MEMBRANE CONTACT REACTORS FOR THREE-PHASE CATALYTIC REACTIONS

by

MICHAEL DEAN WALES

B.A., University of California, Santa Cruz, 2011

AN ABSTRACT OF A DISSERTATION

submitted in partial fulfillment of the requirements for the degree

DOCTOR OF PHILOSOPHY

Department of Chemical Engineering
College of Engineering

KANSAS STATE UNIVERSITY
Manhattan, Kansas

2016

Abstract

Membrane contact reactors (MCRs) have been evaluated for the selective hydro-treating of model reactions; the partial hydrogenation of soybean oil (PHSO), and the conversion of lactic acid into commodity chemicals. Membranes were rendered catalytically active by depositing metal catalyst onto the polymer "skin" of an asymmetric membrane. Hydrogen was supplied to the support side of the membrane and permeated from the support side to the skin side, where it adsorbed directly onto the metal surface. Liquid reactant was circulated over the membrane, allowing the liquid to come into direct contact with the metal coated surface of the membrane, where the reaction occurred. Our membrane contact reactor approach replaces traditional three-phase batch slurry reactors. These traditional reactors possess inherent mass transfer limitations due to low hydrogen solubility in liquid and slow diffusion to the catalyst surface. This causes hydrogen starvation at the catalyst surface, resulting in undesirable side reactions and/or extreme operating pressures of 100 atmospheres or more. By using membrane reactors, we were able to rapidly supply hydrogen to the catalyst surface.

When the PHSO is performed in a traditional slurry reactor, the aforementioned hydrogen starvation leads to a high amounts of trans-fats. Using a MCR, we were able to reduce trans-fats by over 50% for equal levels of hydrogenation. It was further demonstrated that an increase in temperature had minimal effects on trans-fat formation, while significantly increasing hydrogenation rates; allowing the system to capture higher reaction rates without adversely affecting product quality. Additionally, high temperatures favors the hydrogenation of polyenes over monoenes, leading to low amounts of saturated fats. MCRs were shown to operator at high temperatures and: (1) capture high reaction rates, (2) minimize saturated fats, and (3) minimize trans-fats.

We also demonstrated lactic acid conversion into commodity chemicals using MCRs. Our results show that all MCR experiments had faster reaction rate than all of our controls, indicating that MCRs have high levels of hydrogen coverage at the catalyst. It was also demonstrated that changing reaction conditions (pressure and temperature) changed the product selectivities; giving the potential for MCRs to manipulate product selectivity.

MEMBRANE CONTACT REACTORS FOR THREE-PHASE CATALYTIC REACTIONS

by

MICHAEL DEAN WALES

B.A., University of California, Santa Cruz, 2011

A DISSERTATION

submitted in partial fulfillment of the requirements for the degree

DOCTOR OF PHILOSOPHY

Department of Chemical Engineering
College of Engineering

KANSAS STATE UNIVERSITY
Manhattan, Kansas

2016

Approved by:

Major Professor
Dr. Mary Rezac

Copyright

Abstract

Membrane contact reactors (MCRs) have been evaluated for the selective hydro-treating of model reactions; the partial hydrogenation of soybean oil (PHSO), and the conversion of lactic acid into commodity chemicals. Membranes were rendered catalytically active by depositing metal catalyst onto the polymer "skin" of an asymmetric membrane. Hydrogen was supplied to the support side of the membrane and permeated from the support side to the skin side, where it adsorbed directly onto the metal surface. Liquid reactant was circulated over the membrane, allowing the liquid to come into direct contact with the metal coated surface of the membrane, where the reaction occurred. Our membrane contact reactor approach replaces traditional three-phase batch slurry reactors. These traditional reactors possess inherent mass transfer limitations due to low hydrogen solubility in liquid and slow diffusion to the catalyst surface. This causes hydrogen starvation at the catalyst surface, resulting in undesirable side reactions and/or extreme operating pressures of 100 atmospheres or more. By using membrane reactors, we were able to rapidly supply hydrogen to the catalyst surface.

When the PHSO is performed in a traditional slurry reactor, the aforementioned hydrogen starvation leads to a high amounts of trans-fats. Using a MCR, we were able to reduce trans-fats by over 50% for equal levels of hydrogenation. It was further demonstrated that an increase in temperature had minimal effects on trans-fat formation, while significantly increasing hydrogenation rates; allowing the system to capture higher reaction rates without adversely affecting product quality. Additionally, high temperatures favors the hydrogenation of polyenes over monoenes, leading to low amounts of saturated fats. MCRs were shown to operator at high temperatures and: (1) capture high reaction rates, (2) minimize saturated fats, and (3) minimize trans-fats.

We also demonstrated lactic acid conversion into commodity chemicals using MCRs. Our results show that all MCR experiments had faster reaction rate than all of our controls, indicating that MCRs have high levels of hydrogen coverage at the catalyst. It was also demonstrated that changing reaction conditions (pressure and temperature) changed the product selectivities; giving the potential for MCRs to manipulate product selectivity.

Table of Contents

List of Figures

List of Tables

Acknowledgements

First, I would like to thank and express my deepest gratitude to my advisors Dr. Mary Rezac and Dr. Peter Pfromm. They provided me invaluable guidance, encouragement, and infinite patience. I appreciate my time spend with them and feel very fortunate to have had them as my advisors.

I would also like to thank all of my committee members, Dr. Gurpreet Singh, Dr. Stefan Bossmann, and Dr. Donghai Wang, for taking the time to serve on my committee and for their valuable suggestions and comments.

A special thank you must go out to my undergraduate workers, Logan Joos and Wade Traylor. Much of the data in this thesis is because of their hard work and dedication.

I would also like to thank all of my current and former group membranes, John Stanford, Michael Heidlage, Matthew Young, Yixiao Li, Cared Carson, Dr. Leslie Schulte, Shuzhen Qiu, Dr. Sebastian Wendel, Alexandru Avram, Dr. Fan Zhang, and Dr. Ronald Michalsky. Thank for you friendship, advice, and being my sounding board.

I also wish to thank Andrea Blair and everyone at the Student Access Center. They are always welcoming and encouraging to all of their students.

Thank you to Joseph Weeks and Phillip Defoe for ICP help, and Dr. Dan Boyle for SEM help.

Dedication

To my wife, Sheryll, you provided endless inspiration, love, encouragement, and much need laughs. Whenever I am feeling overwhelmed, I think about what you went through, and I know that I can make it through whatever I am dealing with.

To my parents, Richard and Mary, thank you for everything…Dad, "you won".

To my big sister, Pauline, who always inspired me, I have always looked up to you.

To my step mother, Lorell, thank you for everything

To the Kilcrease family: Justin, Ryan, Anne (Lawrence Kilcrease), Casey (Truax), Randy, and the rest of the family.

To the Biko Moving Crew, and all my Santa Cruz urban tribe: R.D., Carmen, Steve, Meeshi, Thomas, Ivan, Leann, Iris, Sarmad, Jake, and Rodrigo.

To all of my friends from "back home": Omar, Mellissa, Aaron, Chris, Rob, Scott, Jessica, Juan, Vu, Randle.

And to my advisor, Dr. Mary Rezac, you took a chance on me when a lot of other schools wouldn't. I will be always be grateful.

So many people have had a positive impact on my life, this is dedicated to all of you. If there is anyone I left off, this is dedicated to you too.

Chapter 1 - Introduction

1.1 Thesis Outline

1.1.1 Introduction

This thesis is comprised of chapters which are papers that: (1) are accepted for publication, (2) have been submitted for publication, or (3) we plan on submitting for publication. Being part of the National Science Foundation Integrative Graduate Education and Research Traineeship Program (NSF IGERT) at Kansas State University, my research focus on sustainable biofuels and biobased products from an interdisciplinary perspective. In addition to my own personal research, I was involved in group projects involving PhD students from a diverse range of disciplines. This thesis will report on the works involved in both my collaboration projects, and my solitary research.

My non-collaboration work involves the development of membrane contact reactors for use in three-phase catalytic reactions actions. The two reactions studied are the partial hydrogenation of soybean oil (PHSO), and the aqueous-phase conversion of lactic acid. Both of these reactions, when operated in traditional slurry reactors, possess inherent mass transfer limitations due to low hydrogen solubility in the liquid phase and slow diffusion to the catalyst surface. This results in hydrogen scarcity at the catalyst surface, causing slow reaction rates, undesirable side reactions, or both[1,2]. In the case of the PHSO, hydrogen starvation at the catalyst cites is directly linked to the production of trans-fats[3]. In the hydrotreating of lactic acid, operating pressures of over 100 atmospheres of pressure are commonly employed[4].

My collaboration work involved using cyclopentyl methyl ether (CPME) as a green solvent alternative for chloroform in the liquid-liquid extraction of oleaginous yeast oils. In addition to wet oil extractions, CPME has also attracted interest as a green ether for various other

processes; however, there is a lack of fundamental studies involving CPME interactions with other chemicals[5,6]. This thesis reports on the liquid-liquid equilibria of four water-alcohol-CPME systems; the alcohols are methanol, ethanol, 1-propanol, and 2-propanol[7].

1.1.2 Outline

Chapter 2 is in the peer-review process. It has been accepted with revisions for Catalysis Today[8]. It is reproduced as it was prepared for publication. It involves our initial investigations into converting commercially available hollow fiber membranes into catalytic membrane reactors. We use the model reaction of the PHSO to explore the effects that temperature and hydrogen pressure have on the production of trans-fats, kinetics, and selectivities.

Chapter 3 continues the work of using commercial "off the shelf" membrane modules as membrane reactors from chapter 2. This chapter explores different catalysts, expands the temperature range of the previous experiments form 80°C to 140°C, tests different membrane configurations, and investigates catalyst deactivation. This paper is prepared for publication.

Chapter 4 reports on the catalytic conversion of lactic acid using ruthenium coated polymeric membranes. This reaction involves several parallel and series reactions taking place simultaneously. The temperature and pressure of the system were varied in an attempt to control product selectivity.

Chapter 5 is in the peer-review process. It has been accepted with revisions for The Journal of Chemical and Engineering Data[7]. It is reproduced as it was prepared for publication. This chapter reports on the liquid-liquid equilibria of CPME ternary systems. The purpose was to obtain thermodynamic data that can be useful for incorporating CPME as a green process solvent. Four water-alcohol-CPME systems were studied. Ternary diagrams with binodal curves and tie-lines were determined.

Chapter 6 is comprised of conclusions and recommendations for future work.

1.2 Background and Theory

1.2.1 Membranes

The field of membrane science is a mature field with some of the earliest works being traced back to experiments done on pig bladders in 1748[9]. Since these early works, the field has expanded to include a diverse range of materials, applications, membrane types, and configurations. There are polymer, metal, ceramic, and liquid membranes. Applications range from water desalination, to gas separations, to membrane assisted chemical reactions, to medical devices. Some of the principle types of membranes include isotropic microporous, nonporous dense films, Loeb-Sourirajan anisotropic, and thin film composite anisotropic membranes[10]. The three basic module configurations are flat sheet, spiral wound, and hollow fiber. The choice of membrane material and configuration is governed by the conditions and compatibility of the stream constituents to the membrane material. While both inorganic and polymeric are applicable to gas and liquid separations, inorganic membranes are usually chosen for high temperatures operations, while polymeric membranes can be used at more modest temperatures (< 200 °C)[11-13]. Both polymeric and inorganic membranes have widespread industrial use[13,14].

Gas transport across a membrane can be divided into three categories depending on the pore size: (1) convective transport occurs when the pores are larger than the mean free path (λ), (2) Knudsen diffusion occurs when the pores are smaller than λ, and (3) solution diffusion occurs when the membranes are dense or non-porous. Because we propose to use membranes as contact reactors, the membranes must also act as a barrier against liquid phase transport, this study will only focus on membranes with Knudsen and solution diffusion.

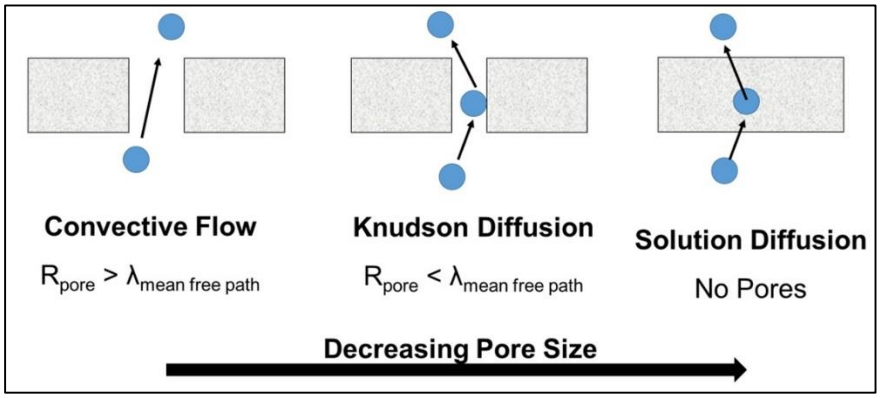

Figure 1.1 – Different types of gas transport through a membrane

The governing equation for one dimensional diffusion can be represented by Fick's first law of diffusion:

$$J_A = -D_A\frac{dC}{dx} \qquad \textbf{Equation 1.1}$$

Integrating over the thickness of the membrane, the flux becomes:

$$J_A = -D_A\frac{dC}{dx} = -D_A\frac{C_1-C_2}{l} \qquad \textbf{Equation 1.2}$$

where J_A is the molar flux of species A, D_A is the diffusion coefficient for A, C_1 is the concentration of A on the feed side of the membrane, C_2 is the concentration of A on the permeate side of the membrane, and l is thickness of the membrane. Although Fick's law can be used for both Knudsen and solution diffusion, the diffusion coefficients are calculated differently.

Knudsen diffusion occurs when the pore radii become smaller than the mean free path of the molecules (λ), under these conditions the gas molecules will have collisions with the pore walls more frequently than with another gas molecule[15]. The Knudsen diffusion coefficient (D_{kn}) can be estimated by:

$$\mathbf{D_{kn}} = \frac{\mathbf{1}}{\mathbf{3}}\boldsymbol{dv} \qquad \textbf{Equation 1.3}$$

where d is the pore diameter, and v is the molecular velocity. Because a molecule's kinetic energy ($\frac{1}{2}mv^2$) is equal to $k_B T$, rearranging for v gives:

$$\boldsymbol{v} = \sqrt{\frac{\mathbf{2}\boldsymbol{k_B}\mathbf{T}}{\boldsymbol{m}}} \qquad \textbf{Equation 1.4}$$

where k_B is the Boltzman constant, T is the temperature, and m is the molecular mass. Combining eq. 1.3 and 1.4 gives:

$$\mathbf{D_{kn}} = \frac{\boldsymbol{d}}{\mathbf{3}}\left[\frac{\mathbf{2}\boldsymbol{k_B}\mathbf{T}}{\boldsymbol{m}}\right]^{\mathbf{1/2}} \qquad \textbf{Equation 1.5}$$

Gases with different masses will have different velocities, and different Knudsen diffusion coefficients. Because molecule-molecule collisions are rare in Knudsen diffusion, it is possible to use a porous membrane to separate gas mixtures. The separation (α) achieved can be calculated by dividing D_{kn} of species A by D_{kn} of species B and taking the inverse. This is also equal to the ratio of the square root of molar masses of each species:

$$\boldsymbol{\alpha_{A/B}} = \mathbf{D_{kn(B)}} / \mathbf{D_{kn(A)}} = \sqrt{\boldsymbol{m}}_{\mathbf{B}} \; / \sqrt{\boldsymbol{m}}_{\mathbf{A}} \qquad \textbf{Equation 1.6}$$

Solution-diffusion occurs in a dense non-porous polymer. Molecules permeate through the free volume of the polymer chains, with the free volume cavities changing due to thermal motion of the polymer chains[16]. In solution diffusion, a gas molecule must first absorb into the dense polymer. It then diffuses through the membrane. And finally desorbs out the other end. The permeability of a membrane is the product of the diffusion coefficient (D) and the sorption coefficient (S):

$$\mathbf{P = D * S} \qquad \textbf{Equation 1.7}$$

The diffusion coefficient is a kinetic term; it relates the energy required for a gas molecule to diffuse through the membrane. The sorption coefficient is a thermodynamic term, it is a measure of the concentration of gas that can be adsorbed into the polymer membrane[16]. Both of these terms are temperature dependent and can be described with the following Arrhenius type equations:

$$\mathbf{S = S_0 \exp\left\{\frac{-H_s}{RT}\right\}} \qquad \textbf{Equation 1.8}$$

$$\mathbf{D = D_0 \exp\left\{\frac{-E_d}{RT}\right\}} \qquad \textbf{Equation 1.9}$$

Combining equations 1.7-1.9 yields:

$$\mathbf{P = P_0 \exp\left\{\frac{-E_P}{RT}\right\}} \qquad \textbf{Equation 1.10}$$

E_d is the diffusion activation energy, H_s is the heat of sorption, and E_p is the activation energy for permeation. S_0, D_0, and P_0 are the pre-exponential factors. The sorption coefficient typically decreases with temperature, while the diffusion coefficient typically increases with temperature. Generally, an increase in temperature increases permeability; however, this is not always the case. Depending on the gas, polymer, and temperature range, the permeability can actually decrease with temperature.

The governing equation for gas transport across a dense membrane is given by:

$$\mathbf{J_A = P_A \frac{p_1 - p_2}{l}} \qquad \textbf{Equation 1.11}$$

where J_A is the molar flux of species A, P_A is the permeability coefficient for A, p_1 is the partial pressure of A on the feed side of the membrane, p_2 is the partial pressure of A on the permeate side of the membrane, and l is thickness of the membrane. This equation shows that the driving force for gas transport across a membrane is the difference in partial pressure between the feed and permeate side.

In solution diffusion, the maximum ability of a membrane to separate two gases is defined as the ideal selectivity and is calculated as the ratio of the pure gas permeability coefficients:

$$\alpha^*_{A/B} = \frac{P_A}{P_B} \qquad \textbf{Equation 1.12}$$

Membrane properties are characterized via measurements of pure gas flux values. Values of $\alpha^*_{A/B}$ less than that of the polymer are an indication of surface defects.

1.2.2 Mass Transfer Resistances in Traditional Three-Phase Reactions

Consider a simplified three-phase heterogeneous hydrogenation reaction:

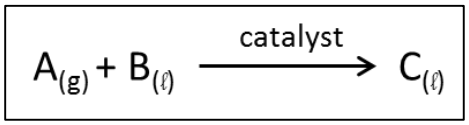

Figure 1.2 – Simplified three-phase reaction scheme

where A is a gas reactant (hydrogen), B is a liquid reactant, and C is a liquid product. In order for the A to reach the catalyst surface, so the reaction can take place, the following steps have to occur[17]:

1. Transport of A from the bulk gas to the gas-liquid interface
2. Transport of A from gas-liquid interface to bulk liquid
3. Transport of A and B from bulk liquid to catalyst surface
4. Diffusion of reactants through the pores of the catalyst (pore diffusion)
5. Adsorption of reactants onto active sites of catalyst
6. Surface reaction

Similar to resisters in series, the overall resistance to mass transfer (R_{tot}) of A from the bulk gas to the catalyst surface can be derived from the individual mass transfer resistances in steps 1-4[18]:

$$\mathbf{R_{tot} = R_1 + R_2 + R_3 + R_4}$$ (Total mass transfer resistance) **Equation 1.13**

$$\mathbf{R_1} = \frac{\mathbf{1}}{\boldsymbol{k_g a}}$$ (mass transfer resistance in the gas phase) **Equation 1.14**

$$\mathbf{R_2} = \frac{\mathbf{1}}{\boldsymbol{k_l a}}$$ (mass transfer resistance in the liquid phase at the gas-liquid interface)

Equation 1.15

$$\mathbf{R_3} = \frac{\mathbf{1}}{\boldsymbol{k_l a_s}}$$ (mass transfer resistance in the liquid phase at the liquid-solid interface)

Equation 1.16

$$\mathbf{R_4} = \frac{\boldsymbol{d_p}}{\mathbf{6}\boldsymbol{D_i a_p \phi}\ \mathbf{\tanh}(\boldsymbol{\phi})}$$ (mass transfer resistance in pores) **Equation 1.17**

$$\boldsymbol{\Phi} = \frac{\boldsymbol{d_p}}{\mathbf{6}}\sqrt{\frac{\boldsymbol{k_r'' a_s}}{\boldsymbol{D_i}}}$$ **Equation 1.18**

where C_A^* is solubility of A in B, $k_l a$ is the gas-liquid mass transfer coefficient, $k_l a_s$ is the liquid-solid mass transfer coefficient, and Φ is the Thiele modulus; see List of Symbols for the full definitions. Several correlations have been developed based on reactor type, reactor geometry, and physical properties of the reactants to calculate the mass transfer coefficients[17].

Additionally, criteria has been established to test whether gas-liquid (α_1), liquid-solid (α_2), and pore diffusion (Φ) mass transfer resistances are significant; they are considered significant if the following inequalities hold true[17]:

$$\boldsymbol{\alpha_1} = \frac{\boldsymbol{R_H}}{\boldsymbol{C_a k_l a}} > \mathbf{0.1}$$ **Equation 1.19**

$$\boldsymbol{\alpha_2} = \frac{\boldsymbol{R_H}}{\boldsymbol{C_a k_l a_s}} > \mathbf{0.1}$$ **Equation 1.20**

$$\boldsymbol{\Phi} > \mathbf{0.2}$$ **Equation 1.21**

where R_H is hydrogenation rate. R_H is an observed value taken from experimental data.

As mentioned above, the three-phase reactions investigated in this thesis, the partial hydrogenation of soybean oil[3] and the lactic acid conversion[19,20], are known to possess one more of these mass transfer limitations. The use of membrane contact reactors are proposed as a means to reduce or eliminate these mass transfer resistances.

1.2.3 Membrane Reactors

The use of a membrane to influence the composition within a chemical reactor is termed a "Membrane Reactor" (MR). A membrane reactor is a unit that takes advantage of the separation properties of membranes and combines them with a chemical reactor into a single unit, the concept was introduced in the 1960's by Gryaznov[21]. There are several configurations that membrane reactors can be operated in, each having its own distinct advantage. Figure 1.3 shows two configurations: an extractor configuration where products are selectively removed from the reactor as they are being formed as a means to the shift equilibrium to the right, and a distributor configuration where a reactant is selectively added to a reactor to minimize the formation of undesired products.

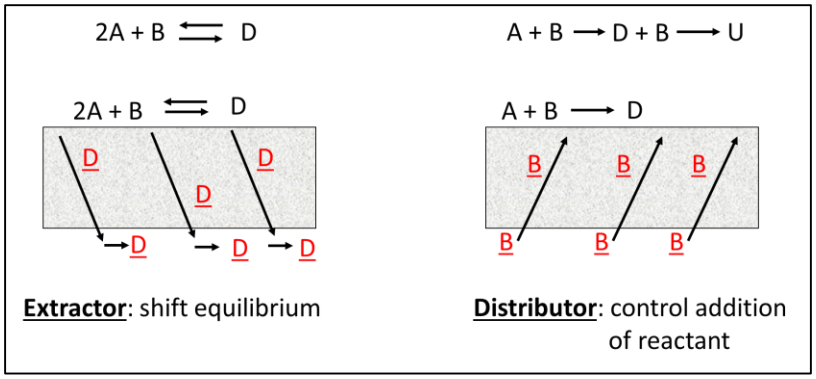

Figure 1.3 – Membrane reactors in (left) extraction configuration and (right) distributor configuration. Species "D" represent a desired product and species "U" represents an undesired product.

Figure 1.4 shows two different configurations for membrane contact reactors (MCRs), "flow-through" and "flow-over" modes. MCRs in the flow-through mode use a porous membrane with either Knudsen or convective transport. Catalyst is attached inside the pores, and premixed reactants are forced through the membrane; an early name for these MCRs was "catalytic filter"[22,23]. The function of the membrane is to provide a reaction surface and a controlled residence time. These type of membranes provide excellent contact between reactants and catalyst, and are a good choice of reactors if pore diffusion is a limiting factor.

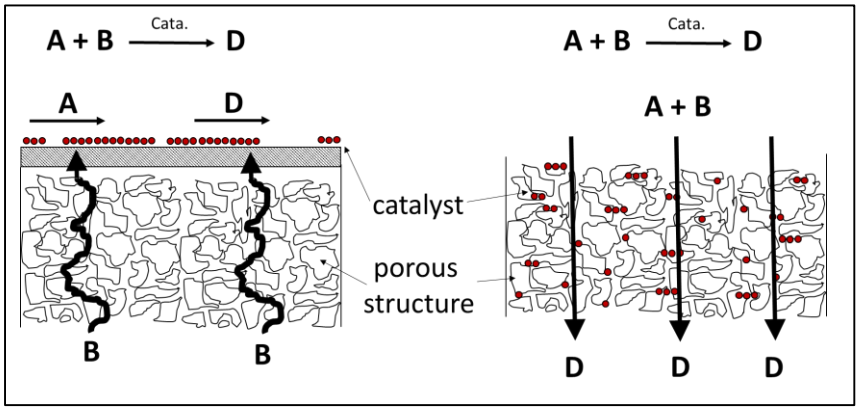

Figure 1.4 – Schematic for catalyst membrane contact reactors in the (left) flow-over configuration and (right) flow-through configuration.

In flow-over operations, catalyst is attached to one side of the membrane and one reactant flows over the catalyst. The second reactant is supplied to the membrane from the opposite non-catalytic side of the membrane, where it must permeate through the membrane to reach the catalyst cites. By forcing the second reactant to permeate through the membrane, it is possible to control its concentration at the catalyst surface, which allows for the ability to control product selectivity. Another benefit of this configuration arises when using three-phase reactions in which the gas phase has low solubility in the liquid phase, such as the two reactions reported on in this thesis. By using the flow-over configuration, it has been shown that hydrogen starvation at the catalyst cites can be eliminated and reactions can be operated under kinetically controlled conditions[8]. For these reasons, only membrane contact reactors operated in the flow-over configuration were investigated in our studies.

1.2.4 List of Symbols

J_A	molar flux of species A, $mol/m^{-2}\ s^{-1}$
D_A	diffusion coefficient of A, m^2/s
C_1	concentration of A on the feed side of the membrane, mol/m^3
C_2	concentration of A on the permeate side of the membrane, mol/m^3
l	thickness of the membrane, m
D_{kn}	Knudsen diffusion coefficient, m^2/s
d	pore diameter, m
v	molecular velocity, m/s
m	mass, kg
k_B	Boltzman constant, $m^2\ kg\ s^{-2}\ K^{-1}$

T	temperature, K
$\alpha_{A/B}$	separation factor, dimensionless
P	permeability, Barrer = 10^{-10} (cm^3(STP) / cm. sec. cmHg)
S	sorption coefficient, dimensionless
E_d	diffusion activation energy, J/mol
H_s	heat of sorption, J/mol
E_p	activation energy for permeation, J/mol
S_0	sorption pre-exponential factor, dimensionless
D_0	diffusion pre-exponential factor, Barrer = 10^{-10} (cm^3(STP) / cm. sec. cmHg)
P_0	permeation pre-exponential factor, Barrer = 10^{-10} (cm^3(STP) / cm. sec. cmHg)
R	gas constant
p_1	partial pressure of feed side, Pa
p_2	partial pressure of permeate side, Pa
$\alpha^*_{A/B}$	ideal selectivity, dimensionless
R_{tot},	resistances to mass transfer, s
R_1, R_2, R_3,R_4	
k_g	gas-side mass transfer coefficient, m/s
a	specific gas-liquid contact area, m^2/m^3
k_l	liquid-side mass transfer coefficient, m/s
c_A^*	gas solubility, c_L/c_g at equilibrium
a_s	specific external surface area of solid, m^2/m^3
d_p	particle diameter, m

D_i impeller diameter, m

ϕ Thiele modulus, dimensionless

$\boldsymbol{k_r''}$ first order surface reaction rate constant, m/s

R_H overall hydrogen rate, kmol m^{-3} s^{-1}

$\boldsymbol{C_a}$ saturation solubility of H_2 in liquid phase, kmol/m^3

Chapter 2 - Composite Catalytic Tubular Membranes for Selective Hydrogenation in Three-Phase Systems

2.1 Introduction

Three-phase catalytic reactions involve liquid-phase and gas-phase reactants coming into contact with a solid-phase catalyst. These three-phase heterogeneous reactions are widely used in industrial applications from pharmaceuticals to food processing. These reactions are typically carried out in batch slurry systems or trickle bed reactors. However, these traditional reactors possess inherent mass transfer limitations due to low hydrogen solubility in the liquid phase and slow diffusion to the catalyst surface. This results in hydrogen starvation at the catalyst surface, causing slow reaction rates, undesirable side reactions, or both[1,2]. In the case of the partial hydrogenation of soybean oil (PHSO), the model reaction chosen for this study, the undesired side reaction is the production of trans-fats[24,25].

PHSO is the process of chemically adding hydrogen to a fat molecule in the presence of a catalyst. This process converts some of the double bonds of unsaturated fatty acids to single bonds[26]. Industrial hydrogenation, or hardening, of vegetable oil has been carried out since the early parts of the 1900's[27]. Hydrogenation improves the oxidative stability, flavor stability, and changes the melting point of the oil. Unfortunately, hydrogenation also results in conversion of some *cis* double bonds to the *trans* configuration. These isomers are collectively referred to as trans-fats or trans-fatty acids[3,26,27]. The accepted reaction scheme for hydrogenation of a polyunsaturated fatty acid is shown in Figure 2.1[3].

The scheme consists of three consecutive first order reactions in which linolenic acid is hydrogenated to linoleic acid, to oleic acid, to steric acid. This is a simplified scheme and neglects shunt reaction, isomerization, or double bond migration. The overall hydrogenation rate

for vegetable oils in a dead end batch reactor has been shown to follow first order kinetics[3]. The rate constant is defined as:

$$\mathbf{k} = \frac{ln\left(\frac{IV_0}{IV}\right)}{t} \qquad \textbf{Equation 2.1}$$

where t is time of reaction, IV_0 is the initial iodine value, and IV is the iodine value at time t. The units of k are $\frac{1}{time}$.

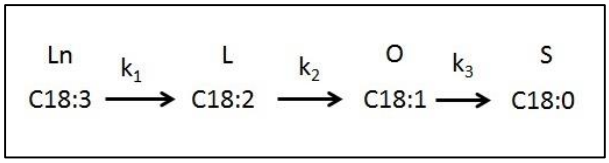

Figure 2.1 - Simplified consecutive reaction scheme for hydrogenation of soybean oil. The accepted nomenclature for lipids is expressed as [Cx:y], where x is the number of carbon atoms in the lipid and y is the number of double bonds present.

PHSO reactions are typically carried out in a batch autoclave with a nickel catalyst under the following conditions: 110-190°C, 2.0-5.0 bar, and 0.01-0.15 wt% nickel[3]. These conditions are necessary to increase the solubility of hydrogen gas in the oil and to accelerate the hydrogenation reaction rate on the catalyst surface. Unfortunately, while the high reaction temperatures promote rapid reaction, they decrease hydrogen solubility in the oil resulting in low hydrogen coverage on the catalyst, and accelerate the production of *trans*-fatty acids[3].

Palladium has been widely studied as an alternative catalyst[28-31]. Palladium has an activity that is 15-20 times greater than nickel, and palladium can give lower trans-fat isomerization if the reaction can be run in the absence of mass-transfer limitation[31]. However, when palladium is used in place of nickel under the normal operating conditions of the latter, mass transfer limitations are known to exist and palladium produces more trans-fats than nickel[31].

A possible solution to overcome these mass transfer limitations, and lower the production of trans-fats, is the application of catalytic membrane contact reactors (CMCRs). CMCRs are created by impregnating an asymmetric membrane with a catalyst on the selective "skin" of a membrane. Hydrogen is supplied from the support side of the membrane and permeates from the support side to the skin side, where it adsorbs directly onto the metal surface. Liquid reactant is circulated over the skin side, allowing the liquid to come into direct contact with the metal coated surface of the membrane where the hydrotreating occurs, Figure 2.2. CMCRs have the potential to eliminate hydrogen starvation by changing the transport mechanism of hydrogen delivery to the catalyst surface, thus changing the reaction from mass transfer limited to kinetically limited. In the PHSO, the mass transfer of gas into the liquid phase is known to be the rate limiting step[3]. With CMCRs, the gas delivery to the catalyst surface is governed by the transport mechanism of the gas through the membrane: solution diffusion, Knudsen diffusion, or convection.

The system configuration shown in Figure 2.2 is referred to as a "flow-over" system; because the liquid reactant is circulated over the surface of the catalyst. Another configuration that has received interest is the pore "flow-through" method[32]. In the flow-through configuration, catalyst is embedded inside the pores of the membrane and premixed reactants are forced through the membrane; an early name for these CMCRs was "catalytic filter"[22,23]. By forcing the reactants through membrane pores, with either convective or Knudsen transport, excellent contact is achieved between reactants and catalyst, and pore diffusion can be eliminated as a limiting factor. We chose the flow-over system because a flow-through system is still limited by the low hydrogen solubility in the oil phase, as the oil and hydrogen must be premixed prior to flowing though the pores[33]. A study hydrogenating sunflower oil showed that this

excellent catalyst-oil contact, coupled with low hydrogen solubility leads to higher trans-fat formation than a slurry reactor[33].

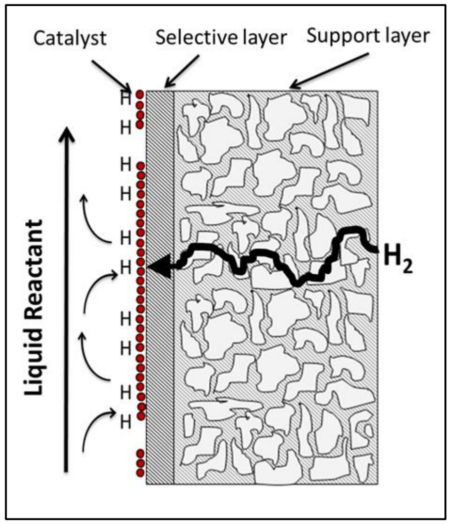

Figure 2.2 - Schematic of catalytic membrane contact reactor (CMCR). Catalyst is attached to the selective layer, hydrogen is supplied to the support side, oil is circulated over the selective layer; allowing the oil to come into contact with the catalyst.

The concept of the catalytic membrane reactors was first introduced by Gryaznov in the 1960's[21,34]. These early works focused on thick non-porous metal membranes. Additionally, much of the early work on catalytic membrane reactors focused on gas-phase reactions[35,36]; while more recent work in the gas phase includes the novel destruction of chemical warfare agents[37]. Since then, CMCRs have been demonstrated using asymmetric membranes for three-phase reactions. These works include CMCRs for hydrogenation of dissolved oxygen in water[38,39], hydrogen peroxide synthesis[40], and the hydrogenation of various vegetable oils[41]. Previous bench scale studies in our lab have shown that bench scale flat sheet membrane reactors are able to reduce the amount of trans-fats formed by up to 70% in the PHSO[42-44]. However, extending this technology from the bench scale to commercial use requires a more complete understanding of how process conditions and reactor design influences system performance.

The objective of this study was to access the potential to scale-up CMCRs for the partial hydrogenation of soybean oil. CMCRs were prepared using commercially available hollow fiber membranes. The influence of the process temperature and pressure on reaction rate and selectivity was measured. The CMCR results are compared to those of the traditional slurry system and viability for large-scale design.

2.2 Materials and Methods

2.2.1 Materials

Commercial available composite tubular membranes and module (PVM-035) were purchased from Pervatech BV (Netherlands). Refined, bleached, and deodorized soybean oil (iodine value, IV = 129-132) was purchased from a local grocery store, Dillon's Food Store Inc. Poly(N-vinyl-2-pryyolidone) (PVP) average M.W. 58,000, K29-32 and palladium(II) chloride with a purity of 99.999, was purchased from ACROS Organics™. Methanol (MeOH) 99.8% (Certified ACS Reagent Grade) was purchased from Fisher Scientific. Hydrogen and nitrogen, ultra high purity (99.999%), were purchased from Linweld Inc.

2.2.2 Virgin Membrane

The membranes used are a polymeric/ceramic composite with a substrate layer of α-Al_2O_3 (outside/shell side), an intermediate layer of γ-Al_2O_3/titania, and a polydimethylsiloxane (PDMS) top layer (inside/bore side). The dimensions are 500 x 10 x 7 mm (length x O.D. x I.D.) The PDMS layer is listed as non-porous with a thickness ranging from 3 to 5 μm.

All membranes used were flux tested using a constant-pressure variable volume apparatus as a means of quality control, a similar device is described elsewhere[45]. All flux measurements were performed at a feed pressure of 4.2 bar gauge, 0 bar gauge permeate

pressure, and 25°C. The normalized gas fluxes are determined, and the pure gas selectivities ($\alpha_{i/j}$) were calculated. $\alpha_{i/j}$ is the ratio of normalized flux of pure gas *i* over pure gas *j*. Gas fluxes are reported in gas permeation units (GPU); where one GPU equals $10^{-6}\frac{cm^3_{(STP)}}{cm^2*sec*cmHg}$. A membrane is considered defect free if it has an $\alpha_{i/j}$ equal to the ratio of the permeance of gas *i* and gas *j* for material of the selective skin layer (PDMS). Any skin defects in the membrane will lower this selectivity.

For this study membrane permeance and selectivities for the pure gases hydrogen and nitrogen were tested. The purpose of testing for pure gas selectivity is to probe for structural damage to the selective skin of the membrane. A small amount of skin defects were acceptable; all membranes used were required to have an $\alpha_{i/j}$ greater than Knudsen diffusion selectivity.

2.2.3 Catalyst Deposition

Membranes were rendered catalytically active by wet impregnation of a polymer-palladium complex. A catalyst solution was prepared by dissolving 0.4g PVP and 0.2g $PdCl_2$ in MeOH into a 50 mL centrifuge tube and sonicated overnight in a water bath. The membranes were coated by first plugging one end of the membrane tube and filling it with 9 mL of the PVP-$PdCl_2$-MeOH solution. The second end was then plugged, and the membrane was inverted several times. The membranes were drained of the PVP-$PdCl_2$-MeOH solution and placed in an oven at 60°C and allowed to dry for 30 min. This process was repeated five times. The coated membranes were reduced from $PdCl_2$ to Pd under a hydrogen atmosphere for two hours prior to use. Catalyst reduction was confirmed using powder x-ray diffraction (XRD).

Because the catalyst was deposited on the inside of the membrane (diameter ≈ 7mm), we were unable to perform XRD directly on the membrane. Instead, reduction was performed on a model surface. A PDMS film was coated with the PVP-$PdCl_2$ and reduced under identical

conditions; XRD was performed on this sample. The bottom two diffraction patterns in Figure 2.3 are the unreduced $PdCl_2$; the bottom most pattern (—) shows pure $PdCl_2$ powder, the 2nd pattern from the bottom (—) shows the PDMS film coated with our PVP-$PdCl_2$ catalyst. The top two diffraction patterns show the reduced palladium; the 3rd pattern from the bottom (—) shows palladium on a XRD slide, and the top most pattern (—) shows the reduced PVP-Pd on a PDMS film. Both of the unreduced samples (bottom two patterns) show characteristic peaks at $2\theta \approx$ 17°, 27°, 28°, and 38° representing the $PdCl_2$ (020), (011), (120) , and (111) planes respectively; these peaks are not present in the reduced samples (top two patterns). The reduced patterns shows characteristic peaks at $2\theta \approx$ 40°, 46°, and 67° representing the (111), (200), and (220) planes respectively. Figure 2.3 shows that our initial catalyst solution of PVP-$PdCl_2$ contains a mixture of $PdCl_2$ and Pd, indicating that some of the $PdCl_2$ was reduced prior to the deposition of the metal (during the catalyst solution preparation step); this is expected as methanol is known to reduce $PdCl_2$[46]; however, figure 3 clearly shows that our final PVP-Pd contains no metal salt. Figure 2.3 also shows the amorphous halo of the PVP polymer.

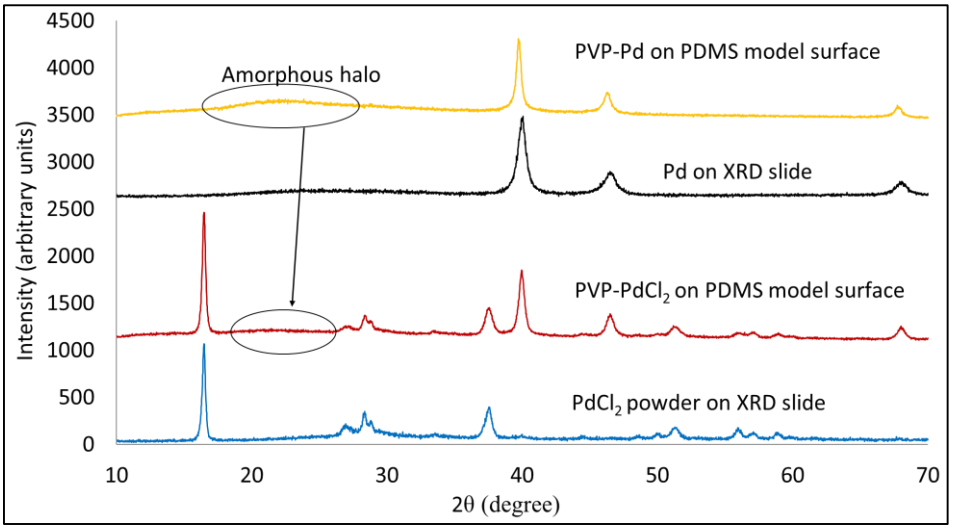

Figure 2.3 - XRD results for catalyst reduction on PDMS film model surface. XRD spectrum clearly show reduction of $PdCl_2$ to Pd, even in the presence of the anchoring polymer PVP. Additionally, the amorphous halo of the PVP is present.

Similar to Gao et al.[35], we found that the metal salt alone could not be irreversibly adhered on the polymeric skin of the membrane; however, the PVP anchored metal complex was able to adhere onto the skin of the membranes. Inductively coupled plasma (ICP) tests, at a detection limit of 5 mg/L, performed on oil samples showed no signs of catalyst leaching into the liquid phase (ICP results not shown). Figure 2.4 shows that the coated membrane on the right has a darker color, indicating that PVP-Pd catalyst adhered to the selective layer of the membrane.

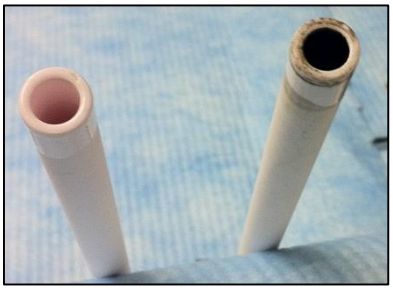

Figure 2.4 - Virgin membrane (left side) and catalytic membrane (right side). The darker color on the bore side of the membrane on the right indicates that PVP-Pd catalyst adhered to the selective layer.

2.2.4 Reactor Set-up

A schematic of the reactor system employed is shown in Figure 2.5. Oil is circulated through the CMCR using a positive displacement pump (Q1CSY**,** Fluid Metering Inc.). The recirculation loop was constructed of ¼ inch stainless steel tubing (Swagelok Company), wrapped in a heating tape (BSAT051006, BriskHeat Corporation). Hydrogen was supplied to the shell side of the reactor (support side of the membrane). Nitrogen was supplied to the oil

side of the membrane; the oil side was kept at a higher pressure than the hydrogen pressure to prevent the selective skin of the membrane from being damaged.

Immediately following catalyst reduction, 19.8 gram of oil was added to the system and circulated at 1 mL/sec. The system was then pressurized and purged with nitrogen, and the heating tape was turned on. Once the system equilibrated at the desired temperature, the hydrogen pressure was applied; this was recorded as the start of the reaction. 0.09g samples were collected periodically and saved for fatty acid methyl ester analysis. At the end of each experiment, the system was drained of oil and flushed with five volumes of hexane.

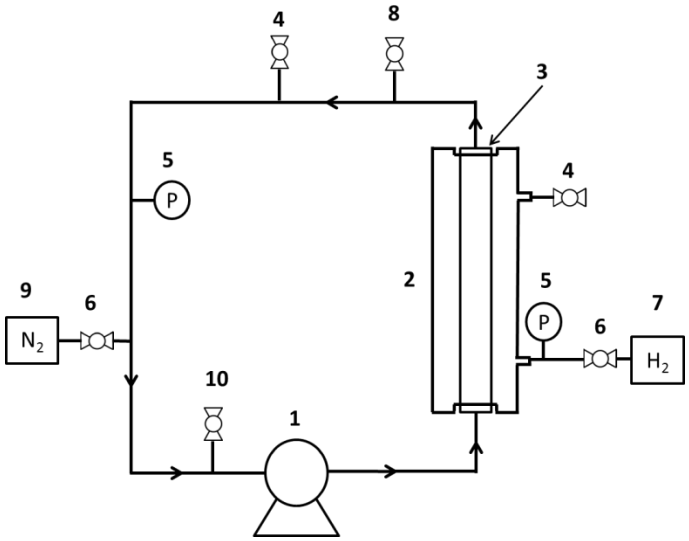

Figure 2.5 - Schematic of the membrane reactor setup for the PHSO experiments: (1) Piston pump; (2) membrane module; (3) membrane; (4) purge valve; (5) pressure gauge; (6) check valve; (7) hydrogen source (8) thermal couple; (9) nitrogen source; (10) sample port.

2.2.5 Sample Analysis

Triglycerides were converted to fatty acid methyl esters (FAMEs) using American Oil Chemists' Society (AOCS) official method Ce 2-66[47]. The corresponding FAMEs were analyzed on a gas chromatogram (GC), equipped with a flame ionization detector (FID); Hewlett-Packard 6890 series. The GC method employed was AOCS official method Ce 1h-05[48]. The column used was a 100m CP-Sil 88 (Agilent Technologies), the injector port and detector were kept at 220 °C with a 100:1 split ratio, the oven was operated isothermally at 180 °C, and the carrier gas was helium at 1.0 mL per min. From the GC results, we were able to determine the iodine value (IV) of the samples using AOCS official method cd 1c-85[49].

2.2.6 Error Analysis

The error bars shown represent the propagation of error present in each measurement. There were three important sources of error for the measurements reported: IV, mass of oil, and time. The error in IV (±1.2) was determined by performing the transesterification and the subsequent GC analysis 10 times on the same sample of oil. The range from these 10 runs was used as the error in IV. The error in the total mass of oil initially charged to the reactor was taken to be ±0.99 g. This was determined by filling and draining the system 10 times, the range from these 10 points was used. And the error in time used was ±1.0 minute; this was the accuracy of the clocks used. These values were used to propagate the error in the results section. There are two other sources of error, temperature and pressure, ±1 °C and ±0.2 bar respectively. However, these values were not used in any calculations and thus not propagated further. Temperature and pressure were usually independent variables, and errors bars were not added in the x-axis of plots.

2.3 Results and Discussion

2.3.1 Pressure Effects

The driving force for hydrogen flux across the membrane is the difference in hydrogen partial pressure between the two sides of the membrane. As the hydrogen pressure is increased on the shell side an increase in hydrogen flux and hydrogen availability at the catalyst surface is expected. As long as hydrogen consumption is greater than the ability to delivery hydrogen to the catalyst, we should expect the reaction rate to increase as the hydrogen flux is increased. However, once hydrogen delivery is greater than hydrogen consumption, the reaction rate will reach a maximum. This is indeed what we see in Figure 2.6.

Figure 2.6 shows the reaction rate as a function of hydrogen pressure for the PHSO at 65 °C ± 2 using three different membranes. Each data point is a separate experiment. CMCR 1, CMCR 2, and CMCR 3 represent different membranes; however, they are structurally identical (i.e. the same catalogue number), so any variation in gas transport properties would come from variations in the manufacturing processes. The data can be divided into two regions: (1) $\leq$ 2 bar of hydrogen pressure, and (2) > 2 bar of hydrogen pressure. In the first region, the reaction rate increased with an increase in hydrogen pressure; however, in the second region the reaction rate remained fairly constant with increasing hydrogen pressure. In the low pressure region, the reaction is hydrogen delivery limited. Above some threshold ($\approx$ 3 bar for this study), the reaction is kinetically limited.

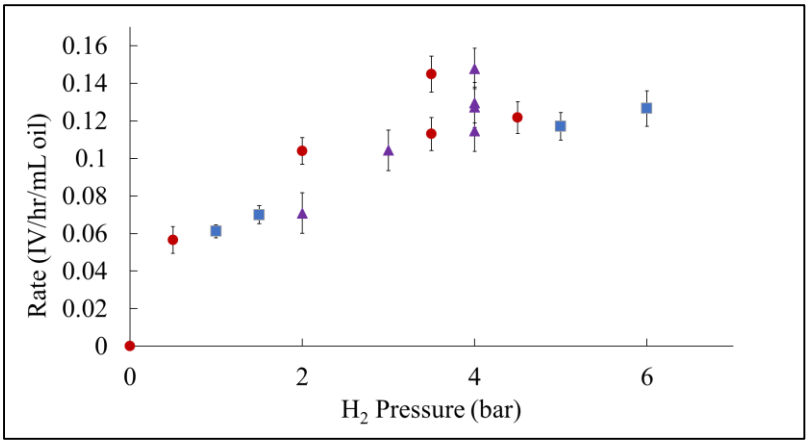

Figure 2.6 - Reaction rate as a function of hydrogen pressure for the partial hydrogenation of soybean oil at 65°C ±2 for three different membranes. CMCR 1 (●), 2 (▲) and 3 (■) (represent different membranes; however, structurally they are identical {i.e. the same catalog number}, and with identical catalyst application). The graph shows two regions: (1) at hydrogen pressures ≤ 2 bar, hydrogen delivery limited region, where an increase in hydrogen pressure causes an increase in reaction rate, (2) at hydrogen pressures ≥ 3.5 bar, kinetically limited region, where the limiting factor is catalyst availability.

The reaction order for the runs with hydrogen pressure ≥ 3.5 bar was determined to be -0.1 ± 0.2 with respect to hydrogen pressure (Figure 2.7). This zero-order type behavior would indicate that the system was operating under kinetically controlled conditions and the catalyst had sufficient hydrogen coverage throughout the experiments. In contrast, a slurry system with a Pd catalyst, operating at over 50 bar hydrogen pressure, has a reaction order of 0.6[28], indicating that the reaction is limited by hydrogen availability at the catalyst. The reported slurry system is believed to be free of pore diffusion limitations[28], thus any hydrogen starvation must be due to low hydrogen solubility into the oil phase. Our CMCR system is able to produce kinetically controlled conditions at pressures > 4 bar, while slurry systems at pressures in excess of 50 bar are not.

The variability in the reaction rates given in Figure 2.6 is probably due to the lack of control in the catalyst deposition. After each experiment, the membrane was sonicated in hexane overnight, dried, and fresh catalyst was redeposit. Without a means to control the precise amount of catalyst applied for each experiment, variability in the amount and availability of catalyst is to be expected. Although CMCR 1, CMCR 2, and CMCR 3 are physically different membranes, they are treated exactly the same; the procedures for depositing catalyst and cleaning the membranes are consistent thought out the experiments. Nevertheless, Figure 2.6 clearly demonstrates that a CMCR can supply hydrogen sufficiently fast to achieve high and constant catalyst surface coverage that ultimately achieves fast and selective conversation.

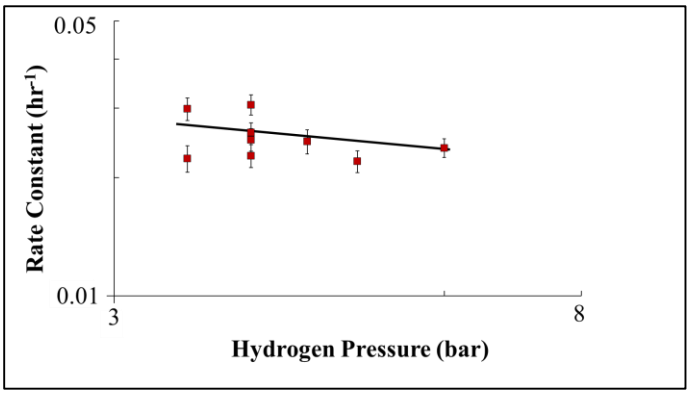

Figure 2.7 - Reaction order with respect to hydrogen pressure equals -0.1 ± 0.2, for data points ≥ 3.5 bar from Figure 2.6 (kinetically limited region). This zero order behavior indicates that the catalyst surface maintains high hydrogen coverage throughout the experiments.

As discussed in the experimental section, the membranes used are ceramic/polymer composites. The goal of composites is to produce a membrane that contains a very thin, selective, top layer that is supported by a nonselective porous layer[50,51]. The ceramic layer acts as the porous support, and provides essentially no resistance to gas transport, its purpose is to

provide mechanical strength to the top polymer layer. The top polymer (PDMS) layer is non-porous, approximately 3-5 μm thick, and essentially provides all of the resistance to gas transport. By minimizing the thickness of the top layer, and using a very permeable support layer, it is possible to produce a membrane that has high flux and close to the intrinsic selectivity of the selective PDMS layer[50,51]. Which is what Table 2.1 shows for the unmodified membranes having hydrogen fluxes between 100-300 GPU, and selectivities close to the intrinsic α_{H_2/N_2} = 2.23 at 35°C[52].

Table 2.1 also shows a significant jump in hydrogen and nitrogen flux for CMCR 1 and CMCR 2 after use, while the fluxes for CMCR 3 essentially stayed constant. We believe that this is due to the repeated process of: (1) using the membranes, (2) depositing and reducing catalyst, and (3) cleaning (described above); this repeated cycle induced defects into the membrane skin. Because the selective PDMS layer is ultrathin, even small defects can lead to a large increases in gas fluxes[53,54]. CMCR 1 and CMCR 2 were exposed to this cycle 14 and 10 times (respectively), while CMCR 3 was only used 4 times; with more uses, we expect CMCR 3 to also see an increase in flux. Table 2.1 also shows the selectivities of the unmodified vs. modified membranes, the selectivities can provide insight into the nature of the type of defects that are being created in the membranes.

The selectivities are between the intrinsic selectivity of PDMS (2.23 at 35°C)[52] and Knudsen selectivity (3.74). This would indicate the induced defects are small; in Knudsen range or smaller. If the defects were large, then the gas transport would be convective flow and the membrane would become non-selective i.e. α_{H_2/N_2} would become 1. Knudsen diffusion occurs when the pores are smaller than the mean free path of the gas. When this is the case, the gas molecules will have collisions with the walls of the pores more frequently than with other gas

molecules[53]. The α_{H_2/N_2} for Knudsen diffusion is $\alpha_{H_2/N_2} = \sqrt{\frac{MW_{N2}}{MW_{H2}}}$, where MW_{N2} and MW_{H2} stand for the molecular weight nitrogen and hydrogen, respectively[53].

Table 2.1 - Membrane flux at 25°C and 4.2 bar: prior to metal deposition and after completion of reactions.

	Virgin membranes (permeance, GPU)			After reaction (permeance, GPU)			
	N_2	H_2	$\frac{H_2}{N_2} selectivity$	Number of Reactions	N_2	H_2	$\frac{H_2}{N_2} selectivity$
CMCR 1	32.8	113.7	3.5	14	350	1160	3.3
CMCR 2	107	263	2.5	10	550	1760	3.2
CMCR 3	88	220	2.5	4	93	196	2.1

2.3.2 Temperature Effects

In a traditional slurry reactor, an increase in temperature increases the rate of hydrogen consumption at the catalyst, while simultaneously decreasing hydrogen solubility in the liquid phase. These factors lead to a decrease in hydrogen coverage on the catalyst and a corresponding increase in trans-fat production[3]. Figure 2.8 compares the trans-fat formed, for equal levels of hydrogenation (IV ≈ 115), as a function of the reaction temperature. A slurry reactor with a Pd/Al_2O_3 catalyst shows a signification increase in trans-fat as temperature is increased[29]. However, for the CMCR system, the production of trans-fat is essentially temperature independent. Additionally, the CMCR's trans-fat formed at all tested temperatures is less than the trans-fat formed at 23 °C for the slurry reactor. This allows the CMCR system to be operated at high temperatures, capturing higher reaction rates without adversely affecting product quality.

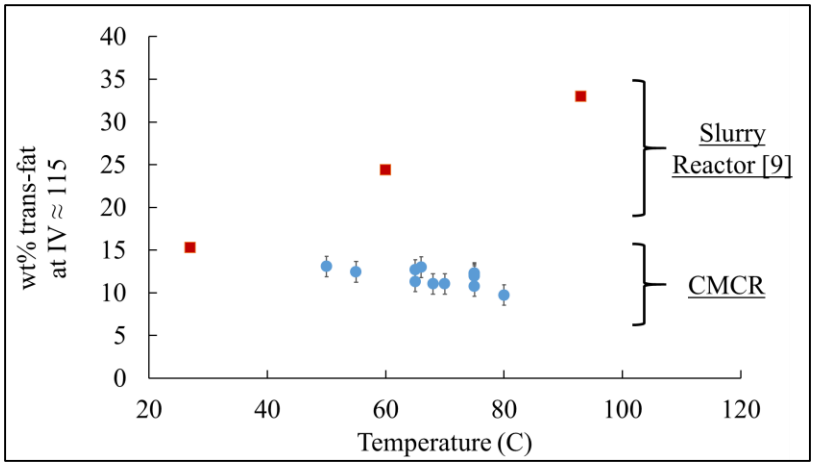

Figure 2.8 - Trans-fat formation as a function of temperature. Trans-fat formation is essentially temperature independent using membrane reactors. The slurry reactor (■) show a significant increase in trans-fat formation as the temperature increases. Membrane reactors (●) operated between 2-5 bar hydrogen pressure, slurries were 3.5 bar [29]

2.3.3 Kinetics

Albright[55] developed the kinetic equations for the reaction scheme shown in Figure 2.1. The governing equations are:

$$[Ln] = [Ln_0]\, e^{-k_1 t} \qquad \textbf{Equation 2.2}$$

$$[L] = [Ln_0]\left(\frac{k_1}{k_2-k_1}\right)\left(e^{-k_1 t} - e^{-k_2 t}\right) + [L_0]\, e^{-k_2 t} \qquad \textbf{Equation 2.3}$$

$$[O] = [Ln_0]\left(\frac{k_1}{k_2-k_1}\right)\left(\frac{k_2}{k_3-k_1}\right)\left(e^{-k_1 t} - e^{-k_3 t}\right) - \qquad \textbf{Equation 2.4}$$

$$[Ln_0]\left(\frac{k_1}{k_2-k_1}\right)\left(\frac{k_2}{k_3-k_2}\right)\left(e^{-k_2 t} - e^{-k_3 t}\right) +$$

$$[L_0]\left(\frac{k_2}{k_3-k_2}\right)\left(e^{-k_2 t} - e^{-k_3 t}\right) +$$

$$[O_0]\, e^{-k_3 t}$$

where $[Ln_0]$,$[L_0]$, and $[O_0]$ are the starting wt% of linolenic acid, linoleic acid, and oleic acid respectively. [Ln], [L], and [O] are the wt% of linolenic acid, linoleic acid, and oleic acid at time

(t). The individual rate constants (k_1, k_2, k_3) were calculated by solving for the three simultaneous equations above.

The temperature dependence of the rate constants are correlated using the Arrhenius equation:

$$\boldsymbol{k = Ae^{-E_a/RT}} \qquad \textbf{Equation 2.5}$$

where k is the rate constant, A is the preexponential factor, E_a is the apparent activation energy, R is the gas constant, and T is the temperature in kelvin. The E_a of a reaction can be determined by carrying out the reaction at different temperatures and plotting the ln(k) versus 1/T. The resulting Arrhenius plot will have a slope equal to $-E_a/R$. These plots were used to determine the apparent activation energy for the over rate of hydrogenation (k), and for the individual rate constants (k_1, k_2, and k_3); denoted as:

E_a = apparent activation energy for the overall rate of hydrogenation (k)

E_{a1} = apparent activation energy for linolenic acid to linoleic acid (k_1)

E_{a2} = apparent activation energy for linoleic acid to oleic acid (k_2)

E_{a3} = apparent activation energy for oleic acid to steric acid (k_3)

The apparent activation energy for overall (E_a), and the individual reactions (E_{a1}, E_{a2}, and E_{a3}) for our CMCR system were determined. The system was filled with oil and operated as described above (section 2.4) at four different temperatures. Four samples were taken at each temperature. After the forth sample at a given temperature, the hydrogen pressure was turned off and the temperature was increased. The system was allowed 30 minutes to equilibrate to the new temperature and hydrogen pressure was reapplied. This was repeated for the final two temperatures (Figure 2.9). The Arrhenius plots for CMCR system was graphed and the apparent activation energies were determined, Table 2.2.

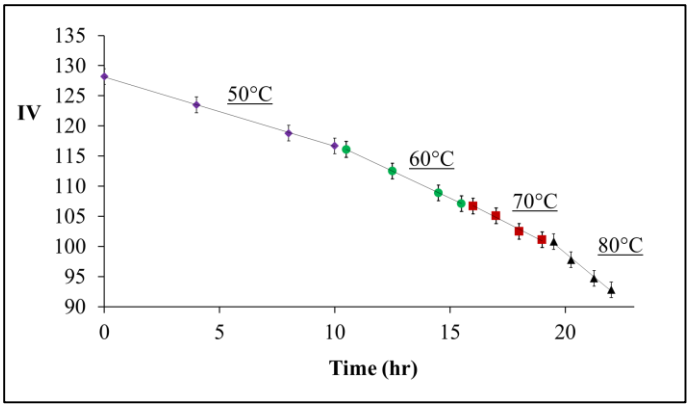

Figure 2.9 - Partial hydrogenation of soybean oil at four temperatures for a catalytic membrane: 50°C (♦), 60°C (●), 70°C (■), 80°C (▲). The overall and individual rate constants (k, k_1, k_2, k_3) were determined as well as the apparent activation energies (E_a, E_{a1}, E_{a2}, E_{a3}).

Because activation energy of a catalyst should be system independent (absent of mass transfer limitations) we compared the E_a of our CMCR to that of a slurry system. We found that the results for the CMCR system compares similarly to a slurry reactor with Pd/alumina, 36.4 kJ/mol compared to 30.1 – 35.9 kJ/mol respectively,

Table 2.3[28]. Additionally, the Arrhenius plots for both systems were linear. The agreement of apparent activation energies and linearity of the plots would indicate that both systems are free of mass transfer limitations. However, the CMCR system achieved this at 4 bar hydrogen pressure compared to 51 bar for the slurry. This further demonstrates the ability of CMCRs to operate in the kinetically controlled region at greatly reduced pressures.

2.3.4 Selectivities

When hardening soybean oil, the aim is to hydrogenate linolenate (Ln, C18:3), while maintaining linoleate (L, C18:2), and minimizing stearate formation (S, C18:0). These

preferences are expressed as the linolenate (S_{Ln}) and linoleate (S_L) selectivities[3,55]. These selectivities are defined as:

$$\mathbf{S_{Ln}} = \frac{k_1}{k_2} \qquad \textbf{Equation 2.6}$$

$$\mathbf{S_L} = \frac{k_2}{k_3} \qquad \textbf{Equation 2.7}$$

The apparent activation energy for individual hydrogenation steps show that $E_{a1} > E_{a2} > E_{a3,}$ Table 2.2. This is consistent with literature for both nickel[3] and palladium[3,28,29,31] slurry reactors. This is credited to preferred adsorption of the polyenes over the monoenes[56]. This increasing activation energy means that it is advantageous to run the reaction at higher temperatures, as the higher temperatures will improve selectivities (Figure 2.10). Because $E_{a1} > E_{a2} > E_{a3}$, as the temperature is increased, k_1 will increase at a greater rate than k_2, and k_2 will increase at a greater rate than k_3. According to equations 2.6 and 2.7, this results in higher S_L and S_{Ln} at higher temperatures, as demonstrated in Figure 2.10. Because increasing temperatures in a slurry reactor causes an increase in trans-fats, slurries are forced to choose between improved selectivities or lower trans-fats. Membrane reactors are not forced to choose between this tradeoff; CMCRs can run at higher temperatures without the increase in trans-fats, allowing them to capture the improved selectivities.

Table 2.2 - Summary of apparent activation energies for the CMCR

	Apparent Activation Energy (kJ/mol)	R^2 of Arrhenius plot
E_a (Overall)	36.4	0.9484
E_{a1} (Ln → L)	46.9	0.9503
E_{a2} (L → O)	43.9	0.9835
E_{a3} (O → S)	28.9	0.9995

Table 2.3 - Apparent activation energy: Membrane systems, and slurry systems

System	H_2 Pressure (bar)	Temperatures (°C)	Ea (kJ/mol)
CMCR	4.0	50-80	36.4
Pd/alumina[28]	51.7	50-110	30.1 – 35.9

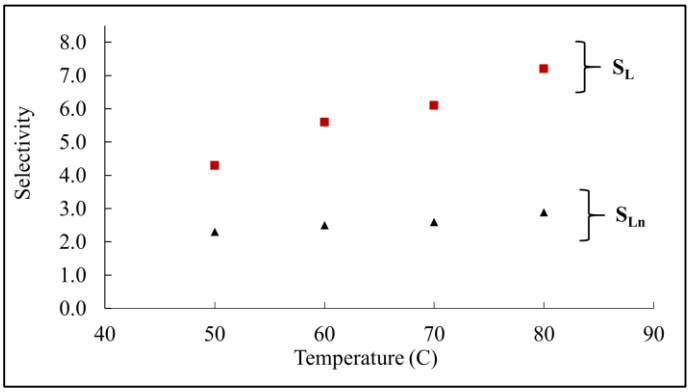

Figure 2.10 - Temperature effects on selectivities for CMCR. As the temperature is increased, both the S_{Ln} (▲) and S_L (■) selectivities increase. Higher selectivities are desired as S_{Ln} represents the selectivity of polyunsaturated fats over monounsaturated fats. And S_L represents the selectivity of monounsaturated fats over saturated fats.

2.3.5 Scale-up

The membrane and module combination were chosen for three reasons, they are: (1) commercially availability, (2) available in the hollow fiber configuration, and (3) several module sizes were available. When accessing the scale-up feasibility of using membrane reactors on a commercial scale, commercial availability is important as this allows for easy and cheap replacement of key components. The hollow fiber configuration is important, as this is the most efficient configuration for membrane packing density[57]. We chose the smallest module available

(one tube, 0.005 m^2 membrane surface area), and have used its performance as a basis for estimation of a pilot CMCR system for the PHSO. Ray[29] reported that 600 mL of oil, at 12 IV/hour, with 0.004% Ni loading, was an acceptably fast reaction rate for the PHSO. Extrapolating our data of 22 mL of oil, at 4.2 IV/hr, with 0.005 m^2 surface area for the CMCR, we would require 0.39 m^2 to equal the slurry's space time yield (assuming reaction rate is constant with scale-up).

When using a CMCR, all of the catalyst is attached to the surface of the membranes, thus, the amount of catalyst that a reactor can contain is limited to the available surface area of the membrane. Whereas, with a slurry reactor, there is no limit to the amount of catalyst that can be used. This can lead to large amounts of required surface area if the reaction rate is slow; the example used above would require 0.39 m^2 of surface area. However, if the temperature can be increased without adversely effecting selectivity, as we demonstrated above, then the reaction rate can be increased while simultaneously lowering the membrane surface area required. Commercially treatment of 5-20 tonnes of oil for an IV reduction of 40 points in 8-10 hours is standard. To accomplish this using current technology would require 1500-7300 m^2. This could be realized in one to a few hollow fiber modules[57].

2.4 Conclusion

It was demonstrated that a Pd-PVP complex could be attached to commercially available membrane for use as a CMCR. The partial hydrogenation of soybean oil was used as model reaction in comparison to three phase batch slurry reactor to investigate mass transfer limitations of the gas phase delivery to the catalyst surface. It was found that at hydrogen pressures as low as 2 bar, CMCRs are able to maintain a high level of hydrogen coverage at the catalyst, with a

reaction order of (-0.1 ± 0.2) with respect to H2 pressure. This allowed our system to produce significantly less trans-fat than a slurry reactor (12 wt% vs. 30 wt% trans-fats at equivalent temperature and extent of reaction). Additionally, trans-fat formation for our CMCRs is essentially temperature independent, contrary to slurry reactors which show a clear correlation between increased temperature and increased trans-fats. Kinetic studies were performed and the Ea for the overall rate of hydrogenation of the system was found to be 36.4 kJ/mol at 4 bar hydrogen pressure; this value is in agreement with a slurry reactor operating at over 50 bar hydrogen pressure.

Chapter 3 - Platinum and Palladium Composite Catalytic Membrane for Three-Phase Hydrogenation

3.1 Introduction

Catalytic membrane contact reactors (CMCRs) have received considerable attention as a possibly alternative to three-phase batch slurry reactors for many hydrogenation reactions[38,39,41]. These traditional reactors possess inherent mass transfer limitations due to low hydrogen solubility in the liquid phase and slow diffusion to the catalyst surface. This causes hydrogen starvation at the catalyst surface, resulting in undesirable side reactions and/or extreme operating pressures[1,2]. CMCRs have the potential to increase hydrogen available at the catalyst at reduced operating pressures and temperatures.

A schematic for CMCRs is shown in Figure 3.1. Hydrogen is supplied to the side of the membrane opposite the catalyst, permeates through the membrane, where it adsorbs directly onto the metal surface. Liquid reactant is circulated over the catalyst, allowing the liquid to come into direct contact with the metal coated surface of the membrane where hydrogenation occurs. With CMCRs, the gas delivery to the catalyst surface is governed by the transport mechanism of the gas through the membrane: solution diffusion, Knudsen diffusion, or convection. By changing the rate of hydrogen delivery to the catalyst surface, CMCRs can change the limiting factor in a reaction from mass transfer limited, to kinetically limited

The early concepts of membrane reactors dates to the 1960s. Gryanov et al.[21,34] wanted to take advantage of hydrogen's ability to diffuse through palladium, and couple palladium membranes to hydrogenation and dehydrogenation reactions. Various liquid phase hydrogenation reactions were proposed;[34,58,59] however, these employed thick non-porous metal membranes, which are both expensive and provide low hydrogen flux. An alternative to a solid,

non-porous metal layer, are composite membranes. Composite membrane can be produced by dispersing a metal catalyst onto a membrane; either into the porous support[60,61], or the nonporous "skin"[42] of the membrane, Figure 3.1. The membranes can be polymeric[44], ceramic[41,62], or a ceramic/polymeric composite[8].

Early work in our lab involved sputter coating polymer membranes with platinum for the partial hydrogenation of soybean oil (PHSO)[42-44]. In the PHSO, low hydrogen solubility into the liquid phase is known to cause hydrogen starvation at the catalyst, leading to the production of trans-fats at high levels (>30wt%)[3]. These sputter coated membranes were able to reduce trans-fats by over 70%, indicating high hydrogen coverage at the catalyst was achieved. In more recent work in our lab, commercially available ceramic/polymeric were rendered catalytically active and used in the PHSO with promising results[8]. However, these latest results were limited to a narrow temperature range due to the operating limits of the membrane, and only reported on one type of catalyst. Here we extend the temperature range and report on results for additional catalysts.

In this study, various membrane/catalyst combinations and configurations are prepare and investigated for the PHSO. All membranes used are tubular ceramic/polymeric composites, with the ceramic providing a porous layer and the polymer being a non-porous layer. Catalyst was deposited in either the porous ceramic or attached to the non-porous skin of the membrane with palladium and platinum being the catalysts studied. We report reaction selectivities, trans-fat formation, and reaction rates of CMCRs. These results are compared to slurry reactors, which are the industrial standard for the PHSO.

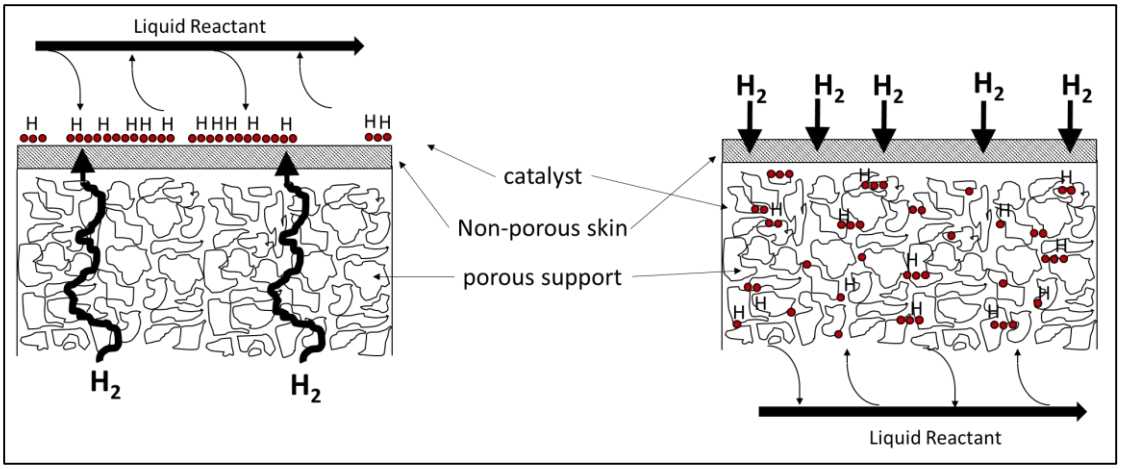

Figure 3.1 - Catalytic membrane contact reactors (CMCRs) in the flow-over configuration, with catalyst attached to the selective skin of the membrane (left), and catalyst embedded in the porous support (right).

3.2 Experimental

3.2.1 Materials

Refined, bleached, and deodorized soybean oil (iodine value, IV = 129-132) was purchased from a local grocery store, Dillon's Food Store Inc. Poly(N-vinyl-2-pryyolidone) (PVP) average M.W. 58,000, K29-32, platinum(II) chloride (99.999% pure), and palladium(II) chloride (99.999% pure), were purchased from ACROS Organics™. Methanol (MeOH) 99.8% (Certified ACS Reagent Grade) was purchased from Fisher Scientific. Hydrogen and nitrogen, ultra high purity (99.999%), were purchased from Linweld Inc. Deionized (DI) water was produced in-lab.

3.2.2 Membranes

Commercial available composite tubular membranes and module (PVM-035) were purchased from Pervatech BV (Netherlands). Two different types of membranes were used in this study, both types are a polymeric/ceramic composite with dimensions of 500 x 10 x 7 mm

(length x O.D. x I.D.). The ceramic portion of the membranes are porous and provide structural support, and the polymer is a thin non-porous layer. One type has a substrate layer of α-Al_2O_3 (outside/shell side), an intermediate layer of γ-Al_2O_3/titania, and a polydimethylsiloxane (PDMS) top layer (inside/bore side), we will refer to these type of membranes as "PDMS"[63]. The 2nd type has a substrate layer of α-Al_2O_3 (outside/shell side), an intermediate layer of γ-Al_2O_3, and a hybrid silica (HybSi®) on top layer (inside/bore side)), we will refer to these type of membranes as "HybSi"[64]. More information on the HybSi® structure, processes, and fabrication can be found elsewhere[65-68].

All membranes used were flux tested using a constant-pressure variable volume apparatus as a means of quality control, a similar device is described elsewhere[45]. All flux measurements were performed at a feed pressure of 4.2 bar gauge, 0 bar gauge permeate pressure, and 25°C. The normalized gas fluxes are determined, and the pure gas selectivities ($\alpha_{i/j}$) were calculated. $\alpha_{i/j}$ is the flux ratio of pure gas *i* relative pure gas *j*. Gas fluxes are reported in gas permeation units (GPU); where one GPU equals $10^{-6}\frac{cm^3_{(STP)}}{cm^2*sec*cmHg}$. A membrane is considered defect-free if the experimental $\alpha_{i/j}$ equals the ratio of the permeabilities for the gas pair through the polymer employed. Any skin defects in the membrane will lower this selectivity. At the test conditions, the ideal selectivities (indicating defect-free behavior) for hydrogen/nitrogen equals 2.23 for PDMS[69] and 20.7 for HybSi[70].

For this study membrane permeance and selectivities for the pure gases hydrogen and nitrogen were tested. The purpose of testing for pure gas selectivity is to probe for structural damage to the selective skin of the membrane. A small amount of skin defects were acceptable; all membranes used were required to have an $\alpha_{i/j}$ greater than Knudsen diffusion selectivity.

3.2.3 Catalyst

Three catalyst solutions were prepared, two different palladium solutions and one platinum solution. One type of palladium catalyst was prepared by dissolving 0.2g of $PdCl_2$ and 0.4g PVP into a 50 mL of MeOH. The second type of palladium catalyst was prepared by dissolving 0.2g of $PdCl_2$ into a 50 mL of MeOH; no PVP was added. The platinum catalyst was prepared by dissolving 0.2g of $PtCl_2$ and 0.4g PVP into 50 mL of DI water. All solutions were sonicated overnight in a water bath.

We found that solutions of the metal salts alone, both $PdCl_2$ and $PtCl_2$, would not adhere to the polymer skin on the tube side of the membranes. Consequently, all catalyst used on the tube side experiments are the PVP-anchored solutions. The tube side depositions was accomplished by plugging one end of the membrane tube and filling it with 9 mL of the catalyst solution. The second end was then plugged, and the membrane was inverted several times. The membranes were drained of the catalyst solution placed in an oven at 60°C and allowed to dry for 30 min. This process was repeated five times.

The shell side of the membranes were able to irreversible adhere the palladium salt without the aid of the PVP. Catalyst was applied to the shell side (support side) of the membrane by assembling the module and 20 mL of catalyst solution was aliquoted into the shell side of the module. The module was inverted and shaken several times, and the solution was drained. The membrane was allowed to air dry and the process was repeated five times.

Through this process, three different type of membrane/catalyst combinations were prepared with catalyst on the tube side, and one type for catalyst on the shell side. These combinations are named after the membrane used (PDMS or HybSi), followed by the catalyst

used. For example, PDMS/Pd-PVP represents a PDMS membrane (described above) impregnated with the Pd-PVP catalyst. This nomenclature will be used throughout this report.

All catalytic membranes were reduced by flowing hydrogen through the appropriate side of the module (shell side or tube side) at 1 mL/sec two hours, at room temperature. Catalyst leaching was tested using inductively coupled plasma (ICP), at a detection limit of 5 mg/L, on the used oil after experiments, neither the palladium or platinum metals were found in the oil phase (ICP results not shown).

3.2.4 Reactors

A schematic of the reactor systems employed is shown in Figure 3.2. Oil is circulated over the catalyst side of the membrane using a positive displacement pump (Q1CSY**,** Fluid Metering Inc.). The recirculation loop was constructed of ¼ inch stainless steel tubing (Swagelok Company), wrapped in a heating tape (BSAT051006, BriskHeat Corporation). Hydrogen was supplied to the side of the membrane that did not contain the catalyst, Figure 3.1. For the tube side experiments, nitrogen was supplied to the tube side at a pressure 1.0 bar greater than the hydrogen pressure; this was done to prevent the membrane skin from becoming damaged. This precaution was not taken with the shell side experiments. Unless otherwise stated, all reactions were performed within two hours of catalyst reduction. Once reduction was completed, oil was loaded into the system and circulated at 1.0 mL/sec; shell side experiments used 99g of oil, tube side experiments used 19.8g of oil. Once the system equilibrated at the desired temperature, the hydrogen pressure was applied; this was recorded as the start of the reaction. 0.09g samples were collected periodically and saved for fatty acid methyl ester analysis. At the end of each experiment, the system was drained of oil and flushed with five volumes of hexane.

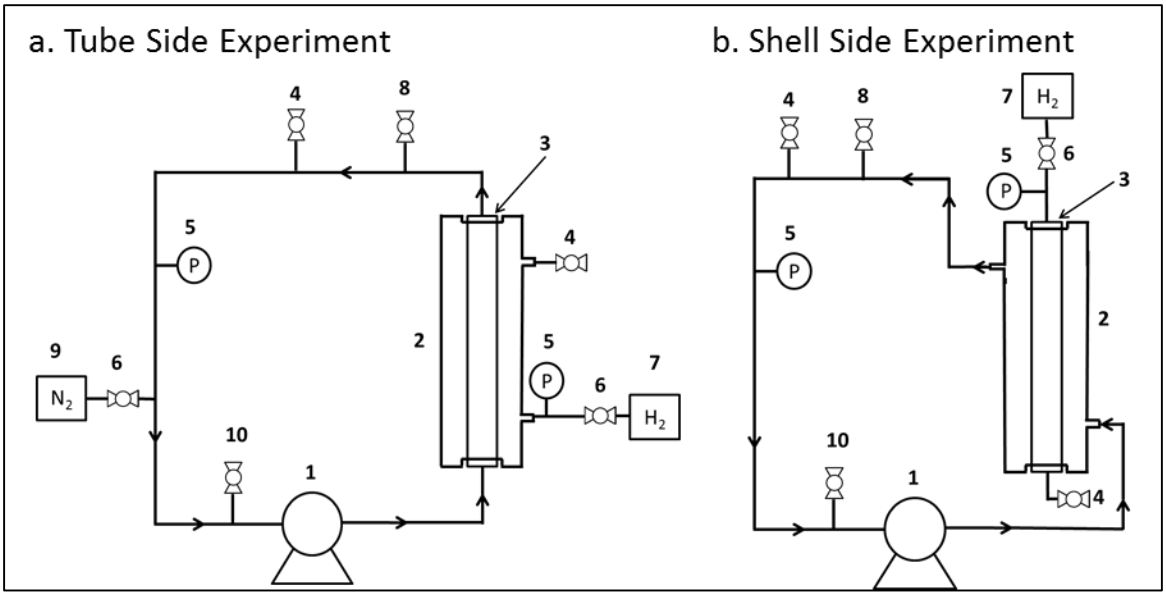

Figure 3.2 - Schematic of the membrane reactor setup for the PHSO experiments: (1) piston pump; (2) membrane module; (3) membrane; (4) purge valve; (5) pressure gauge; (6) check valve; (7) hydrogen source (8) thermal couple; (9) nitrogen supply; (10) sample port.

3.2.5 Sample Analysis

The iodine value (IV) of the samples were determined using AOCS official method cd 1c-85[49]:

$$IV = (C18:1 \times 0.86) + (C18:2 \times 1.72) + (C18:3 \times 2.58) \qquad \text{Equation 3.1}$$

where [Cx:y], x is the number of carbon atoms in the fatty acid and y is the number of double bonds present. Triglycerides were converted to fatty acid methyl esters (FAMEs) using American Oil Chemists' Society (AOCS) official method Ce 2-66[47]. The corresponding FAMEs were analyzed on a gas chromatogram (GC), equipped with a flame ionization detector (FID); Hewlett-Packard 6890 series. The GC method employed was AOCS official method Ce 1h-05[48]. The column used was a 100m CP-Sil 88 (Agilent Technologies), the injector port and detector

were kept at 220 °C with a 100:1 split ratio, the oven was operated isothermally at 180 °C, and the carrier gas was helium at 1.0 mL per min.

3.2.6 Error Analysis

Unless otherwise stated, the error bars shown represent the propagation of error present in each measurement. There were four important sources of error for the measurements reported: IV, wt% trans-fat, mass of oil, and time. The error in IV (±1.2), and wt% trans-fat (0.56%) were determined by performing the transesterification and the subsequent GC analysis 10 times on the same sample of oil. The range from these 10 runs were used as the error. The error in the total mass of oil initially charged to the reactor was taken to be ±0.99 g. This was determined by filling and draining the system 10 times, the range from these 10 points was used. And the error in time used was ±1.0 minute; this was the accuracy of the clocks used. These values were used to propagate the error in the results section. There are two other sources of error, temperature and pressure, ±1°C and ±0.2 bar respectively. However, these values were not used in any calculations and thus not propagated further. Temperature and pressure were independent variables, and errors bars were not added in the x-axis of plots.

3.3 Results and Discussion

3.3.1 Temperature and Selectivities (Tube Side)

Figure 3.3 represents the reaction scheme for the PHSO[3]. Vegetable oils are tri-esters with three fatty acids attached to a glycerol molecule. The fatty acids in soybean oil contain 0, 1, 2, or 3 double bonds. When hydrogenating these double bonds, the goal is to hydrogenate the trienes over the dienes, and dienes over the monoenes; these preferences are expressed as the

linolenate (S_{Ln}) and linoleate (S_L), (equations 3.2 and 3.3). The preference to minimize trans-fat formation is given as the isomerization selectivity (S_i), equation 3.4:

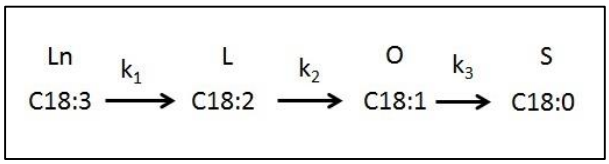

Figure 3.3 – Reaction scheme for the hydrogenation of linolenate (Ln)

$$\mathbf{S_{Ln}} = \frac{k_1}{k_2} \qquad \textbf{Equation 3.2}$$

$$\mathbf{S_L} = \frac{k_2}{k_3} \qquad \textbf{Equation 3.3}$$

$$\mathbf{S_i} = \frac{\Delta IV}{\Delta trans\text{-}fats} \qquad \textbf{Equation 3.4}$$

where ΔIV is the change in iodine value, and Δtrans-fat is the increase in wt% trans-fat. The objective of our CMCR system is to maximize S_i, S_{Ln}, and S_L.

Figure 3.4 shows the S_i as a function of temperature for the three different membrane/catalyst combinations. A previous study in lab our looking at a PDMS/Pd-PVP CMCR showed that trans-fat formation was independent of reaction temperature[8]. While, slurry reactors see a significant increase in trans-fat formation as the temperature is increased and a corresponding reduction in S_i, Figure 3.4[29]. This is because increasing the temperature in a slurry reactor simultaneously increases the hydrogen consumption (increased reaction rate) and decreases the hydrogen solubility in the oil. This leads to hydrogen scarcity at the catalyst surface and increased trans-fat formation[3].

This study was able to extend our results to temperatures up to 140 °C using the HybSi membrane; whereas the previous study was limited to 80 °C. As with the previously

investigated PDMS/Pd-PVP, the two new membrane/catalyst combinations are able to out preform the slurry reactor at all temperatures studied. All membrane/catalyst systems produced trans-fats at rates that were independent of temperature. Figure 3.4 shows HybSi/Pd-PVP essentially has the same S_i at 50 °C as 140 °C; which are both greater than the S_i of the slurry at 23 °C. This would indicate that CMCRs have high levels of hydrogen coverage at the catalyst at all temperatures. For slurry reactors, in general, high pressure and low temperatures are favorable for low trans-fat formation, conversely, CMCR are able to combine high temperature with low pressures and still produce low amounts of trans-fats. Figure 3.4 also shows that the Pt-PVP catalyst produces about half the trans-fat as the Pd-PVP catalysts; this is be expected, as supported platinum is known to produce less trans-fats than supported palladium for the hydrogenation of vegetable oils[3].

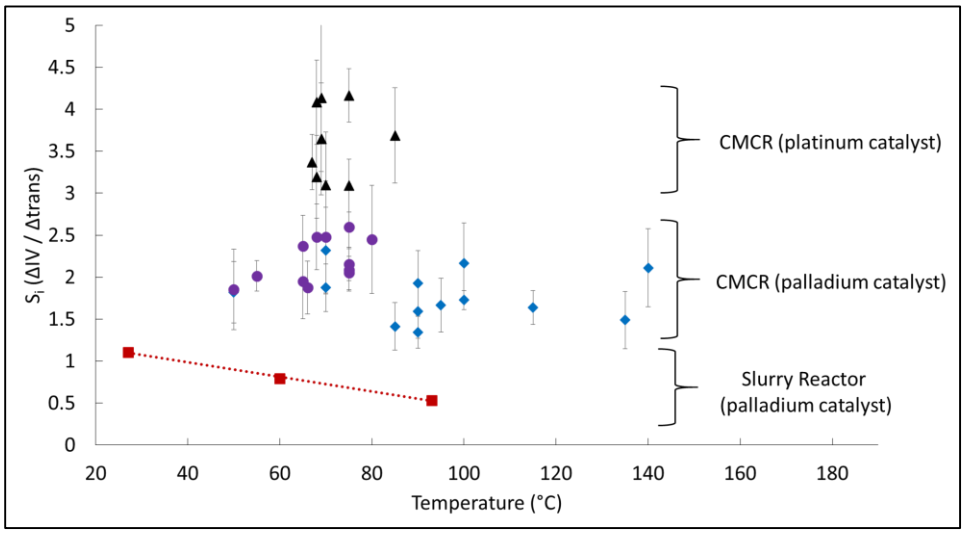

Figure 3.4 - Isomerization selectivity as a function of temperature for tube side experiments. The slurry reactor (■) with a Pd [29] catalyst shows a significant decrease in selectivity as the temperature is increased. The selectivity for all three combinations of CMCR/catalyst are virtually temperature independent. The PDMS/Pt-PVP membrane (▲) showed the highest selectivity, with the HybSi/Pd-PVP (♦) and PDMS/Pd-PVP (●) showing equivalent levels of selectivity. All reactions were between 2-4 bar hydrogen.

Figure 3.5 compares the linolenate and linoleate selectivities of the same catalyst on two different membranes; PDMS/Pd-PVP and HybSi/Pd-PVP. As with the S_i, the S_L and S_{Ln} trends from our previous study held true; S_{Ln} and S_L increase with increasing temperatures. These results are desirable, as higher S_{Ln} and S_L equate to lower amounts of the saturated fat, stearic acid (C18:0), for equal levels of hydrogenation. The results of temperatures effects on selectivity would indicate that CMCRs should be able to run at the highest allowed operating temperature of the membranes to achieve the highest S_{Ln} and S_L selectivities, while producing an oil product with consistently low trans-fat content.

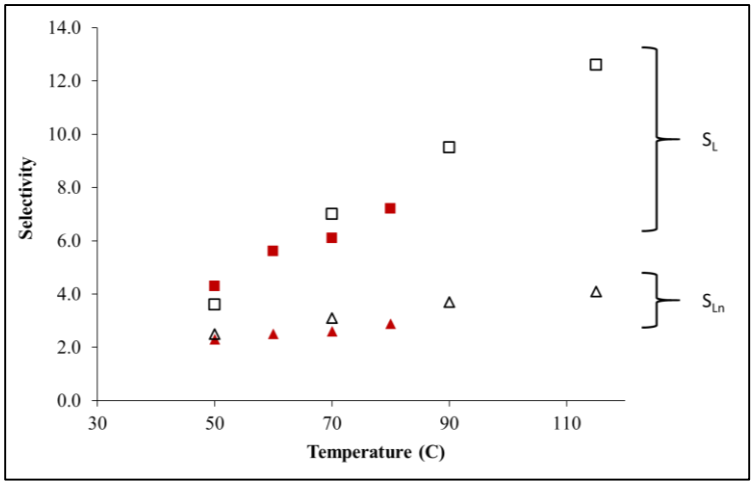

Figure 3.5 - Linolenate (S_{Ln}) and linoleate (S_L) selectivities as a function of temperature. Both the HybSi/(Pd-PVP) S_{Ln} (Δ) and S_L(□) [8], and the PDMS/(Pd-PVP) S_{Ln}(▲) and S_L(■) follow the same trend of increasing selectivity with increasing temperature.

3.3.2 Reaction Rates (Tube Side)

Table 3.1 shows the reaction rate for three different membrane/catalyst combinations. The PDMS/Pt-PVP has a reaction rate of 0.048 (IV/hr/mL oil), this is the average of the points in Figure 3.4 that are between 67-75 °C. The PDMS/(Pd-PVP) has a reaction rate of 0.13 ± 0.01,

this is the average of the points in Figure 3.4 between 63-67 °C. And the HybSi/(Pd-PVP) has a reaction rate of 0.14 ± 0.02, this is the average of the points at 70 °C from Figure 3.4. The Pt-PVP catalyst reaction rate was significantly lower than the two Pd-PVP catalyst. This is be expected, as supported platinum is known to have lower reaction rates than supported palladium for the hydrogenation of vegetable oils[3].

Table 3.1 also shows that both the PDMS and HybSi membranes with Pd-PVP catalyst have the same reaction rate. We concluded in our previous study that our CMRCs are zero order with respect to hydrogen and are operating under kinetically controlled conditions[8]; that is, the reaction rate is controlled by the amount of catalyst deposited and is not limited by hydrogen availability. If we extend this conclusion to the HybSi membrane, then equal reaction rates would indicate that the PDMS and HybSi CMCRs have equal amounts of available catalyst.

Table 3.1 – Reaction rates and operating conditions for three different tube side membrane/catalyst combinations

Membrane/catalyst	reaction rate (IV/hr/ml oil)	error	Pressure range (bar)	Temperature range (°C)
PDMS/(Pt-PVP)	0.048	± 0.014*	2.0 - 4.0	67 - 75
PDMS/(Pd-PVP)	0.125	± 0.013**	3.5 - 6.0	63 - 67
HybSi/(Pd-PVP)	0.142	± 0.011***	3.0 - 4.0	70

*range of the two points used to calculate rate
**standard deviation of the six points used to calculate rate
***standard deviation of the eight points used to calculate rate

3.3.3 Reaction Rates (Shell Side)

We had two factors in mind when we ran experiments with catalyst on the shell side of the membrane. We wanted to take advantage of the fact that the outside of the membrane has a

greater surface area than the inside of the membrane, 75 cm^2 to 50 cm^2 respectively. Additionally, we hypothesized that the catalyst would more readily adhere to the ceramic pores of the membrane than to the non-porous polymer skin. According to these two criteria, the shell side experiments were a success. As noted in the experimental section, neither palladium nor platinum were able to adhere to the polymeric skin layer of the membrane without the aid of the PVP polymer; yet, the palladium is able to deposit onto the shell side of the membrane without the use of the PVP. However, despite the increased surface area, when comparing reaction rates of the same membrane/catalyst combination, the shell side was over an order of magnitude slower than the tube side experiments, (0.0065 vs. 0.142 $\frac{IV}{hr*mL\ oil}$ respectively), Figure 3.6. Additionally, the reported shell side reaction was ran at 90 °C while the three other reported rates were ran between 63-70 °C, further exasperating these differences in rates. We believe that these lower reaction rates are caused by oil in the pores of membrane causing increased mass transfer resistant for the hydrogen to reach the catalyst cites. When the catalyst is attached to the membrane skin, the only barrier for hydrogen transport is hydrogen diffusing through the membrane. If oil is in the membrane pores, hydrogen would have to diffuse through both the membrane and the oil to reach the catalyst surface. Flux data from Table 2.1 would seem to support these hypothesizes.

The flux for this membrane after a reaction was too low to be measured on a constant pressure variably volume system. After the first reaction reported in Figure 3.7, the membrane was sonicated in hexane overnight in an attempt to remove the oil from the pores, however this proved unsuccessful. Although the hydrogen flux was too low to measure, it was not stopped altogether; as Figure 3.7 shows that the CMCR was still able to hydrogenate soybean oil even after it was "clogged". The three runs represent different PHSO experiments using the shell side

membrane, fresh catalyst was not applied in-between runs. The slope of each run was linear, all runs have a R^2 value greater than 0.991, indicating that oil transport from the bulk, to the catalyst inside the membrane pores, and back to the bulk, occurred at constant rate; the membrane was not becoming "more clogged" over time. The change in slope of subsequent runs in is attributed to catalyst deactivation, 39% loss in reaction rate from the first run to the third.

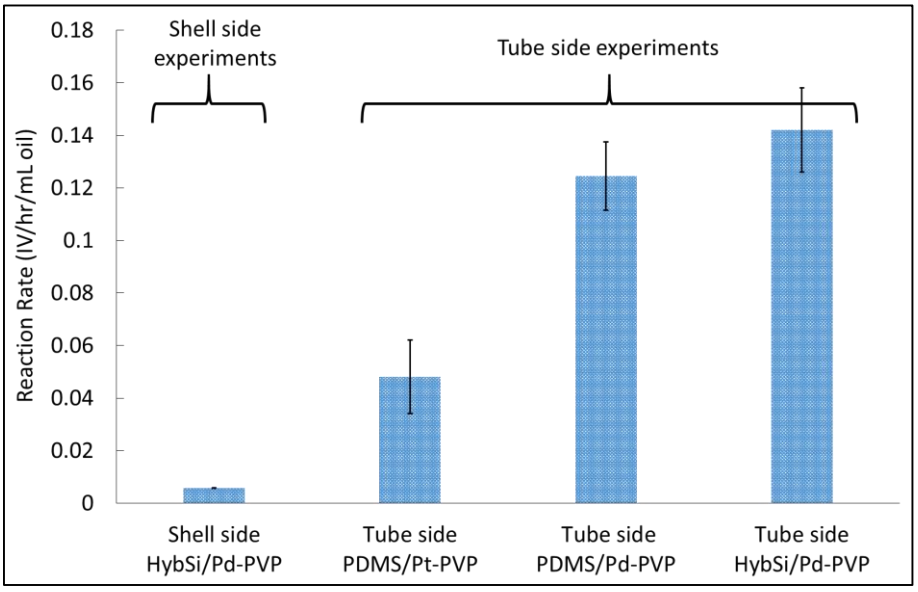

Figure 3.6 - Reaction rates for various membrane/catalyst configurations. The shell side experiment (far left) is considerably slower than the tube side experiment of the same membrane/catalyst combination (far right).

Table 3.2 – Shell side experiments flux data shows membrane clogging

	Flux (GPU)								
	virgin membrane			coated and reduced			after reaction		
	N_2	H_2	$\frac{H_2}{N_2}$ selectivity	N_2	H_2	$\frac{H_2}{N_2}$ selectivity	N_2	H_2	$\frac{H_2}{N_2}$ selectivity
HybSi (Pd, shell side)	45	1062	23	30	390	13	n/a*	n/a*	n/a*
n/a* - flux was too slow to measure using constant pressure flux system									

3.3.4 Catalyst Deactivation

The oil used in this study was typical of soybean oil used in industrial hydrogenation; it was degummed, neutralized, bleached, and deodorized[27]. These oils are known to contain catalyst poisoning material: sulfur and phosphorous organic compounds, oxidation products, soaps, and free fatty acids[71-73]; with sulfur having the greatest impact on deactivation, followed by phosphorus compounds[74]. Sulfur poisoning is known to increase trans-fat isomerization[75], while phosphorus poisoning does not affect the linolenate (S_{Ln}), linoleate (S_L), or isomerization (S_i) selectivities[72,73]. Another possible reason for catalyst deactivation is the formation of coke on the catalyst[76,77].

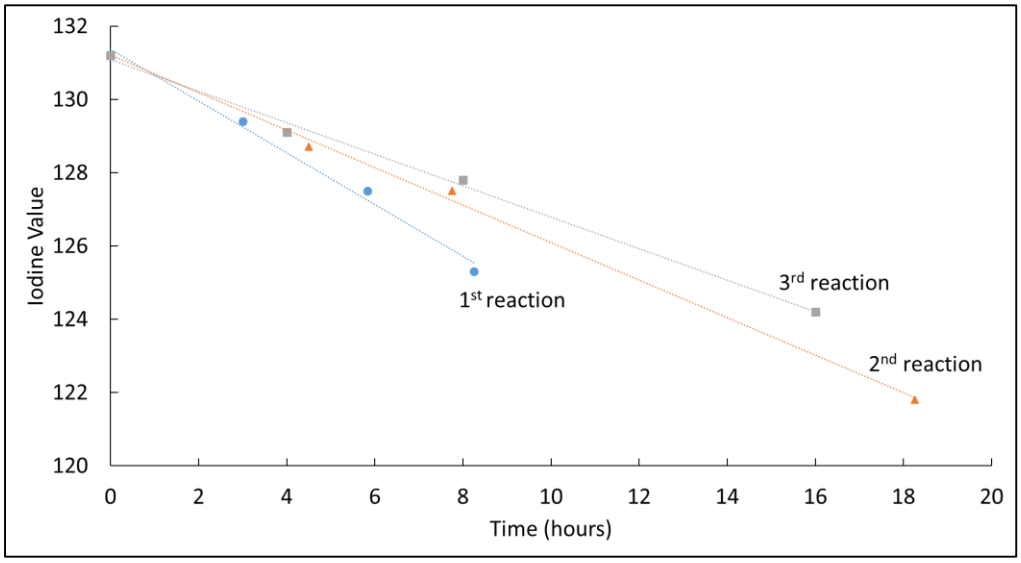

Figure 3.7 - Catalyst Deactivation - Shell side membrane ran three PHSO experiments without applying fresh catalyst in-between runs. All reactions ran at 90 °C and 4 bar hydrogen pressure. 1st reaction (●), 2nd reaction (▲), and 3rd reaction (■) have reaction rates of 0.007, 0.005, and 0.004 IV/hr/mL oil, respectively.

Mäki-Arvela et al.[77] studied linoleic acid to stearic acid using Pd/C supported catalyst to elucidate the catalyst deactivation. They concluded that the deactivation for their experiments were caused by coke forming on the active cites of the catalyst, or coke formation blocking the pores of the catalyst support; citing a lowering of specific surface of reacted catalyst as evidence. They ruled out catalyst poisoning because they used pure, analytical grade linoleic acid. Edvardsson et al.[76] studied coke formation on Pd/α-Al_2O_3 and Pd/γ-Al_2O_3 catalyst for the hydrogenation of sunflower oil methyl esters. Coke formation was continuous with repeated use for the Pd/γ-Al_2O_3, accompanied with a >50% loss in catalytic activity after four repeated uses. Alternatively, Pd/α-Al_2O_3 showed essentially no coke formation and no deactivation.

Table 3.3 summarizes the reaction rate and selectivities for each run in Figure 3.7. We did not see a change in selectivities from run to run. Additionally, the substrate layer of our membrane, which is the layer that catalyst was deposited on, is α-Al_2O_3, which Edvarsson found no coke formation[76]. These would indicate that our catalyst deactivation is from a non-phosphorus poisoning, not coking. Although a more thorough characterization of our spent catalyst would provide greater insight.

Table 3.3 – Reaction rates and selectivities of successive runs

PHSO run	Reaction Rate (IV/hr/mL oil)	S_{Ln}	S_L	S_i
1	0.0065	0.53	1.80	1.90
2	0.005	0.54	1.94	1.93
3	0.004	0.64	1.88	1.88

3.4 Conclusion

In this study we used several CMCR with different membrane/catalyst combinations for the PHSO with high selectivities. We were able to extend the results from the previous study to higher temperature (up to 140 °C), incorporate a new catalyst (platinum), and a new membrane

(HybSi). For tube side experiments, we used three different membrane/catalyst combinations: (1) PDMS/Pd-PVP, (2) HybSi/Pd-PVP, and (3) PDMS/Pt-PVP. We found that the trend of trans-fat formation being independent of reaction temperature held for all three different membrane/catalyst combinations and for the entire temperature range studied. Additionally, we successfully deposited Pd catalyst into the porous support of a composite ceramic/polymeric tubular membranes. Running PHSO oil experiments with the oil on the porous support side of the membrane led to slower reaction rates than running the catalyst and oil on the selective skin side of the membrane. These slower rates are believed to be caused by oil clogged in the pores of the membrane, leading to lower hydrogen transport rates to the catalyst surface. Catalyst deactivation was observed over time for successive runs; with the reaction rate decreasing by 42% from the first run to the third. This deactivation is believed to be from catalyst poisoning.

Chapter 4 - Lactic Acid to Commodity Chemicals using Ruthenium Coated Polymeric Membranes

4.1 Introduction

The conversions of renewable carbohydrates to lactic acid (L.A.) is one of the largest fermentation processes currently employed[78-80]. Lactic acid is used in the food and beverage industry as a preservative, flavouring, and pH adjuster[81-83]. It also sees widespread application in the cosmetic industry[84,85] in a variety of applications: treat wrinkles[86], moisturizer[87], and skin whitening[88]. Because L.A. contains both a hydroxyl and carboxylic acid functional groups, it is highly reactive and offers several novel routes to commodity chemicals[89,90], several possible routes are shown in Figure 4.1. Acetaldehyde[91,92], 1,2 propanediol[93-95], pyruvic acid[96,97], acrylic acid[98-100], 2,3 propanediol[100], propionic acid[101], and ethyl lactate[102-104] can all be derived from lactic acid. Because of this versatility, the US Department of Energy has labelled lactic acid one of its top 30 chemical building block candidates from sugar[105] and a top 15 platform chemicals from a biorefinery carbohydrates[105]. However, several of these reactions suffer from inadequate hydrogen coverage on the catalyst due to extremely low hydrogen solubility in water[106,107], which results in an unselective spread of products[101]. Elevated pressures are often used to achieve sufficient hydrogen concentration in the liquid phase, Table 4.1. The use of membrane contact reactors (MCRs) offers a possibility to simultaneously lower operating pressures and controlling selectivities.

One type of MCR that has received considerable attention in recent years for hydrogenation reactions are metal coated polymeric membranes[36,39,43]. These consist of an asymmetric polymeric membrane, the membrane contains a porous support layer with a non-porous dense polymer “skin”, and metal catalyst is attached to the membrane skin. The

hydrogen gas is supplied to the support side of the membrane, permeates from the support side to the skin side, and is immediately adsorbed onto the catalyst surface. A second reactant, gas or liquid phase, is passed over the skin of the membrane, allowing all reactants and catalyst to come into contact. Because the driving force for gas transport across the membrane is the difference in partially pressure from the feed side to the permeate side, it is possible to control the rate of hydrogen delivery to the catalyst by changing the hydrogen pressure applied to the support side of the membrane. This gives MCRs the potential to control product selectivities[61,108].

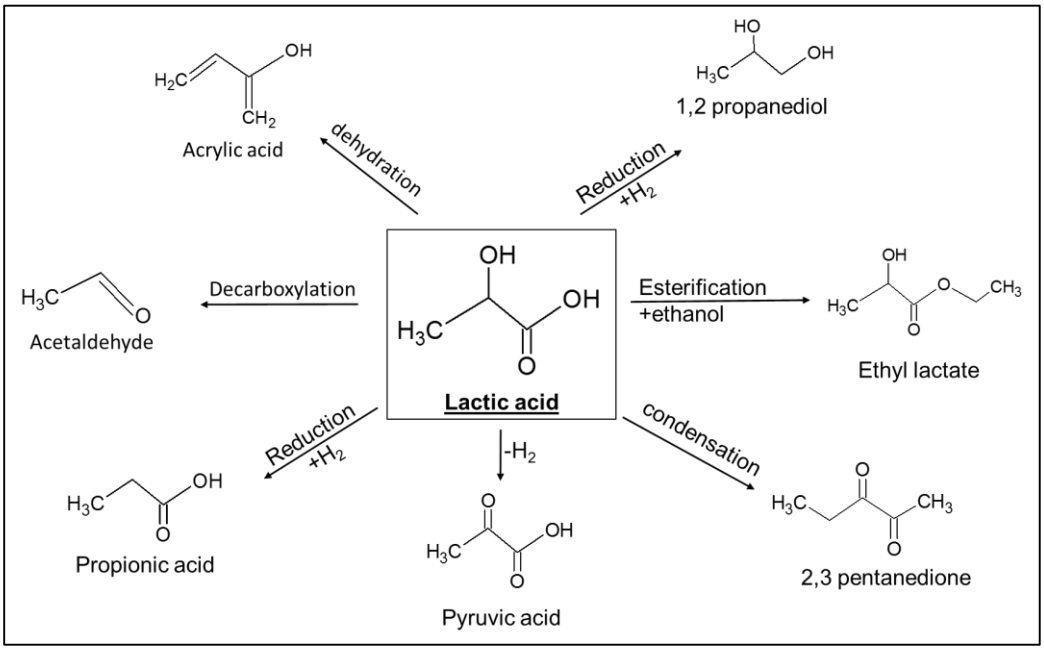

Figure 4.1 – Possible conversion pathways for lactic acid to commodity chemicals

Table 4.1 – Reaction conditions for aqueous phase lactic acid reactions

Product	Temp. (°C)	Press. (bar)	Source
acetaldehyde	300	57	91
Propionic acid	350	57	101
1,2 propanediol	170	140	95
2,3 pentanedione	370	100	100
acrylic acid	385	345 bar	98

Gao et al. used a MCR for the selective hydrogenation of cyclopentadiene[35]. Gao showed that by changing the hydrogen partial pressure, they were able to control the rate at which the double bonds were hydrogenated, and control the rate that cyclopentene was formed vs. cyclopentene. In the case of three-phase reactions, Singh et al. used MCRs for the selective hydrogenation of soybean oil[109]. Low hydrogen solubility in the liquid phase (oil) is known to cause hydrogen starvation at the catalyst; this hydrogen starvation is the known cause for trans-fat production for this reaction. Singh was able to show that CMRs were able to produce a hydrogenated oil with a 70% reduction in trans-fa, demonstrating that membrane reactors maintain high levels of hydrogen coverage at the catalyst surface.

The purpose of this study is to access the potential of MCR for the catalytic conversion of lactic acid. Asymmetric polyetherimide membranes were produced in-house and ruthenium metal was attached through a spin coating process. Experiments were run at temperatures between 130 – 170 °C, and pressures between 0 – 10 bar hydrogen pressure. We report the effects of reaction conditions on selectivity, conversion, and reaction rates.

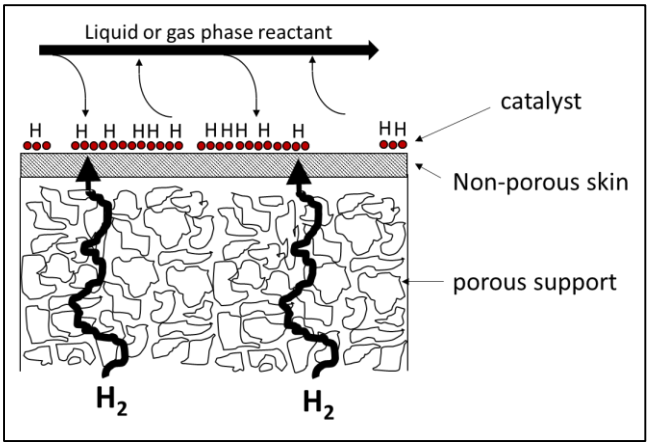

Figure 4.2 – Schematic of a metal coated asymmetric membrane for use as a membrane contact reactor.

4.2 Experimental

4.2.1 Materials

Deionized water was produced on-site. Hydrogen and nitrogen gas (99.999%) were purchased from Linweld Inc. Polyetherimide (UltemTM 1000) was purchased from Saudi Basic Industries Corporation (SABIC), Figure 4.3. Lactic acid was purchased as 85 wt% L.A. in water, and diluted to 2 wt% prior to use. All other chemicals used are listed in Table 4.2.

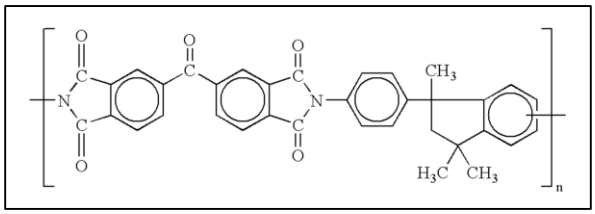

Figure 4.3 – Ultem 1000, polyetherimide

Table 4.2 – Chemicals used

Compound	Source	Purity
1,2 propanediol	Sigma-Aldrich	>99.5%
pyruvic acid	Sigma-Aldrich	0.95
2,3 pentanedione	Sigma-Aldrich	0.97
acrylic acid	Acros Organics	>95.5%
ethyl lactate	Acros Organics	>99.5
acetaldehyde	Acros Organics	>99.5
lactic acid	Acros Organics	0.85
ethanol	Decon Labs	>99.5
methanol	Fisher	>99.5
2-propanol	Fisher	>99.5
1-propanol	Fisher	>99.5
Propionic acid	Fisher	>99.5

4.2.2 Integrally Skinned Asymmetric Membranes

PEI asymmetric membranes were fabricated through a phase inversion method developed by Peinemann [110]. Dichloromethane (54.6 wt%), 1,1,2,2 tetrachloroethane (4.8 wt%), p-xylene (17.8 wt%), acetic acid (6.9wt%), and PEI (15.9wt%) were combine in a glass jar and allowed to stir for 48 hours at room temperature. After all of the polymer was dissolved, the resulting solution was cast on a glass plate using a Gardner casting knife at a thickness of 400 μm. Immediately following casting, the membranes were placed in an acetone bath. After 30 min, the membrane sheets were remove from the acetone bath and hang dried overnight. After hang drying, the membranes were placed in a vacuum over at 80 °C for a minimum of 24 hours. 4.2 cm diameter membrane stamps were cut out of the sheets and flux tested for defects. All membranes used had an overall thickness (support + skin) between 202-259 μm.

Membranes were flux tested using a constant-volume variable-pressure apparatus as a means of quality control, a similar device is described elsewhere[111]. All flux measurements were

performed at a feed pressure of 4.2 bar gauge and 35°C. The normalized gas fluxes are determined, and the pure gas selectivities ($\alpha_{i/j}$) were calculated. $\alpha_{i/j}$ is the ratio of normalized flux of pure gas i over pure gas j. Gas fluxes are reported in gas permeation units (GPU); where one GPU equals $10^{-6}\frac{cm^3_{(STP)}}{cm^2*sec*cmHg}$. A membrane is considered defect free if it has an $\alpha_{i/j}$ equal to the ratio of the permeance of gas i and gas j for material, ($\alpha_{i/j}$ = 117-129 for Ultem 1000)[112,113]. The membranes were tested pre and post catalyst deposition Table 4.3. The membranes used had an effective skin thickness between 140 – 460 nm; effective thickness is back calculated by dividing the measured permeance by the known nitrogen permeability[112,113]. These data include membranes that have a selectivity higher than 80 from Table 4.3, as selectivities lower than this will have significant defects and return an imprecise skin thickness that is too thin.

Table 4.3 – Membrane flux and selectivities

Reaction conditions		Virgin membranes			Coated and reduced		
Pressure	Temp (°C)	H_2 flux (GPU)	N_2 flux (GPU)	selectivity	H_2 flux (GPU)	N_2 flux (GPU)	selectivity
1	130	31	0.32	97	n/a	n/a	n/a
3	130	29	0.35	82	16	0.85	19
6.5	130	53	0.38	140	n/a	n/a	n/a
7	130	53	0.32	165	435	126.00	3
1	150	26	0.16	161	18	0.26	69
6.5	150	31	0.19	165	n/a	n/a	n/a
7	150	34	0.97	35	10	2.30	4
10	150	45	0.30	150	32	1.61	20
1	170	21	0.11	191	13	0.45	29
3	170	30	0.20	150	24	0.45	54
7	170	43	1.74	25	17	0.65	25

4.2.3 Catalyst

Catalyst solution was prepared by combining 0.6 g of $RuCl_3$ and 50 mL of ethanol into a centrifuge tube and sonicating overnight. Membranes were coated through a spin coating process. Virgin membranes were placed on the chuck of a spin coater with the support side down and the skin side facing up. Approximately 1.5 mL of catalyst solution was pipetted onto the membrane, with the spinning process beginning within 5 second of the pipetting. The spin coater was run at 2500 RPM for 30 seconds, with an acceleration of 250 RPM/sec. After 30 seconds, the spin coater was stopped, and the process was repeated a total of 15 times. The coated membrane was allowed to dry at room temperature overnight. After drying, the catalytic membranes were reduced at 120 °C in a hydrogen atmosphere. Figure 4.4 shows that the virgin membranes are white, followed by the $RuCl_3$ coating as a brownish color, and the reduced membrane is shown as a shiny metallic color.

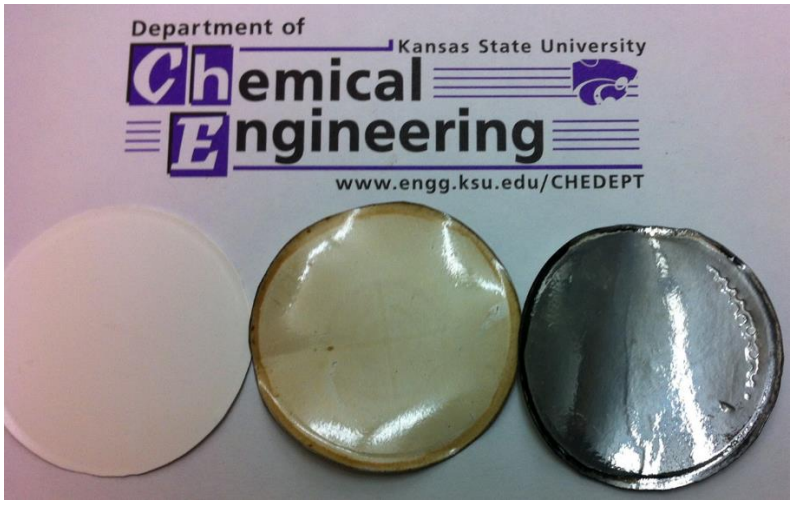

Figure 4.4 – PEI membranes that are: (left) virgin, (middle) coated with $RuCl_3$, and (right) coated and reduced.

4.2.4 Reactor

The reaction systems (Figure 4.5) consists of a loop of ¼ inch stainless steel tubing (Swagelok®). Liquid was circulated using a gear pump (Micropump®), through a stainless steel membrane cell (Millipore XX4404700). The feed side was over pressurized with nitrogen to avoid damaging the skin layer of the membrane. Hydrogen was used as a sweep gas on the permeate side of the membrane at a flow rate of 1.0 mL/min. The sweep gas was collected using two cold traps in series; the first trap was cooled using ice water, the 2nd trap was cooled using liquid nitrogen. Both the feed and permeate lines were wrapped in heating tapes. The permeate side was heated to ensure that liquid did not condense before reaching the cold traps.

All reactions were started within two hours of catalyst reduction. The system was loaded with 60 mL of 2 wt% lactic acid in water. The system was purged and then pressurized with nitrogen to a pressure of 1 bar higher than the anticipated hydrogen pressure. After the nitrogen, the system is pressurized with hydrogen; it was pressurized in this order to ensure that the membrane skin stays intact. The heat is then turned on, and this marks the start of the reaction (time = 0). Samples from both the feed and permeate were collected periodically. All experiments reported have >92% mass recovery.

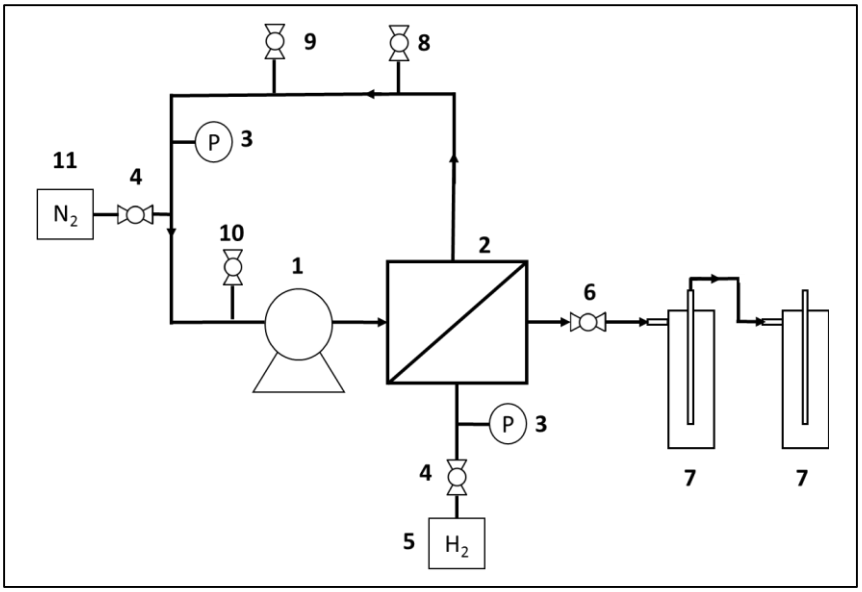

Figure 4.5 – Reaction system: (1) gear pump, (2) membrane cell, (3) pressure gauge, (4) check valve, (5) hydrogen supply, (6) metering valve, (7) cold trap, (8) thermos couple, (9) purge valve, (10) sampling port, (11) nitrogen supply.

4.2.5 Product Analysis

Samples were analyzed using a high pressure liquid chromatograph (HPLC), Shimadzu LC-10A, with an Aminex HPX-87H column. Injection volumes were 10 μL, the flow rate was 0.6 mL/min, the column was maintained at 55°C, and the mobile phase was 5mM H_2SO_4 in water. All compounds were calibrated with a 6-point calibration curve with concentration ranging from 5 - 20,000 ppm. All calibrations were fit to a linear regression with an $R^2 >$ 0.9900.

4.3 Results and Discussion

4.3.1 Reaction Rates

Three different controls were run to compare with the MCRs. One control was a slurry reactor operated at 170 °C, 10 bar hydrogen pressure, and the catalyst was three spin coated

membranes. The membranes were treated the same as the membranes used in the MCR experiments, three membranes were used to ensure that the control had an equal or greater amount of catalyst as the MCRs. A second control was a MCR experiment in which the hydrogen and nitrogen lines were switch. The purpose of the second control is to run an experiment in which the hydrogen delivery mechanics are the same as a slurry reactor, but the flow patterns are the same as the MCR experiments. The third control was run in the same set-up as the MCR experiments; however, there was no hydrogen applied to the system. As Figure 4.6 shows, all of the MCR experiments ran at a fast reaction rate than all of the controls. If hydrogen availability at the catalyst is a limiting factor in the reaction rate, then these results would indicate that MCRs have higher levels of hydrogen coverage at the catalyst cites.

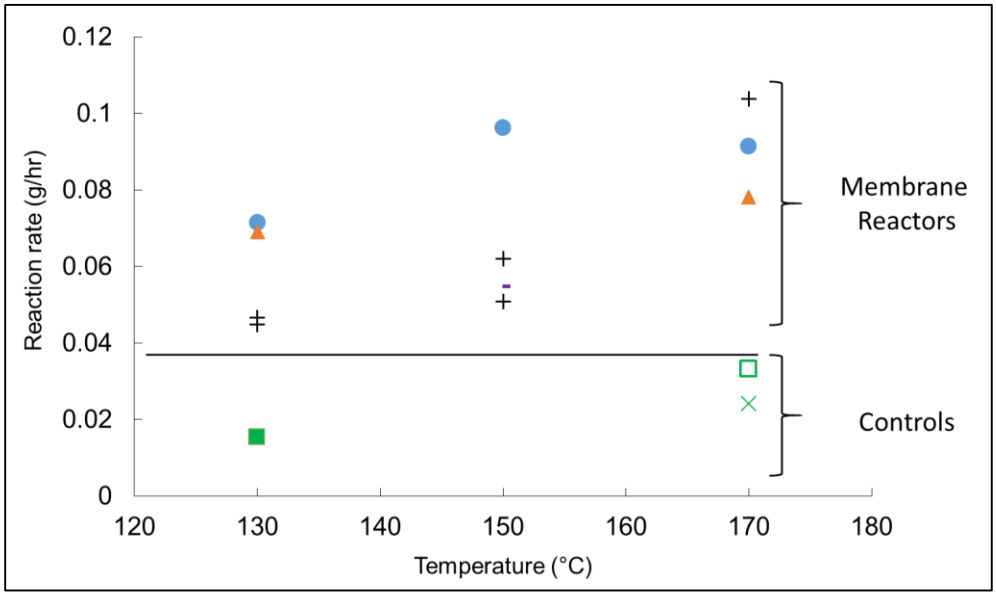

Figure 4.6 – Membrane reactors outperform controls for every combination of temperature and pressure. Controls: membrane reactor with no hydrogen pressure (■), parr reactor with three catalytic membranes (X, 10 bar), membrane reactor with hydrogen on the feed side (□, 10 bar). Membrane reactors: 1 bar (●), 3 bar (▲), 7 bar (+), and 10 bar (-).

Figure 4.7 shows the lactic acid conversion as a function of pressure for the three temperatures used, 130 °C, 150 °C, and 170 °C. There were no discernible patterns between hydrogen pressure and reaction rate. This may be due to our catalyst deposition method; we do not believe that we were depositing equal amounts of catalyst consistently. As Table 4.3 and Figure 4.8 show, the spin coating process dramatically alters the transport characteristics of the membrane; the decrease in selectivities would indicated that defects are being introduced into the membrane skin. Alcohols are known to swell membranes[114], and we noticed physical deformations in the membrane turning the coating process; they curly inwards, or become wavy, Figure 4.4. If the membranes are not perfectly flat, then we should expect variations in the spin coating process. Surface roughness is another parameter that effects spin coating depositions; although atomic force microscope (AFM) measurements were not perform, we could assume that the surface roughness varied from membrane to membrane. In future studies it would be advisable to develop a sputter coating technique for catalyst deposition. This would provide consistent catalyst deposition from sample to sample, while maintaining the integrity of the membrane skin[109].

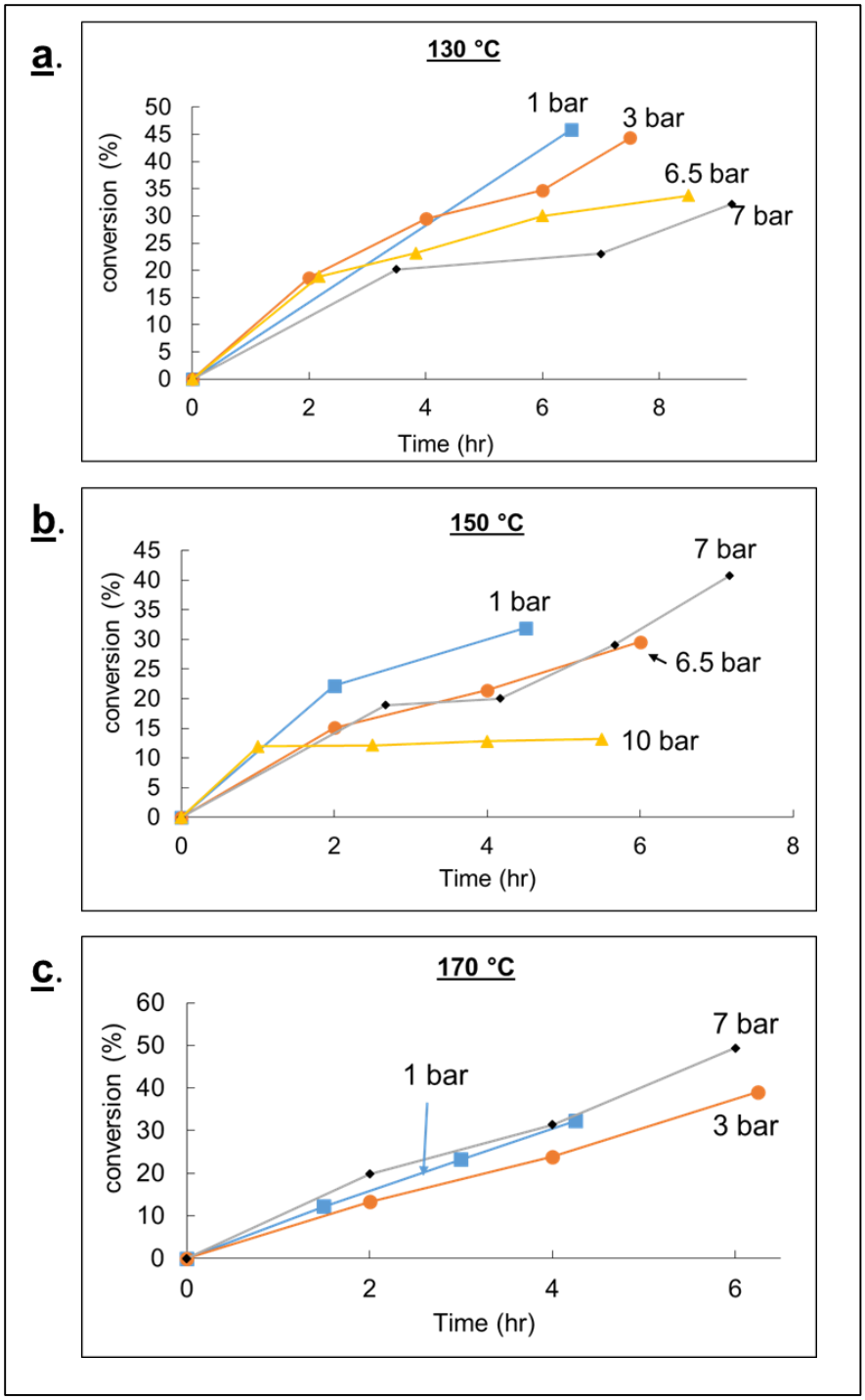

Figure 4.7 – Effects of pressure on lactic acid conversion in MCRs for: (a.) 130 °C, (b.) 150 °C, and (c.) 170 °C. Lines are added for visual aid, they do not suggest a mathematical relation.

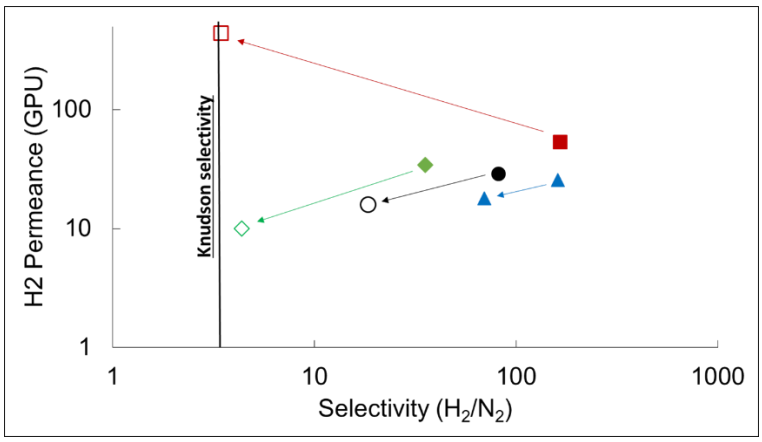

Figure 4.8 – Effects of spin coating and reducing catalyst on PEI membranes. Solid marks are the virgin membrane, and hollow marks are the coated and reduced. Membranes typically see a decrease in hydrogen flux and selectivity; except in the case that the of Knudsen selectivity, where in increase in flux was observed.

4.3.2 Selectivities

Figure 4.9 shows the final product composition (lactic acid was not included) of all the reported reactions. All unidentified peaks, and unaccounted for mass were combined into, "other". Although each combination of temperature and pressure produces different compositions over time, Figure 4.10 – 4.12, as in the case of conversion rates, patterns in the selectivity are hard to identify. As mentioned above, the spin coating process does not deposit catalyst consistently from membrane to membrane, and variation in catalyst amount is known to effect product selectively in ruthenium catalysed lactic acid[95]. However, with that being said, there are still some trends of note.

All of the reactions at 130 °C show large amounts of "other" being formed. These missing masses could be in the form of gaseous products. Zhang et al.[95] studied lactic acid conversion over Ru/C catalyst, and found that at temperatures < 170 °C, the major products were

methane, ethane, and propane. However, we did not test the gas phase, further sample analysis is require to test this hypothesis.

Another results that stands out is the fact that the control with no hydrogen pressure reacted. The major products were acetaldehyde (36%), methanol, (36%), ethyl lactate (15%), and other (5%). Halpern et al. studied the reaction pathways for fumaric acid and maleic acid (both are acids with a hydroxyl and carboxyl group) with a ruthenium catalyst, using deuterium tracer labeling. They found that hydrogenation of the acids occurred with D_2 in H_2O, and yielded undeuterated products[115]. Conversely, hydrogenation with H_2 in D_2O yielded deuterated products. They concluded that hydrogen atoms participating in the reactions originated from the water, and not the gas phase. This could explain why our control with no hydrogen still reacts and forms produces. Another possible explanation is the fact that lactic acid is known to undergo self-esterification in the absence of catalyst and hydrogen[116]. It is probably a combination of both of these properties.

Also, ethyl lactate and pyruvic acid were produced in every reaction. The ethyl lactate could be explained due the self-esterification explained above. All of the literature on lactic acid to pyruvic acid are vapor-phase experiments or enzyme catalysed. The vapor experiments available note that direct oxidation of L.A. to pyruvate produces low yields as this reaction competes with acetaldehyde and CO_2 formation[78,117]; which is what we see in the control. All of the controls see large amounts of acetaldehyde; however, the MCRs do not see large selectivity towards acetaldehyde, indicating some kind of fundamental difference in reaction mechanism between MCRs and slurry reactors.

As Figure 4.10 – 4.12 show, the conversion of lactic acid is a complicated process. There are several parallel reactions occurs, as well as multiple reactions happening in series. Again, it is hard to distinguish trends from these figures.

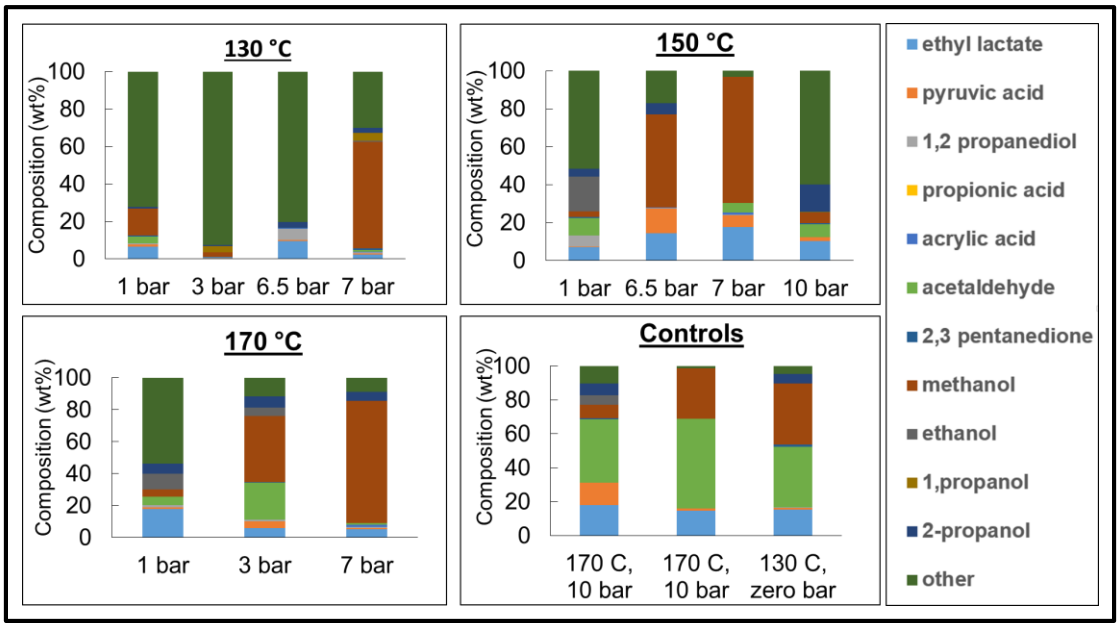

Figure 4.9 – Final product compositions: (top left) 130 °C, (top right) 150 °C, (bottom right) 170 °C, and (bottom right) control reactions.

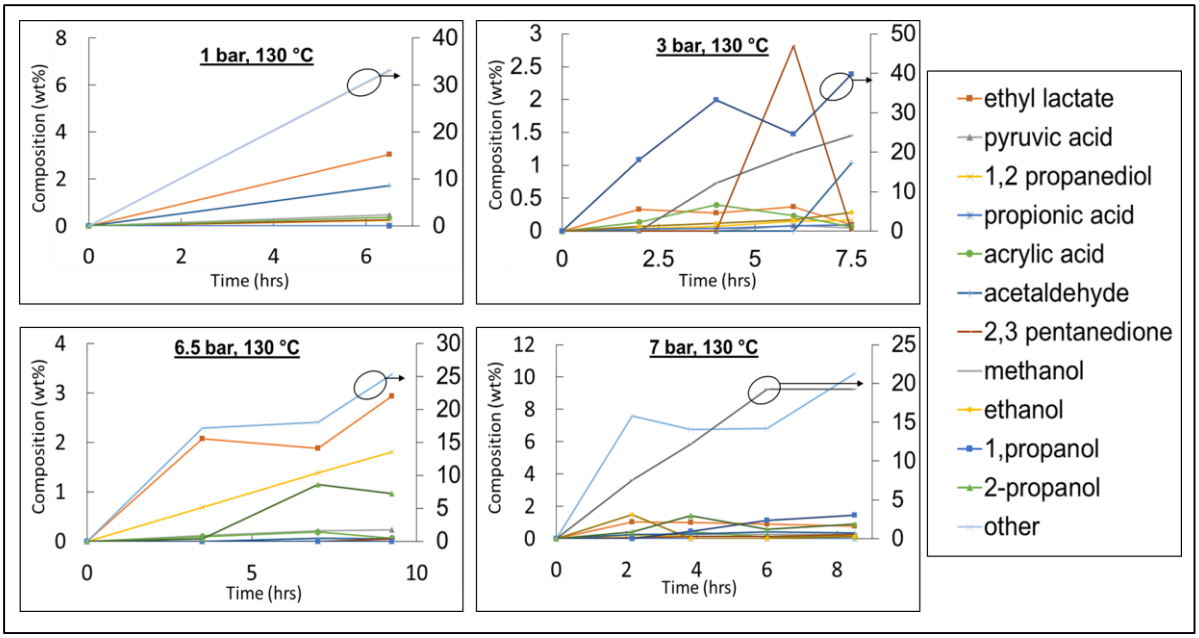

Figure 4.10 – Composition over time for membrane reactors at 130 °C and different hydrogen pressures. Indicated products use the right vertical axis. Lactic acid was included in calculate, but data points were left out. Lines are for visual aid, they do not imply a mathematical relationship.

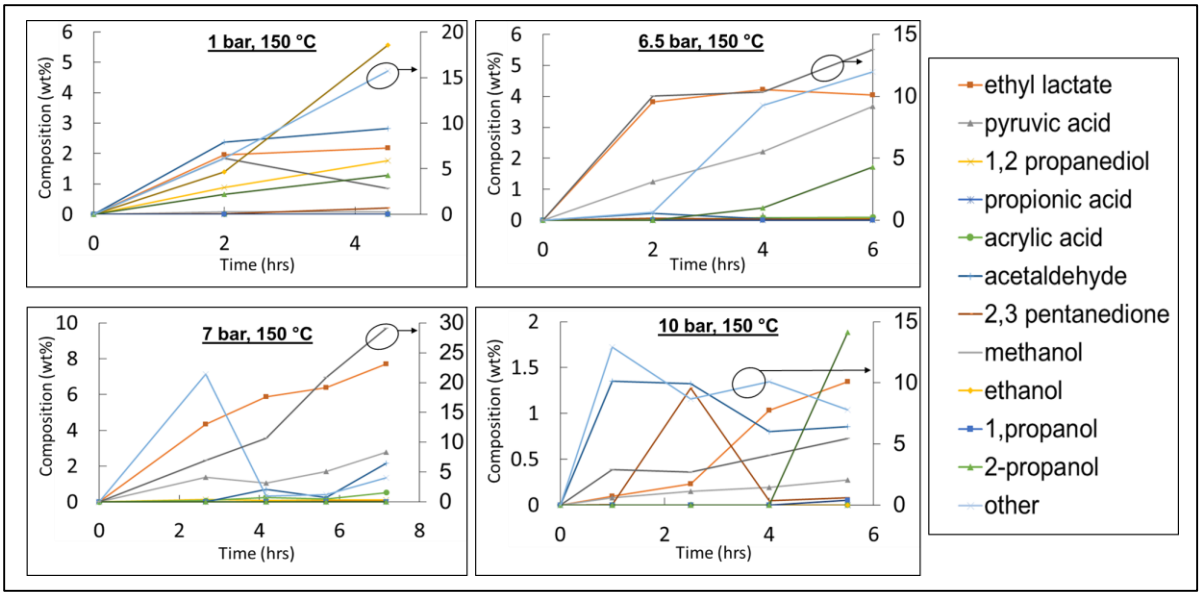

Figure 4.11 - Composition over time for membrane reactors at 150 °C and different hydrogen pressures. Indicated products use the right vertical axis. Lactic acid was included in calculate, but data points were left out. Lines are for visual aid, they do not imply a mathematical relationship.

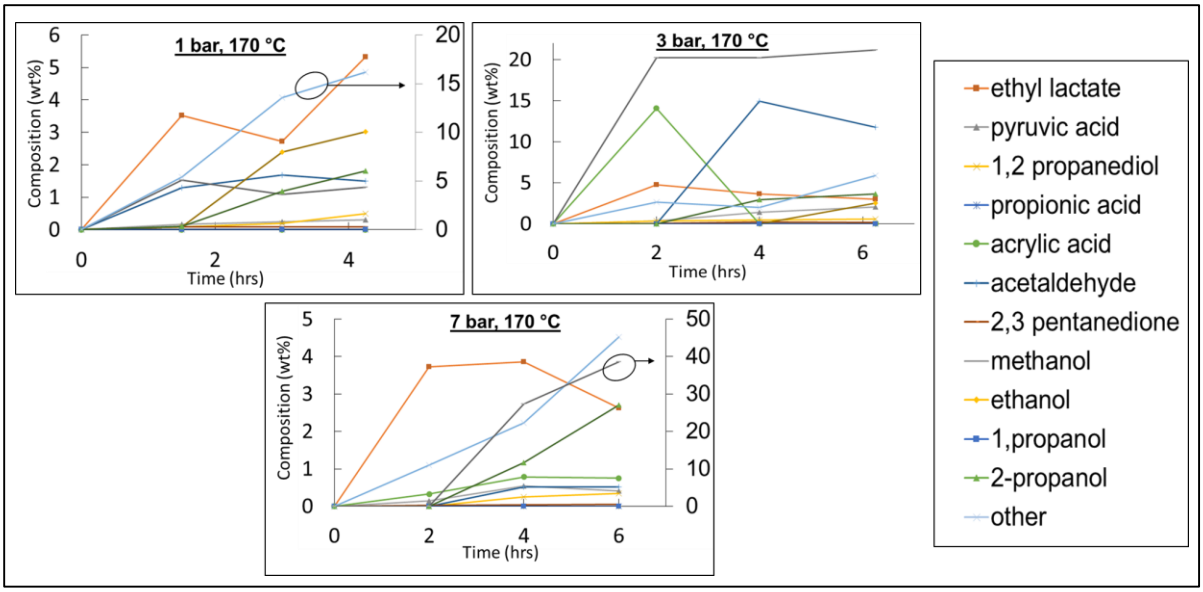

Figure 4.12 - Composition over time for membrane reactors at 170 °C and different hydrogen pressures. Indicated products use the right vertical axis. Lactic acid was included in calculate, but data points were left out. Lines are for visual aid, they do not imply a mathematical relationship.

4.4 Conclusions

The catalytic conversion of lactic acid into valuable commodity chemicals was demonstrated using a membrane contact reactor. By using the MCR, it was expect to overcome gas-liquid mass transfer resistances, thus increasing hydrogen coverage at the catalyst cites. It was further expected that a change in hydrogen pressure would change the hydrogen availability at the catalyst and allow for the manipulation of product selectivity. The results are currently ambiguous. MCRs were shown to have higher reaction rates, indicating higher hydrogen availability. And it was clearly demonstrated that changing pressure while holding the temperature constant, does indeed change product selectivity; however due the large amounts of unknown products, no clear patterns can be interpreted. More sample analysis to identify the unknown products could help elucidate the selectivity trends that the MCRs provide. Additionally, a more consistent metal deposition, such as sputter coating, would ensure repeatability in selectivity and conversions.

Chapter 5 - Liquid-Liquid Equilibria for Ternary Systems of Water + Cyclopentyl Methyl Ether (CPME) + Alcohol; Methanol, Ethanol, 1-Propanol, or 2-Propanol

5.1 Introduction

Oleaginous microalgae[118-120] and yeast[121-123] are two types of non-crop based renewable oils that have received considerable attention in recent years. These renewable oil sources have been considered in a wide range of commercial applications from nutritional supplements[124,125], to biodiesel[119,124,126], to feed stock for fine chemicals[127,128]. However, there is no consensus on large scale lipid extraction of either oleaginous yeast or microalgae[129,130]. The methods of Bligh and Dyer[131], and Folch[132], are generally accepted as the standard procedures to extract lipids from wet materials;[133,134] however, these are only performed on laboratory scale and use large volumes of chloroform. Chloroform's toxicity[135] may prevent its industrial scale use. With this in mind, cyclopentyl methyl ether (CPME) has been proposed as a green solvent alternative for the liquid-based lipid extraction[129].

In addition to oil extraction, CPME has been discussed as a possible green solvent to replace tetrahydrofuran, (THF), diethyl ether, methyl tert-butyl ether (MTBE), 1,4-dioxane, and other commonly used ether solvents in chemical synthesis and various extractions[5,136,137]. The advantageous properties of CPME include: (1) resistance to peroxide formation, (2) low vaporization energy, (3) high hydrophobicity, (4) stable under acidic and basic conditions, (5) high boiling point, and (6) low solubility of salts[5,6]. To facilitate these operations, a more complete understanding of how CPME fundamentally interacts with various components is of importance. A plethora of liquid-liquid equilibria (LLE) data of ternary systems exists for the

above mentioned ethers (MTBE,[138-140] 1,4-dioxane,[141,142] THF,[140,143] etc.); however, LLE data for CPME ternary systems is lacking[144,145].

The purpose of this study is to measure LLE data for the four ternary systems of water + CPME + alcohol, with the alcohols being methanol, ethanol, 1-propanol, and 2-propanol. The binodal points were determined using the cloud point method[146,147] and tie-line data were determined from gas chromatography (GC). Measurements were carried out at 298.15K and atmospheric pressure. The tie-line data were verified using the Othmer-Tobias[148] and Hand[149] correlations. Additionally, distribution coefficients and separation factors were calculated. The LLE data determined in this study were compared to LLE data for the water + methanol + chloroform system as a possible green alternative for the Bligh and Dyer[131] extraction method.

5.2 Experimental

5.2.1 Chemicals

HPLC grade water (CAS Registry No. 7732-18-5), methanol (CAS Registry No. 67-56-1), 1-propanol (CAS Registry 71-23-8), and 2-propanol (CAS Registry No. 67-63-0) were purchased from Fisher Scientific. Ethanol (CAS Registry No. 64-17-5) was purchased from Decon Labs Inc. CPME was purchased from Sigma-Aldrich (CAS Registry No. 5614-37-9). All reagents used had a mass fraction purity >0.999, Table 5.1.

Table 5.1 - Suppliers and Purity of Chemicals

Chemical Name	Source	Initial Mass Fraction Purity[a]	Purification Method	Final Mass Fraction Purity	Analysis Method
Water	Fisher	> 0.999	none	> 0.999	GC[b]
Methanol	Fisher	> 0.999	none	> 0.999	GC[b]
Ethanol	Decon Labs	> 0.995	none	> 0.999	GC[b]
1-Propanol	Fisher	> 0.999	none	> 0.999	GC[b]
2-Propanol	Fisher	> 0.999	none	> 0.999	GC[b]
CPME	Sigma-Aldrich	> 0.999	none	> 0.999	GC[b]

[a]Manufacturer listing [b]Gas chromatography

5.2.2 Procedure

The experimental setup for the binodal curve data includes a 50 mL water jacketed cell, magnetic stir plate, recirculating water bath, a glass burette, and a thermocouple. Data for the bimodal curve were constructed using both the cloud point method[146,147], and by determining tie-lines. Twelve cloud point measurements were performed for each ternary system; six points were determined for the water-rich sides of the bimodal curves, and six points for the CPME rich sides. Initially samples were prepared that contained 100/0, 90/10, 80/20, 70/30, 60/40, and 50/50 (wt%/wt%) water/alcohol. These samples were prepared by weighing the appropriate components into a 40 mL sample vial containing a magnetic stir bar, using an A&D® GR-120 analytical balance ±0.0001 g. The vial was then placed in a 50 mL jacketed cell. Water was circulated at a temperature of 298.15 K using a Lauda-Brinkmann RC 6 water bath ± 0.05 K. The jacked cell was placed on a magnetic stir plate, and the temperature was monitored using a thermal couple probe, Omega® KTSS-HH, connected to a thermal couple, Amprobe TMD-50 ± 0.1 K. CPME was titrated into the water-alcohol mixture using a burette with an accuracy of 0.05 mL. The endpoint was determined when the mixture went from homogeneous, to cloudy, to

a heterogeneous mixture. The data points for the solvent-rich side of the curves were determined in much the same way. CPME and alcohol were weighed out in the 100/0, 90/10, 80/20, 70/30, 60/40, and 50/50 (wt%/wt%) mixtures, and water was titrated in until heterogeneity was reach. The error for the cloud point measurements were determined using error propagation. The error in the components that were weight are ± 0.0001 g and the error in the titrated components are ±0.05 mL, this volume is converted to mass according to each components density. The reported error for the cloud point mass fraction data is reported as ± 0.003. Each data point actually has a different error, as each data point propagated error to a different amount; however only one value for error is reported per table. We picked the data point with the greatest error and reported that error for the entire table. The data generated from these cloud point measurements gave a rough guide for the binodal, and were used as a guide to prepare the tie-line samples.

The tie-line samples were prepared using the same experimental setup described above. Various water-alcohol-CPME mixtures were prepared at compositions within the two phase region of the ternary plots. The samples were prepared by weighing the components into a 40 mL glass vial with a magnetic stir bar, total weight was approximately 30 g for each sample. The vial was placed in the jacketed cell and vigorously stirred for a minimum of 2 hours. After agitation, the heterogeneous mixture was left to settle for at least 2 hours to reach equilibrium. Approximately 300 μL of each phase was removed and analyzed using a gas chromatograph (GC) equipped with a thermal conductivity detector (TCD); Hewlett-Packard 6890 series. The error for the tie-lines are from error in the GC. For each GC calibration curves, we injected six different samples of known concentrations, and back calculated the concentration using the calibration curve. All GC calibration curves were accurate to >0.005 mass fractions for every point checked.

The GC employed an auto-sampler with 1 μL injection volumes. Two capillary columns were connected in series using a press fit connector (Agilent 5190-6979); the first column was a DB-Wax (Agilent 125-7032) followed by a DB-5 (Agilent 122-5032), column flow was constant at 1.2 mL/min, with helium as a carrier gas. The injector port was maintained at 170 °C and operated in split mode with a 150:1 split ratio. The temperature program starts at 50 °C and holds for 1 minute, followed by a 20 °C per minute ramp to 200 °C, total run time is 8.5 minutes. The detector was a TCD operated at 150 °C with helium as the reference gas.

5.3 Results and Discussion

5.3.1 Experimental LLE Data

Table 5.2 lists the experimental cloud point data of the ternary systems water (1) + alcohol (2) + CPME (3). The alcohols are methanol, ethanol, 1-propanol, and 2-propanol. The data was determined at 298.15 K and atmospheric pressure. The compositions are listed as mass fractions. Figure 5.1 and Figure 5.2 show the combine cloud point and tie-line data.

Table 5.2 - Experimental LLE Mass Fraction Obtained using the Cloud Point Method for the Ternary Systems Water (1) + Alcohol (2) + CPME (3) at Temperature T = 298.15 K and Pressure p = 0.1 MPa[a]

	organic phase			aqueous phase		
alcohol	w_1	w_2	w_3	w_1	w_2	w_3
methanol	0.0066	0.0000	0.9934	0.9869	0.0000	0.0131
	0.0443	0.1027	0.8530	0.8823	0.0984	0.0193
	0.0950	0.1867	0.7183	0.7696	0.1986	0.0318
	0.1459	0.2622	0.5919	0.6742	0.2851	0.0407
	0.2155	0.3204	0.4641	0.5493	0.3669	0.0839
	0.2744	0.3734	0.3522	0.4079	0.4085	0.1836
ethanol	0.0066	0.0000	0.9934	0.9943	0.0000	0.0057
	0.0317	0.1067	0.8616	0.8776	0.1001	0.0223
	0.0795	0.186	0.7345	0.7736	0.1935	0.0329
	0.1545	0.2557	0.5898	0.6531	0.2790	0.068
	0.2220	0.3110	0.4670	0.5083	0.3383	0.1533
	0.3278	0.3360	0.3362	0.3394	0.3380	0.3226
1-propanol	0.0131	0.0000	0.9869	0.9870	0.0000	0.0130
	0.0384	0.0984	0.8632	0.8735	0.1042	0.0222
	0.0625	0.1876	0.7499	0.7666	0.1953	0.0381
	0.0794	0.2763	0.6443	0.6626	0.2833	0.0541
	0.1277	0.3494	0.5229	0.5382	0.3594	0.1024
	0.1935	0.4034	0.4031	0.4222	0.4202	0.1576
2-propanol	0.0099	0.0000	0.9901	0.9899	0.0000	0.0101
	0.0259	0.0974	0.8767	0.8685	0.1092	0.0223
	0.0724	0.2018	0.7258	0.7704	0.2000	0.0296
	0.1138	0.2668	0.6195	0.6468	0.2824	0.0708
	0.1619	0.3352	0.5028	0.5224	0.3491	0.1285
	0.2253	0.3898	0.3849	0.3946	0.3988	0.2066

[a]Standard uncertainties u are u(w) = 0.003, u(T) = 0.1 K, and u(p) = 10 kPa

Table 5.3 lists the tie-line values, distribution coefficients (D_i), and selectivities (S). These are defined as:

$$D_1 = \frac{w_1^{org}}{w_1^{aq}} \qquad \textbf{Equation 5.1}$$

$$D_2 = \frac{w_2^{org}}{w_2^{aq}} \qquad \textbf{Equation 5.2}$$

$$S = \frac{D_2}{D_1} \qquad \textbf{Equation 5.3}$$

where D_1 and D_2 are the distribution coefficients for the water and alcohol, respectively, in each phase. w_1 is the water fraction, w_2 is the alcohol fraction. The superscripts org and aq refer to the organic and aqueous phases, respectively. And the selectivity S is the capability of CPME to extract the alcohol from the water phase, Figure 5.3.

Table 5.3 - Experimental LLE Mass Fraction (Tie-Line Data) for the Ternary Systems Water (1) + Alcohol (2) + CPME (3) at Temperature T = 298.15 K and Pressure p = 0.1 MPa[a]

	organic phase		aqueous phase				
alcohol	w_1	w_2	w_1	w_2	D_1	D_2	S
methanol	0.0571	0.1144	0.4398	0.3960	0.13	0.29	2.23
	0.0307	0.0678	0.5444	0.3616	0.06	0.19	3.32
	0.0147	0.0316	0.6872	0.2675	0.02	0.12	5.52
	0.0087	0.0135	0.8120	0.1603	0.01	0.08	7.86
	0.0870	0.1526	0.3767	0.3985	0.23	0.38	1.66
	0.0264	0.0586	0.5719	0.3471	0.05	0.17	3.66
	0.0174	0.0381	0.6530	0.2946	0.03	0.13	4.85
	0.0122	0.0244	0.7290	0.2335	0.02	0.1	6.24
	0.0042	0.0028	0.9296	0.05190	0.00	0.05	11.94
ethanol	0.1585	0.2500	0.5818	0.3147	0.27	0.79	2.92
	0.0986	0.1919	0.6449	0.2845	0.15	0.67	4.41
	0.0745	0.1490	0.6866	0.2616	0.11	0.57	5.25
	0.0411	0.1013	0.7315	0.2301	0.06	0.44	7.84

	0.0145	0.0361	0.8320	0.1428	0.02	0.25	14.51
	0.0085	0.0152	0.9011	0.0763	0.01	0.2	21.12
	0.0198	0.0511	0.8077	0.1669	0.02	0.31	12.49
	0.0368	0.0918	0.7485	0.2194	0.05	0.42	8.51
1-propanol	0.2038	0.4071	0.8234	0.1541	0.25	2.64	10.67
	0.1579	0.3680	0.8408	0.1372	0.19	2.68	14.28
	0.1225	0.3211	0.8538	0.1245	0.14	2.58	17.98
	0.1253	0.3211	0.8538	0.1247	0.15	2.57	17.55
	0.0798	0.2400	0.8747	0.1044	0.09	2.3	25.2
	0.0343	0.1057	0.9096	0.0700	0.04	1.51	40.04
	0.1953	0.4022	0.8304	0.1478	0.24	2.72	11.57
	0.1619	0.3719	0.8418	0.1368	0.19	2.72	14.14
	0.1360	0.3416	0.8518	0.1274	0.16	2.68	16.79
	0.1045	0.2899	0.8636	0.1156	0.12	2.51	20.72
	0.0211	0.0504	0.9338	0.0472	0.02	1.07	47.26
	0.0379	0.1196	0.9031	0.0758	0.04	1.58	37.6
	0.0472	0.1518	0.8934	0.0857	0.05	1.77	33.53
	0.0647	0.2027	0.8848	0.0945	0.07	2.14	29.33
2-propanol	0.1580	0.3387	0.7573	0.2067	0.21	1.64	7.85
	0.122	0.2947	0.7827	0.1872	0.16	1.57	10.1
	0.0816	0.2149	0.8140	0.1605	0.10	1.34	13.36
	0.0258	0.0861	0.8691	0.1096	0.03	0.79	26.46
	0.1866	0.3535	0.7342	0.2235	0.25	1.58	6.22
	0.1370	0.3085	0.7692	0.1987	0.18	1.55	8.72
	0.1220	0.2887	0.7803	0.1896	0.16	1.52	9.74
	0.0742	0.2082	0.8153	0.1594	0.09	1.31	14.35
	0.0247	0.0815	0.8729	0.1054	0.03	0.77	27.33
	0.0121	0.0214	0.9289	0.0532	0.01	0.4	30.88
	0.2537	0.3863	0.7088	0.2431	0.36	1.59	4.44

[a]Standard uncertainties u are u(w) = 0.005, u(T) = 0.1 K, and u(p) = 10 kPa

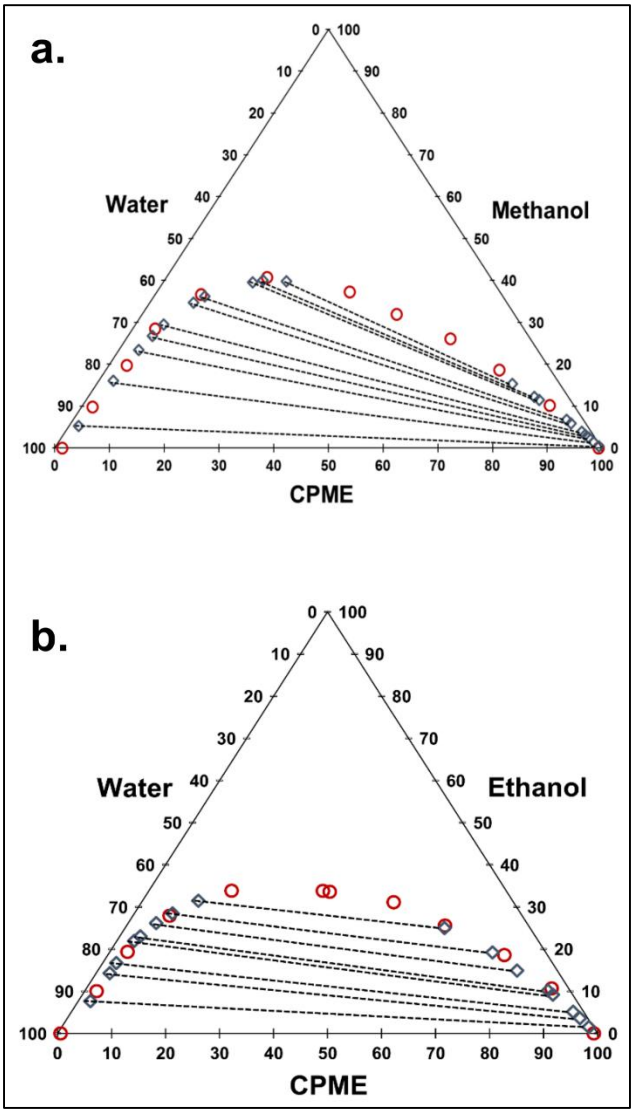

Figure 5.1 - LLE data for the ternary systems (a) {water + methanol + CPME}, and (b) {water + ethanol + CPME} at T= 298.15 K; cloud point data (○), tie-lines (◊).

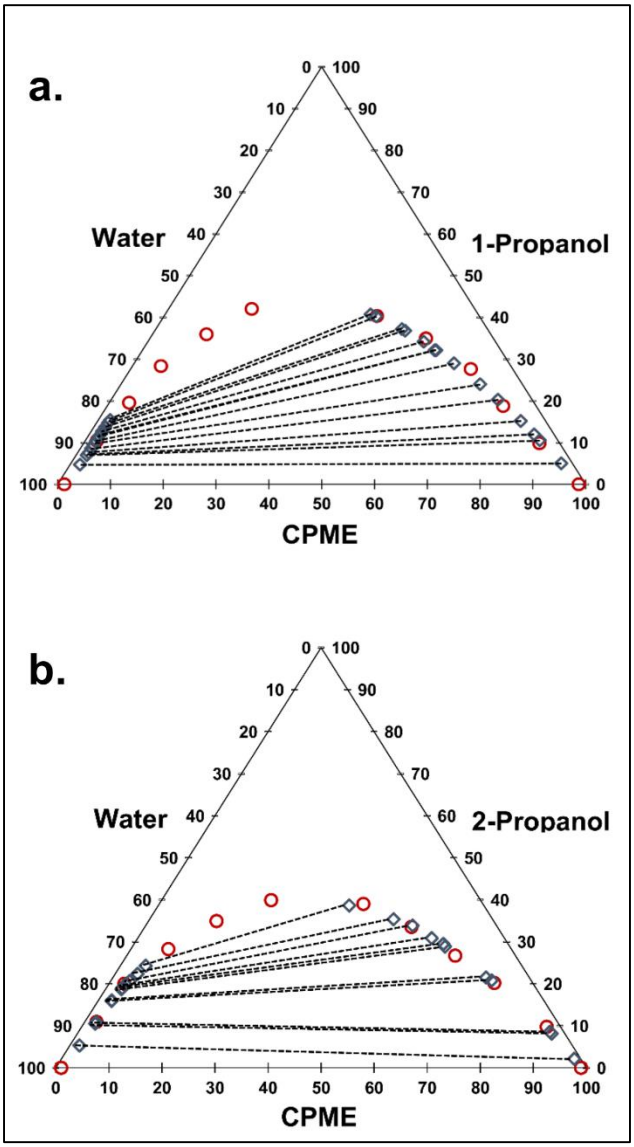

Figure 5.2 - LLE data for the ternary systems (a) {water + 1-propanol + CPME}, and (b) {water + 2-propanol + CPME} at T= 298.15 K; cloud point data (○), tie-lines (◊).

Qualitatively, the tie-lines and cloud point data are in good agreement. Quantitatively, the reliability of the lines were confirmed by plotting the Other-Tobias (equation 5.4) and Hand (equation. 5.5) correlations:

$$ln\left[\frac{1-w_3^{org}}{w_3^{org}}\right] = a + b\ln\left[\frac{1-w_1^{aq}}{w_1^{aq}}\right] \qquad \textbf{Equation 5.4}$$

$$ln\left[\frac{w_2^{org}}{w_3^{org}}\right] = c + d\ln\left[\frac{w_2^{aq}}{w_1^{aq}}\right] \qquad \textbf{Equation 5.5}$$

where w_1, w_2, and w_3 are the mass fraction of water, alcohol, and CPME respectively. The superscripts are as in equations 5.1 and 5.2. a, b, c, d are the fitting parameters for the linear regression, Table 5.4.

Table 5.4 - Fitting Parameter for Othmer-Tobias and Hand Plots

	Othmer-Tobias			Hand		
alcohol	a	b	R^2	c	d	R^2
methanol	-1.9575	1.2268	0.9900	-1.9534	1.4113	0.9866
ethanol	0.1405	1.8305	0.9893	0.0709	1.8042	0.9808
1-propanol	4.9132	2.8968	0.9916	4.0489	2.3819	0.9941
2-propanol	2.6776	2.416	0.9928	2.4227	2.2252	0.9951

5.3.2 Comparison of CPME to Chloroform.

The Bligh and Dyer method for extraction lipids from wet biomass uses a water-methanol-chloroform system[131]. Our system would replace chloroform with CPME and methanol with any of the four possible alcohols, methanol, ethanol, 1-propanol, or 2-propanol. Table 5.5 lists the physical properties of CPME and chloroform. Although relative to chloroform CPME is far less hydrophobic, in absolute terms CPME is hydrophobic. CPME also has a

similar heat of vaporization as chloroform. These terms are important if a separation step is necessary to remove water and/or alcohol from the CPME phase.

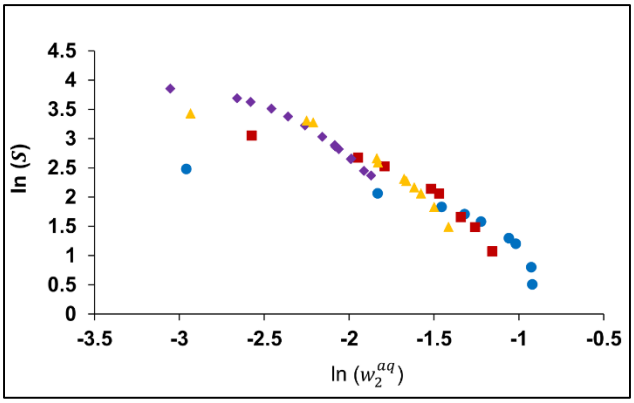

Figure 5.3 - Separation factor (S) for {water + methanol + alcohols} at T = 298.15 K; methanol (●), ethanol (■), 1-propanol (♦), and 2-propanol (▲)

Figure 5.4 shows the LLE ternary diagram for water-methanol-chloroform as well as the four systems studied in this work. As shown in **Figure 5.4**, the miscibility gap for the four systems are fairly similar, with ethanol having the farthest deviation from the Bligh and Dyer. More importantly, the reason that the water-methanol-chloroform system is so successful for lipid extraction is because the oil partitions almost completely into the chloroform phase. Combine this with the slopes of the tie-lines (downward sloping), and upon phase separation the chloroform phase will contain almost no water or methanol, and mostly oil. If CPME acts like chloroform and very little oil partitions into the alcohol, then the water + methanol + CPME system would be preferred; downward sloping tie-line with low selectivity (S). However, if CPME does not capture all of the oil, and some lipids partition into the alcohol, then the water + 1-propanol + CPME system would be preferred; upward sloping tie-lines high selectivity (S).

Table 5.5 - Physical Properties of CPME[5] and Chloroform[150]

property	CPME	Chloroform
molecular weight (g/mol)	100.16	119.38
density (298.15 K) [kg/m^3)	860	1480
boiling Point [K]	379.15	334.15
dielectric constant (298.15)	4.76	4.81
viscosity [mPa·s]	0.55	0.54
heat of vaporization [kJ/kg]	289.3	248.1
azeotropic temperature with water [k]	356.15	326.45
azeotropic composition [solvent/water, wt%/wt%]	83.7/16.3	97.0/3.0
solubility of water in solvent (293.15 K) [g/100g]	0.3	0.06
solubility of solvent in water (293.15 K) [g/100 g]	1.1	0.8

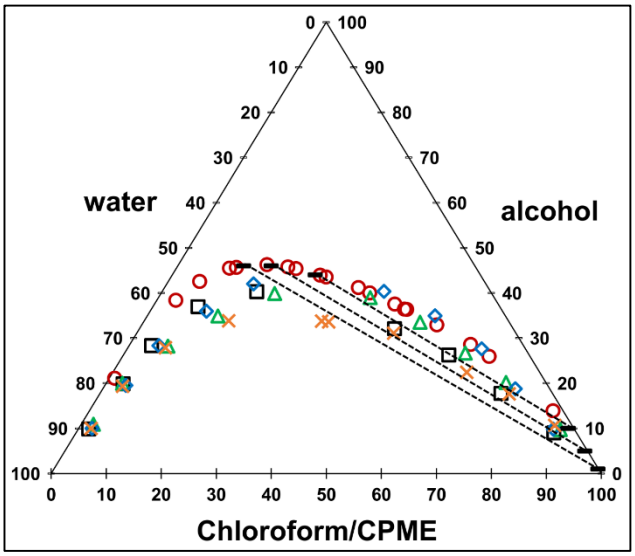

Figure 5.4 - LLE ternary diagrams for water + methanol + chloroform[151] (○), water + methanol + CPME (□), water + ethanol + CPME (x), water + 1-propanol + CPME (◊), and water + 2-propanol + CPME (Δ). Tie-lines (-) correspond to water + methanol + chloroform system.[151]

5.4 Conclusion.

LLE data for four ternary systems, water + alcohol + CPME (the alcohol being methanol, ethanol, 1-propanol, or 2-propanol) were determined at 298.15 K and atmospheric pressure. Both cloud point measurements and tie-line measurement were performed. The accuracy of the tie-line data were checked using the Othmer-Tobias and Hand equations. Distribution coefficients and selectivities were reported. The physical properties and LLE ternary diagrams of CPME was compared to chloroform for the extraction of lipids from wet-biomass. It was concluded that CPME has the potential to replace chloroform, but more studies on oil-CPME-alcohol partitions would are needed.

Chapter 6 - Conclusion

6.1 Summary and Conclusions

This work focused on the development of membrane contact reactors for use in heterogeneous three-phase reactions. It was demonstrated that commercially available membranes could be rendered catalytically active with very little modification, and used in the partial hydrogenation of soybean oil (PHSO) to decrease hydrogen mass transfer resistances. Additionally, the catalytic conversion of an aqueous solution of lactic acid into commodity chemicals was accomplished using ruthenium coated polymeric membranes.

When hydrogenated in a traditional slurry reactor, the PHSO is known to produce high amounts of trans-fats. The low solubility of hydrogen gas in the oil causes significant hydrogen scarcity at the catalyst surface. This lack of hydrogen coverage is the cause of the trans-fats. By using a membrane contact reactor, we were able to reduce trans-fat formation by over 50% compared to a slurry reactor with similar catalyst and equal levels of hydrogenation. We also demonstration that the PHSO reaction is nearly zero order with respect to hydrogen pressure, indicating that the membrane reactor was operating in a kinetically limited region.

Additionally, it was shown that the formation of trans-fats is independent of temperature using the membrane reactor, whereas slurry reactors show a strong positive correlate between temperature and trans-fat production. With slurry reactors, as the temperature is increased, the hydrogen solubility of the oil is reduced, leading to an increase in hydrogen starvation, causing trans-fats to be formed. In addition to producing low trans-fats, it is also desirable to minimize the amount of saturated fat produced. However, minimizing saturated fats is favoured at high temperature, while minimizing trans-fats is favoured at low temperatures; forcing a trade-off scenario for slurry reactors. Membranes reactors, because hydrogen is delivered by permeation

through the membrane (which actually increases with increasing temperature), are able to operate at elevated temperatures without a loss in hydrogen at the catalyst cites, allowing for: (1) increased reaction rate, (2) minimize saturated fats, and (3) minimize trans-fats.

In the lactic acid experiments, flat sheet polymeric membranes (polyetherimide) were fabricated in-house and coated with ruthenium catalyst through a spin coating process. Aqueous phase hydrogenation experiments, similar to the PHSO, are also known to suffer from low hydrogen solubility of the liquid phase; requiring pressures of 100 bar or more of hydrogen pressure. The intended goals were to reduce the operating pressures, improve reaction rates, and control product selectivity with the use of membrane contact reactors. Our results show that the use of membrane reactors was able to increase the reaction rates compared to all control experiments; however the ability to control selectivity is currently uncertain. It was demonstrated that changing reaction conditions (pressure and temperature) was able to change product selectivities; however there were many unknown products, which leads to an uncertain final composition. Further analysis of the unknown compounds is needed to clarify the selectivities. Additionally, a more accurate catalyst deposition technique is required to ensure consistent and even metal loading.

6.2 Future work

If this project were to continue, there are several directions that I could envision this research going. Below I will outline what I believe to be important and attainable avenues of investigation.

6.2.1 Catalyst Deposition and Determination

Knowing the mass of catalyst deposited on the membrane would be immensely important. This would allow for the reaction rates to be normalized on a catalyst mass basis, which would allow for better comparison between membrane reactors and traditional three-phase reactors. Determining the mass of catalyst on the commercial hollow fibers membranes mentioned in chapters 2 and 3 proved difficult because normal elemental analysis techniques, such as acid digestion or energy dispersive spectroscopy (EDS), were not possible due to the location of the catalyst (on the inside of the tube), and the material of the membrane (ceramic). However, if the membranes are flat sheets, it is possible to digest the entire membrane in hydrofluoric acid for inductively coupled plasma **(**ICP) analysis. Alternatively, sputter coating is a technique that allows for both a uniform distribution and a precise amount of material (catalyst) to be deposited[152]. Because the amount of catalyst deposited is known, sputter coating would eliminate the need of additional wet chemistry and instrumentation that ICP requires for metal loading determination.

Moreover, with magnetron sputter coating it is possible to deposit more than one metal at a time. Experiments could be conducted using both single metal and bimetallic depositions. For the bimetallic deposition, first titanium or chromium will be deposited onto the polymer skin, followed by a platinum group metal. Both Cr and Ti are known to be "adhesion" metals, and it is common to uses these adhesion metals as an intermediate layer between two surfaces that will not adhere by themselves. These bimetallic depositions may provide a more robust adhesion than a single metal[153,154].

Another route to preparing catalytic membranes is to deposit catalytic nanoparticles (NPs) onto the surface of a membrane. There is an abundance literature on both NP synthesis[155-

[157] and NPs use in modifying membranes[158-160]. Along with the chemical reactions themselves, surface modifications opens up an entire surface chemistry avenue for research. How are the NPs adhering? What forces are involved?

6.2.2 Surface Modifications

One particular aspect of surface modification that receives considerable study, and could be potentially useful for this project, is chemical cross-linking[114]. Cross-linking can be used to reduce plasticization[161], improve or reduce water flux[162], and increase chemical resistant[163]; with the latter being on interest for this project. With the reactions studied in these works, the solvents/reactants were very mild (oil and water) toward the membranes; however, more aggressive solvents, such as tetrahydrofuran (THF), are known to be detrimental to polyimides[161,164,165].

The crosslinking of polyimides (PIs) with diamines has been shown to improve solvent stability and density[166]. The diamine is first dissolved in an alcohol, and the cross-linking solution is introduced on the surface of the membrane. The alcohol swells the membrane, which allows the diamine access to the polymer chains[161,164,166,167]. The diamine reacts with the end of the polymer chain by breaking the imide bond and makes an intermolecular amide bond/bridge. Although diamines have been studied with polyimides such as P84 and Matrimid, to my knowledge, there are no reported studies on Ultem 1000/diamine cross-linking. Additionally, the instrumentation to study the surface science of the cross-linking, and the above catalyst adhesion questions, are available either within the Chemical Engineering department, or within other Kansas State University departments.

ATR-FTIR (attenuated total reflection – Fourier transform infrared spectroscopy), housed in Biological and Agricultural Engineering, is used to compare original and cross-linked

membranes. ATR-FTIR shows that with increased cross-linking, imide groups are replaced with amide groups. Although the exact chemical shifts are specific for different polyimides, there are three main bands for imide shifts in the unmodified PIs around: (1) 1770-1790 cm^{-1} (C=O asymmetric stretch of imide groups), (2) 1700-1720 cm^{-1} (C= O symmetric stretch of imide groups), and (3) 1340-1360 cm^{-1} (C–N stretch of imide groups)[167,168]. These peaks are shown to decrease with increased cross-linking time, while the characteristic bands of the amide groups increase; ≈1645 cm^{-1} (C=O stretch band of the CONH group)[169] and ≈1530 cm^{-1} (C-N stretch of the C-N-H group)[166].

XPS (X-ray photoelectron spectroscopy), housed in Chemical Engineering, is another common characterization technique that is used to characterized cross-linked membranes. Cross-linking with diamines introduces more nitrogen atoms, while keeping other atoms constant. Overtime, it would be expected to see an increase in nitrogen, thus, the ratio increase of N_{1s} to an orbital from an element that is not being added, is considered an indication of the degree of cross-linking. For example, the PI used by Shao et al.[168] contained fluorine (F), and the cross-linking agent only contained carbon (C), hydrogen (H), and nitrogen (N). They used XPS to show that increased cross-linking time correlated with increased N_{1s}/F_{1s} and N_{1s}/O_{1s} ratios[168].

Because the membranes used are polymers, XRD (X-ray diffraction), housed in Chemical Engineering, does not show sharp, distinct peaks, instead, it returns an amorphous halo. However, diamine cross-linking universally causes shifts to the right, indicating a significant decrease in the d-spacing; with increased cross-linking time associated with a greater decrease in the d-spacing[166-168,170,171]. Additionally, XRD intensity is known to decrease with increased cross-linking time. The drop in d-spacing is thought to be caused by inter-polymer chain bonding[167], or possibly by hydrogen bonding of inter-chain and intra-chain[170]. Both the loss of

intensity and d-spacing are indicative of a tightening of the overall system. Diamine cross-linked membranes are known to densify, which supports the above XRD trends[161,164-166].

In addition to the benefit that the cross-linking would provide to the membrane reactors, the cross-linking characterization would provide an opportunity for an original manuscript. I envision a chemical reaction using the membrane reactor as the long term focus of the project, with the cross-linking as a co-currant side project.

References

1. Klaewkla, R.; Arend, M.; Hoelderich, W. F. A review of mass transfer controlling the reaction rate in heterogeneous catalytic systems. *de Mass Transfer-Advanced Aspects, Germany, InTech* **2011**, 668-684.

2. Rylander, P. N. *Catalytic hydrogenation in organic syntheses;* Academic Press New York: 1979; Vol. 113.

3. Veldsink, J. W.; Bouma, M. J.; Schöön, N. H.; Beenackers, A. A. Heterogeneous hydrogenation of vegetable oils: a literature review. *Catalysis Reviews* **1997**, *39*, 253-318.

4. Fan, Y.; Zhou, C.; Zhu, X. Selective catalysis of lactic acid to produce commodity chemicals. *Catalysis Reviews* **2009**, *51*, 293-324.

5. Watanabe, K.; Yamagiwa, N.; Torisawa, Y. Cyclopentyl methyl ether as a new and alternative process solvent. *Organic process research & development* **2007**, *11*, 251-258.

6. Watanabe, K. The Toxicological Assessment of Cyclopentyl Methyl Ether (CPME) as a Green Solvent. *Molecules* **2013**, *18*, 3183-3194.

7. Wales, M.; Joos, L.; Probst, K.; Vadlani, P.; Rezac, M. Liquid-Liquid Equilibria for Ternary Systems of Water + Methoxycyclopentane (CPME) + Alcohol; Methanol, Ethanol, 1-Propanol, or 2-Propanol. *J. Chem. Eng. Data* **submitted 2015**.

8. Wales, M.; Joos, L.; Traylor, W.; Pfromm, P.; Rezac, M. Composite catalytic tubular membranes for selective hydrogenation in three-phase systems. **submitted, 2015**.

9. Mason, E. From pig bladders and cracked jars to polysulfones: an historical perspective on membrane transport. *J. Membr. Sci.* **1991**, *60*, 125-145.

10. Baker, R. W. *Membrane technology and applications;* John Wiley: Chichester, West Sussex, 2012; , pp 575.

11. Ozdemir, S. S.; Buonomenna, M. G.; Drioli, E. Catalytic polymeric membranes: preparation and application. *Applied Catalysis A: General* **2006**, *307*, 167-183.

12. Vankelecom, I. F. Polymeric membranes in catalytic reactors. *Chem. Rev.* **2002**, *102*, 3779-3810.

13. Zaman, J.; Chakma, A. Inorganic membrane reactors. *J. Membr. Sci.* **1994**, *92*, 1-28.

14. Pabby, A. K.; Sastre, A. M. State-of-the-art review on hollow fibre contactor technology and membrane-based extraction processes. *J. Membr. Sci.* **2013**, *430*, 263-303.

15. Cussler, E. L. *Diffusion: mass transfer in fluid systems;* Cambridge university press: 2009; .

16. Baker, R. W. *Membrane technology;* Wiley Online Library: 2000; .

17. Ramachandran, P.; Chaudhari, R. *Three-phase catalytic reactors;* Gordon & Breach Science Pub: 1983; Vol. 2.

18. Beenackers, A.; Van Swaaij, W. Mass transfer in gas—liquid slurry reactors. *Chemical Engineering Science* **1993**, *48*, 3109-3139.

19. Zhang, Z.; Jackson, J. E.; Miller, D. J. Aqueous-phase hydrogenation of lactic acid to propylene glycol. *Applied Catalysis A: General* **2001**, *219*, 89-98.

20. Zhang, Z.; Jackson, J. E.; Miller, D. J. Kinetics of aqueous-phase hydrogenation of lactic acid to propylene glycol. *Ind Eng Chem Res* **2002**, *41*, 691-696.

21. Gryaznov, V. M. USSR Patent , 1964.

22. Saracco, G.; Montanaro, L. Catalytic ceramic filters for flue gas cleaning. 1. Preparation and characterization. *Ind Eng Chem Res* **1995**, *34*, 1471-1479.

23. Saracco, G.; Specchia, V. Catalytic ceramic filters for flue gas cleaning. 2. Catalytic performance and modeling thereof. *Ind Eng Chem Res* **1995**, *34*, 1480-1487.

24. Hashimoto, K.; Muroyama, K.; Nagata, S. Kinetics of the hydrogenation of fatty oils. *Journal of the American Oil Chemists Society* **1971**, *48*, 291-295.

25. Van der Plank, P. Isomerization phenomena during hydrogenation of methyl oleate and methyl elaidate over nickel-silica catalysts. *Journal of the American Oil Chemists Society* **1972**, *49*, 327-332.

26. Mabrouk, A. F.; Brown, J. The trans fatty acids of margarines and shortenings. *J. Am. Oil Chem. Soc.* **1956**, *33*, 98-102.

27. Bockisch, M. *Fats and oils handbook.* AOCS press: 1998; .

28. Hsu, N.; Dlosady, L.; Rubin, L. Catalytic behavior of palladium in the hydrogenation of edible oils. *Journal of the American Oil Chemists' Society* **1988**, *65*, 349-356.

29. Ray, J. D. Behavior of hydrogenation catalysts. I. Hydrogenation of soybean oil with palladium. *Journal of the American Oil Chemists' Society* **1985**, *62*, 1213-1217.

30. Heldal, J.; Moulton, K.; Fronkel, E. Fixed-Bed continuous hydrogenation of soybean oil with palladium-Polymer supported catalysts. *Journal of the American Oil Chemists' Society* **1989**, *66*, 979-982.

31. Ahmad, M.; Priestley, T.; Winterbottom, J. Palladium-catalyzed hydrogenation of soybean oil. *Journal of the American Oil Chemists' Society* **1979**, *56*, 571-577.

32. Urbanczyk, D.; Dittmeyer, R.; Wolf, A.; Warsitz, R.; Fischer, G.; Voigt, I. Evaluation of porous catalytic membranes operated in pore-flow-through mode for hydrogenation of α-methylstyrene. *Asia-Pacific Journal of Chemical Engineering* **2010**, *5*, 12-25.

33. Schmidt, A.; Schomäcker, R. Partial hydrogenation of sunflower oil in a membrane reactor. *Journal of Molecular Catalysis A: Chemical* **2007**, *271*, 192-199.

34. Gryaznov, V. M. Mechanism of the catalytic redistribution of hydrogen in unsaturated cyclic hydrocarbons. *Russian Chemical Reviews* **1963**, *32*, 188-200.

35. GAO, H.; LIAO, S.; XU, Y.; LIU, R.; LIU, J.; LI, D. Selective Hydrogenation of Cyclopentadiene in a Catalytic Cellulose-Acetate Hollow-Fiber Reactor. *Catal. Lett.* **1994**, *27*, 297-303.

36. Liu, C.; Xu, Y.; Liao, S.; Yu, D. Selective hydrogenation of cyclopentadiene in mono- and bimetallic catalytic hollow-fiber reactors. *J. Mol. Catal. A-Chem.* **2000**, *157*, 253-259.

37. Motamedhashemi, M. Y.; Egolfopoulos, F.; Tsotsis, T. Application of a flow-through catalytic membrane reactor (FTCMR) for the destruction of a chemical warfare simulant. *J. Membr. Sci.* **2011**, *376*, 119-131.

38. Van der Vaart, R.; Lebedeva, V.; Petrova, I.; Plyasova, L.; Rudina, N.; Kochubey, D.; Tereshchenko, G.; Volkov, V.; Van Erkel, J. Preparation and characterisation of palladium-loaded polypropylene porous hollow fibre membranes for hydrogenation of dissolved oxygen in water. *J. Membr. Sci.* **2007**, *299*, 38-44.

39. Volkov, V.; Lebedeva, V.; Petrova, I.; Bobyl, A.; Konnikov, S.; Roldughin, V.; van Erkel, J.; Tereshchenko, G. Adlayers of palladium particles and their aggregates on porous polypropylene hollow fiber membranes as hydrogenization contractors/reactors. *Adv. Colloid Interface Sci.* **2011**, *164*, 144-155.

40. Centi, G.; Dittmeyer, R.; Perathoner, S.; Reif, M. Tubular inorganic catalytic membrane reactors: advantages and performance in multiphase hydrogenation reactions. *Catalysis Today* **2003**, *79*, 139-149.

41. Veldsink, J. W. Selective hydrogenation of sunflower seed oil in a three-phase catalytic membrane reactor. *J. Am. Oil Chem. Soc.* **2001**, *78*, 443-446.

42. Singh, D.; Rezac, M.; Pfromm, P. H. Partial hydrogenation of soybean oil using metal-decorated integral-asymmetric polymer membranes: Effects of morphology and membrane properties. *J. Membr. Sci.* **2010**, *348*, 99-108.

43. Singh, D.; Pfromm, P. H.; Rezac, M. Overcoming mass-transfer limitations in partial hydrogenation of soybean oil using metal-decorated polymeric membranes. *AIChE J.* **2011**, *57*, 2450-2457.

44. Singh, D.; Rezac, M.; Pfromm, P. Partial hydrogenation of soybean oil with minimal trans fat production using a Pt-decorated polymeric membrane reactor. *J. Am. Oil Chem. Soc.* **2009**, *86*, 93-101.

45. Dudley, C.; Schöberl, B.; Sturgill, G.; Beckham, H.; Rezac, M. Influence of crosslinking technique on the physical and transport properties of ethynyl-terminated monomer/polyetherimide asymmetric membranes. *J. Membr. Sci.* **2001**, *191*, 1-11.

46. Roucoux, A.; Schulz, J.; Patin, H. Reduced transition metal colloids: a novel family of reusable catalysts? *Chem. Rev.* **2002**, *102*, 3757-3778.

47. AnonymousPreparation of methyl esters of fatty acids. *Official and Recommended Practices of the AOCS, 5th Edn.* **1997**.

48. AnonymousDetermination of cis-, trans-, saturated, monounsaturated and polyunsaturated fatty acids in vegetable or non-ruminant animal oils and fats by capillary GLC method. *Official and Recommended Practices of the AOCS, 5th Edn.* **2005**.

49. Firestone, D. *Official Methods and Recommended Practices of the American Oil Chemists' Society* **1989**.

50. Henis, J. M.; Tripodi, M. K. Composite hollow fiber membranes for gas separation: the resistance model approach. *J. Membr. Sci.* **1981**, *8*, 233-246.

51. Pinnau, I.; Wijmans, J.; Blume, I.; Kuroda, T.; Peinemann, K. Gas permeation through composite membranes. *J. Membr. Sci.* **1988**, *37*, 81-88.

52. Merkel, T.; Bondar, V.; Nagai, K.; Freeman, B.; Pinnau, I. Gas sorption, diffusion, and permeation in poly (dimethylsiloxane). *Journal of Polymer Science Part B: Polymer Physics* **2000**, *38*, 415-434.

53. Baker, R. W. *Membrane technology;* Wiley Online Library: 2000; .

54. Henis, J. M.; Tripodi, M. K. A novel approach to gas separations using composite hollow fiber membranes. *Sep. Sci. Technol.* **1980**, *15*, 1059-1068.

55. Albright, L. Quantitative measure of selectivity of hydrogenation of triglycerides. *Journal of the American Oil Chemists' Society* **1965**, *42*, 250-253.

56. Albright, L. Mechanism of hydrogenation of triglycerides. *Journal of the American Oil Chemists Society* **1963**, *40*, A16-A29.

57. Kesting, R. E.; Fritzsche, A. *Polymeric gas separation membranes;* Wiley-Interscience: 1993; .

58. Gryaznov, V. Platinum Metals as Components of Catalyst-Membrane Systems. *ChemInform* **1992**, *23*.

59. Gryaznov, V.; Orekhova, N.; Cybulski, A.; Moulijn, J. Structured Catalysis and Reactors. *Marcel Decker, New York* **1998**.

60. Bengtson, G.; Fritsch, D. Catalytic membrane reactor for the selective hydrogenation of edible oil: platinum versus palladium catalyst. *Desalination* **2006**, *200*, 666-667.

61. Liu, C.; Xu, Y.; Liao, S.; Yu, D. Mono- and bimetallic catalytic hollow-fiber reactors for the selective hydrogenation of butadiene in 1-butene. *Appl. Catal. A-Gen.* **1998**, *172*, 23-29.

62. Jiang, H.; Qu, Z.; Li, Y.; Huang, J.; Chen, R.; Xing, W. One-step semi-continuous cyclohexanone production via hydrogenation of phenol in a submerged ceramic membrane reactor. *Chem. Eng. J.* **2016**, *284*, 724-732.

63. AnonymousMicrosoft Word - Datasheet 1-Channel PDMS, Version 27-05-2014.docx - Datasheet-1-Channel-PDMS-Version-27-05-2014.pdf. *http://pervaporation-membranes.com/wp-content/uploads/2014/10/Datasheet-1-Channel-PDMS-Version-27-05-2014.pdf* (accessed 10/19/2015, 2015).

64. AnonymousMicrosoft Word - Datasheet 1-Channel Hybrid Silica membranes, Version 27-05-2014.docx - Datasheet-1-Channel-Hybrid-Silica-membranes-Version-27-05-2014.pdf. *http://pervaporation-membranes.com/wp-content/uploads/2014/10/Datasheet-1-Channel-Hybrid-Silica-membranes-Version-27-05-2014.pdf* (accessed 10/19/2015, 2015).

65. Agirre, I.; Arias, P. L.; Castricum, H. L.; Creatore, M.; Johan, E.; Paradis, G. G.; Ngamou, P. H.; van Veen, H. M.; Vente, J. F. Hybrid organosilica membranes and processes: Status and outlook. *Separation and purification technology* **2014**, *121*, 2-12.

66. Castricum, H. L.; Kreiter, R.; van Veen, H. M.; Blank, D. H.; Vente, J. F.; Johan, E. High-performance hybrid pervaporation membranes with superior hydrothermal and acid stability. *J. Membr. Sci.* **2008**, *324*, 111-118.

67. Castricum, H. L.; Sah, A.; Kreiter, R.; Blank, D. H.; Vente, J. F.; Johan, E. Hybrid ceramic nanosieves: stabilizing nanopores with organic links. *Chemical Communications* **2008**, 1103-1105.

68. Paradis, G. G.; Shanahan, D. P.; Kreiter, R.; van Veen, H. M.; Castricum, H. L.; Nijmeijer, A.; Vente, J. F. From hydrophilic to hydrophobic HybSi® membranes: A change of affinity and applicability. *J. Membr. Sci.* **2013**, *428*, 157-162.

69. Merkel, T.; Bondar, V.; Nagai, K.; Freeman, B.; Pinnau, I. Gas sorption, diffusion, and permeation in poly (dimethylsiloxane). *Journal of Polymer Science Part B: Polymer Physics* **2000**, *38*, 415-434.

70. Kreiter, R.; Rietkerk, M.; Castricum, H.; Van Veen, H.; Ten Elshof, J.; Vente, J. Evaluation of hybrid silica sols for stable microporous membranes using high-throughput screening. *J. Sol Gel Sci. Technol.* **2011**, *57*, 245-252.

71. Chu, Y.; Lin, L. Effects of minor compounds on hydrogenation rate of soybean oil. *Journal of the American Oil Chemists Society* **1992**, *69*, 880-883.

72. Drozdowski, B.; Zajac, M. Effect of concentration of some nickel catalyst poisons in oils on the course of hydrogenation. *Journal of the American Oil Chemists' Society* **1977**, *54*, 595-599.

73. Szukalska, E. The effect of temperature during soybean oil hydrogenation on nickel catalyst poisoning by phospholipids. *Polish journal of food and nutrition sciences* **2003**, *4*.

74. Klimmek, H. Influence of various catalyst poisons and other impurities on fatty acid hydrogenation. *Journal of the American Oil Chemists' Society* **1984**, *61*, 200-204.

75. Abraham, V. Effect of some isothiocyanates on the hydrogenation of canola oil. *Journal of the American Oil Chemists Society* **1987**, *64*, 855-858.

76. Edvardsson, J.; Rautanen, P.; Littorin, A.; Larsson, M. Deactivation and coke formation on palladium and platinum catalysts in vegetable oil hydrogenation. *J. Am. Oil Chem. Soc.* **2001**, *78*, 319-327.

77. Mäki-Arvela, P.; Kuusisto, J.; Sevilla, E. M.; Simakova, I.; Mikkola, J.; Myllyoja, J.; Salmi, T.; Murzin, D. Y. Catalytic hydrogenation of linoleic acid to stearic acid over different Pd-and Ru-supported catalysts. *Applied Catalysis A: General* **2008**, *345*, 201-212.

78. Chojnacka, K. Fermentation products. *Chemical engineering and chemical process technology* , 12.

79. Datta, R.; Henry, M. Lactic acid: recent advances in products, processes and technologies—a review. *Journal of Chemical Technology and Biotechnology* **2006**, *81*, 1119-1129.

80. Taskila, S.; Ojamo, H. *The current status and future expectations in industrial production of lactic acid by lactic acid bacteria;* INTECH Open Access Publisher: 2013; .

81. Das, D.; Goyal, A. Lactic acid bacteria in food industry. In *Microorganisms in Sustainable Agriculture and Biotechnology*Springer: 2012; pp 757-772.

82. De Vuyst, L.; Leroy, F. Bacteriocins from lactic acid bacteria: production, purification, and food applications. *J. Mol. Microbiol. Biotechnol.* **2007**, *13*, 194-199.

83. Leroy, F.; De Vuyst, L. Lactic acid bacteria as functional starter cultures for the food fermentation industry. *Trends Food Sci. Technol.* **2004**, *15*, 67-78.

84. Wee, Y.; Kim, J.; Ryu, H. Biotechnological production of lactic acid and its recent applications. *Food Technology and Biotechnology* **2006**, *44*, 163-172.

85. Kreps, S. I. *Cosmetic compositions containing lactic acid esters of fatty alcohols* **1963**.

86. Smith, W. P. Epidermal and dermal effects of topical lactic acid. *J. Am. Acad. Dermatol.* **1996**, *35*, 388-391.

87. Stiller, M. J.; Bartolone, J.; Stern, R.; Smith, S.; Kollias, N.; Gillies, R.; Drake, L. A. Topical 8% glycolic acid and 8% L-lactic acid creams for the treatment of photodamaged skin: a double-blind vehicle-controlled clinical trial. *Arch. Dermatol.* **1996**, *132*, 631-636.

88. Smith, W. P. The effects of topical L ( ) lactic acid and ascorbic acid on skin whitening. *Int. J. Cosmetic Sci.* **1999**, *21*, 33-40.

89. Fan, Y.; Zhou, C.; Zhu, X. Selective catalysis of lactic acid to produce commodity chemicals. *Catalysis Reviews* **2009**, *51*, 293-324.

90. Holm, M. S.; Saravanamurugan, S.; Taarning, E. Conversion of sugars to lactic acid derivatives using heterogeneous zeotype catalysts. *Science* **2010**, *328*, 602-605.

91. Serrano-Ruiz, J. C.; Dumesic, J. A. Catalytic processing of lactic acid over Pt/Nb2O5. *ChemSusChem* **2009**, *2*, 581-586.

92. Katryniok, B.; Paul, S.; Dumeignil, F. Highly efficient catalyst for the decarbonylation of lactic acid to acetaldehyde. *Green Chem.* **2010**, *12*, 1910-1913.

93. Cortright, R.; Sanchez-Castillo, M.; Dumesic, J. Conversion of biomass to 1, 2-propanediol by selective catalytic hydrogenation of lactic acid over silica-supported copper. *Applied Catalysis B: Environmental* **2002**, *39*, 353-359.

94. Zhang, Z.; Jackson, J. E.; Miller, D. J. Effect of biogenic fermentation impurities on lactic acid hydrogenation to propylene glycol. *Bioresour. Technol.* **2008**, *99*, 5873-5880.

95. Zhang, Z.; Jackson, J. E.; Miller, D. J. Aqueous-phase hydrogenation of lactic acid to propylene glycol. *Applied Catalysis A: General* **2001**, *219*, 89-98.

96. Ai, M.; Ohdan, K. Oxidative dehydrogenation of lactic acid to pyruvic acid over iron phosphate catalyst. *Applied Catalysis A: General* **1997**, *150*, 13-20.

97. Tsujino, T.; Ohigashi, S.; Sugiyama, S.; Kawashiro, K.; Hayashi, H. Oxidation of propylene glycol and lactic acid to pyruvic acid in aqueous phase catalyzed by lead-modified palladium-on-carbon and related systems. *Journal of molecular catalysis* **1992**, *71*, 25-35.

98. Mok, W. S. L.; Antal Jr, M. J.; Jones Jr, M. Formation of acrylic acid from lactic acid in supercritical water. *J. Org. Chem.* **1989**, *54*, 4596-4602.

99. Gunter, G. C.; Langford, R. H.; Jackson, J. E.; Miller, D. J. Catalysts and supports for conversion of lactic acid to acrylic acid and 2, 3-pentanedione. *Ind Eng Chem Res* **1995**, *34*, 974-980.

100. Miller, D. J.; Jackson, J. E.; Langford, R. H.; Gunter, G. C.; Tam, M. S.; Kokitkar, P. B. *From lactic acid or ester* **1998**.

101. Serrano-Ruiz, J. C.; Dumesic, J. A. Catalytic upgrading of lactic acid to fuels and chemicals by dehydration/hydrogenation and C–C coupling reactions. *Green Chem.* **2009**, *11*, 1101-1104.

102. Delgado, P.; Sanz, M. T.; Beltrán, S. Kinetic study for esterification of lactic acid with ethanol and hydrolysis of ethyl lactate using an ion-exchange resin catalyst. *Chem. Eng. J.* **2007**, *126*, 111-118.

103. Choi, J.; Hong, W. H. Recovery of Lactic Acid by Batch Distillation with Chemical Reactions Using Ion Exchange Resin. *J. Chem. Eng. Japan* **1999**, *32*, 184-189.

104. Engin, A.; Haluk, H.; Gurkan, K. Production of lactic acid esters catalyzed by heteropoly acid supported over ion-exchange resins. *Green Chem.* **2003**, *5*, 460-466.

105. AnonymousTop Value Added Chemicals from Biomass: Volume I--Results of Screening for Potential Candidates from Sugars and Synthesis Gas - 35523.pdf. *http://www.nrel.gov/docs/fy04osti/35523.pdf* (accessed 11/6/2015, 2015).

106. Stephen, H.; Stephen, T. *Solubilities of inorganic and organic compounds;* Pergamon Press Oxford: 1963; Vol. 1.

107. Zhang, Z.; Jackson, J. E.; Miller, D. J. Kinetics of aqueous-phase hydrogenation of lactic acid to propylene glycol. *Ind Eng Chem Res* **2002**, *41*, 691-696.

108. Singh, D.; Rezac, M.; Pfromm, P. H. Partial hydrogenation of soybean oil using metal-decorated integral-asymmetric polymer membranes: Effects of morphology and membrane properties. *J. Membr. Sci.* **2010**, *348*, 99-108.

109. Singh, D. *Metal decorated polymeric membranes for low trans partial hydrogenation of soybean oil* **2009**.

110. Peinemann, K. V.; Pinnau, I. *Method for producing an integral asymmetric gas separating membrane and the resultant membrane* **1988**.

111. Rezac, M. E.; Schöberl, B. Transport and thermal properties of poly (ether imide)/acetylene-terminated monomer blends. *J. Membr. Sci.* **1999**, *156*, 211-222.

112. Bayer, B. Thermisch und chemisch stabile Membranen aus vernetzungsfahigkeit Polymermischungen, Institut für Thermische Verfahrenstechnik der Universität Karlsruhe, 1996.

113. Schöberl, B. TemperatureinfluB auf Polymermembranen, Institut für Thermische Verfahrenstechnik der Universität Karlsruhe, 1997.

114. Vanherck, K.; Koeckelberghs, G.; Vankelecom, I. F. Crosslinking polyimides for membrane applications: a review. *Progress in polymer science* **2013**, *38*, 874-896.

115. Halpern, J.; Harrod, J. F.; James, B. R. Homogeneous Catalysis of the Hydrogenation of Olefinic Compounds by Ruthenium (II) Chloride1. *J. Am. Chem. Soc.* **1966**, *88*, 5150-5155.

116. Holten, C. H. *Lactic acid. Properties and chemistry of lactic acid and derivatives.* Weinheim/Bergstr., W. Germany, Verlag Chemie GmbH: 1971; .

117. Sugiyama, S.; Shigemoto, N.; Masaoka, N.; Suetoh, S.; Kawami, H.; Miyaura, K.; Hayashi, H. Vapor-Phase Oxidation of Ethyl Lactate to Pyruvate over Various Oxide Catalysts. *Bull. Chem. Soc. Jpn.* **1993**, *66*, 1542-1547.

118. Mata, T. M.; Martins, A. A.; Caetano, N. S. Microalgae for biodiesel production and other applications: a review. *Renewable and sustainable energy reviews* **2010**, *14*, 217-232.

119. Hu, Q.; Sommerfeld, M.; Jarvis, E.; Ghirardi, M.; Posewitz, M.; Seibert, M.; Darzins, A. Microalgal triacylglycerols as feedstocks for biofuel production: perspectives and advances. *The Plant Journal* **2008**, *54*, 621-639.

120. Singh, A.; Olsen, S. I. A critical review of biochemical conversion, sustainability and life cycle assessment of algal biofuels. *Appl. Energy* **2011**, *88*, 3548-3555.

121. Probst, K. V.; Schulte, L. R.; Durrett, T. P.; Rezac, M. E.; Vadlani, P. V. Oleaginous yeast: a value-added platform for renewable oils. *Crit. Rev. Biotechnol.* **2015**, 1-14.

122. Sabirova, J. S.; Haddouche, R.; Van Bogaert, I.; Mulaa, F.; Verstraete, W.; Timmis, K.; Schmidt-Dannert, C.; Nicaud, J.; Soetaert, W. The 'LipoYeasts' project: using the oleaginous yeast Yarrowia lipolytica in combination with specific bacterial genes for the bioconversion of lipids, fats and oils into high-value products. *Microbial biotechnology* **2011**, *4*, 47-54.

123. Li, Y.; Zhao, Z. K.; Bai, F. High-density cultivation of oleaginous yeast Rhodosporidium toruloides Y4 in fed-batch culture. *Enzyme Microb. Technol.* **2007**, *41*, 312-317.

124. Brennan, L.; Owende, P. Biofuels from microalgae—a review of technologies for production, processing, and extractions of biofuels and co-products. *Renewable and sustainable energy reviews* **2010**, *14*, 557-577.

125. Draaisma, R. B.; Wijffels, R. H.; Slegers, P. E.; Brentner, L. B.; Roy, A.; Barbosa, M. J. Food commodities from microalgae. *Curr. Opin. Biotechnol.* **2013**, *24*, 169-177.

126. Meng, X.; Yang, J.; Xu, X.; Zhang, L.; Nie, Q.; Xian, M. Biodiesel production from oleaginous microorganisms. *Renewable Energy* **2009**, *34*, 1-5.

127. Olguín, E. J. Dual purpose microalgae–bacteria-based systems that treat wastewater and produce biodiesel and chemical products within a Biorefinery. *Biotechnol. Adv.* **2012**, *30*, 1031-1046.

128. Cheirsilp, B.; Suwannarat, W.; Niyomdecha, R. Mixed culture of oleaginous yeast Rhodotorula glutinis and microalga Chlorella vulgaris for lipid production from industrial wastes and its use as biodiesel feedstock. *New Biotechnology* **2011**, *28*, 362-368.

129. Probst, K. V. Single cell oil production using Lipomyces starkeyi : fermentation, lipid analysis and use of renewable hemicellulose-rich feedstocks, Ph.D. Dissertation, Kansas State University, Manhattan, KS, 2014.

130. Axelsson, M.; Gentili, F. A single-step method for rapid extraction of total lipids from green microalgae. *PloS one* **2014**, *9*, e89643.

131. Bligh, E. G.; Dyer, W. J. A rapid method of total lipid extraction and purification. *Canadian journal of biochemistry and physiology* **1959**, *37*, 911-917.

132. Folch, J.; Lees, M.; Sloane-Stanley, G. A simple method for the isolation and purification of total lipids from animal tissues. *J. Biol. Chem.* **1957**, *226*, 497-509.

133. Christie, W. W. Preparation of lipid extracts from tissues. *Advances in lipid methodology* **1993**, *2*, 195-213.

134. Phillips, K. M.; Ruggio, D. M.; Amanna, K. R. Extended validation of a simplified extraction and gravimetric determination of total fat to selected foods. *Journal of Food lipids* **2008**, *15*, 309-325.

135. AnonymousToxicological Review of Chloroform (CAS No. 67-66-3) (PDF) - 0025tr.pdf. *http://www.epa.gov/iris/toxreviews/0025tr.pdf* (accessed 8/31/2015, 2015).

136. Henderson, R. K.; Jiménez-González, C.; Constable, D. J.; Alston, S. R.; Inglis, G. G.; Fisher, G.; Sherwood, J.; Binks, S. P.; Curzons, A. D. Expanding GSK's solvent selection guide–embedding sustainability into solvent selection starting at medicinal chemistry. *Green Chem.* **2011**, *13*, 854-862.

137. Molina, M. C.; Mariscal, R.; Ojeda, M.; Granados, M. L. Cyclopentyl methyl ether: A green co-solvent for the selective dehydration of lignocellulosic pentoses to furfural. *Bioresour. Technol.* **2012**, *126*, 321-327.

138. Chen, Y.; Pan, Z.; Dong, Y. Measurements of liquid-liquid equilibria for quaternary mixtures of water, methyl tert-butyl ether, and diisopropyl ether with methanol or ethanol. *Journal of Chemical & Engineering Data* **2005**, *50*, 1047-1051.

139. Tamura, K.; Chen, Y.; Yamada, T. Ternary and quaternary liquid-liquid equilibria for fuel additives of the water methanol toluene and water methanol toluene methyl tert-butyl ether or tert-amyl methyl ether systems at 298.15 K. *Journal of Chemical & Engineering Data* **2001**, *46*, 1381-1386.

140. Domanska, U.; Żołek-Tryznowska, Z.; Tshibangu, M. M.; Ramjugernath, D.; Letcher, T. M. Separation of an alcohol and a tetrahydrofuran, methyl tert-butyl ether, or ethyl tert-

butyl ether by solvent extraction with a hyperbranched polymer at T= 298.15 K. *Journal of Chemical & Engineering Data* **2010**, *55*, 2879-2885.

141. Wang, B.; Qiu, T.; Li, S. Liquid− Liquid Equilibrium for the System Water 1, 4-Dioxane 2, 6-Dimethyloct-7-en-2-ol over the Temperature Range of (343.2 to 358.2) K. *Journal of Chemical & Engineering Data* **2009**, *55*, 558-560.

142. Eum, K. W.; Gu, H.; Lee, T. G.; Choe, J.; Lee, K.; Song, K. H. Liquid–liquid equilibria for the ternary systems of perfluorohexane methyl nonafluorobutyl ether toluene, 1, 4-dioxane, or dimethylformamide at 298.15 K. *Journal of Chemical & Engineering Data* **2013**, *58*, 915-919.

143. Senol, A. Liquid-Liquid Equilibria for the Ternary Systems of (Water Tetrahydrofuran Polar Solvent) at 298.15 K. *Journal of Chemical & Engineering Data* **2004**, *49*, 1827-1832.

144. Zhang, H. Measurements and Comparative Study of Ternary Liquid–Liquid Equilibria for Water Acrylic Acid Cyclopentyl Methyl Ether at (293.15, 303.15, and 313.15) K and 100.249 kPa. *Journal of Chemical & Engineering Data* **2015**, *60*, 1371-1376.

145. Zhang, H.; Liu, G.; Li, C.; Zhang, L. Liquid–Liquid Equilibria of Water Acetic Acid Cyclopentyl Methyl Ether (CPME) System at Different Temperatures. *Journal of Chemical & Engineering Data* **2012**, *57*, 2942-2946.

146. Alders, L. *Liquid-liquid extraction: theory and laboratory practice;* Elsevier Publishing Company: 1959; .

147. Cehreli, S. Liquid-liquid equilibria of the acetic acid-water-mixed solvent (cyclohexyl acetate-cyclohexanol) system. *Brazil. J. Chem. Eng.* **2002**, *19*, 45-54.

148. Othmer, D.; Tobias, P. Liquid-liquid extraction data-the line correlation. *Industrial & Engineering Chemistry* **1942**, *34*, 693-696.

149. Hand, D. B. Dineric distribution. *J. Phys. Chem.* **1930**, *34*, 1961-2000.

150. Dean, J. A. Lange's handbook of chemistry. **1985**.

151. Bonner, W. D. Experimental Determination of Binodal Curves, Plait Points, and Tie Lines, in 50 Systems, each consisting of Water and Two Organic Liquids. *J. Phys. Chem.* **1910**, *14*, 738-789.

152. Wasa, K.; Kitabatake, M.; Adachi, H. *Thin film materials technology: sputtering of control compound materials;* Springer Science & Business Media: 2004; .

153. Maeder, T.; Sagalowicz, L.; Muralt, P. Stabilized platinum electrodes for ferroelectric film deposition using Ti, Ta and Zr adhesion layers. *Japanese journal of applied physics* **1998**, *37*, 2007-2012.

154. Meille, V. Review on methods to deposit catalysts on structured surfaces. *Applied Catalysis A: General* **2006**, *315*, 1-17.

155. Astruc, D. *Nanoparticles and catalysis;* John Wiley & Sons: 2008; .

156. Zhong, C.; Maye, M. M.; Luo, J.; Han, L.; Kariuki, N. Nanoparticles in catalysis. In *Nanoparticles*Springer: 2004; pp 113-143.

157. Xia, Y.; Yang, H.; Campbell, C. T. Nanoparticles for catalysis. *Acc. Chem. Res.* **2013**, *46*, 1671-1672.

158. Ben-Sasson, M.; Zodrow, K. R.; Genggeng, Q.; Kang, Y.; Giannelis, E. P.; Elimelech, M. Surface functionalization of thin-film composite membranes with copper nanoparticles for antimicrobial surface properties. *Environ. Sci. Technol.* **2013**, *48*, 384-393.

159. Dotzauer, D. M.; Dai, J.; Sun, L.; Bruening, M. L. Catalytic membranes prepared using layer-by-layer adsorption of polyelectrolyte/metal nanoparticle films in porous supports. *Nano letters* **2006**, *6*, 2268-2272.

160. Luo, M.; Zhao, J.; Tang, W.; Pu, C. Hydrophilic modification of poly (ether sulfone) ultrafiltration membrane surface by self-assembly of TiO 2 nanoparticles. *Appl. Surf. Sci.* **2005**, *249*, 76-84.

161. Liu, Y.; Wang, R.; Chung, T. Chemical cross-linking modification of polyimide membranes for gas separation. *J. Membr. Sci.* **2001**, *189*, 231-239.

162. Kaba, M.; Raklaoui, N.; Guimon, M.; Mas, A. Improvement of the water selectivity of ULTEM poly (ether imide) pervaporation films by an allylamine-plasma-polymerized layer. *J Appl Polym Sci* **2005**, *97*, 2088-2096.

163. Koros, W. J.; Mahajan, R. Pushing the limits on possibilities for large scale gas separation: which strategies? *J. Membr. Sci.* **2000**, *175*, 181-196.

164. Tin, P.; Chung, T.; Liu, Y.; Wang, R.; Liu, S.; Pramoda, K. P. Effects of cross-linking modification on gas separation performance of Matrimid membranes. *J. Membr. Sci.* **2003**, *225*, 77-90.

165. Cao, C.; Chung, T.; Liu, Y.; Wang, R.; Pramoda, K. Chemical cross-linking modification of 6FDA-2, 6-DAT hollow fiber membranes for natural gas separation. *J. Membr. Sci.* **2003**, *216*, 257-268.

166. Shao, L.; Chung, T.; Goh, S.; Pramoda, K. The effects of 1, 3-cyclohexanebis (methylamine) modification on gas transport and plasticization resistance of polyimide membranes. *J. Membr. Sci.* **2005**, *267*, 78-89.

167. Qiao, X.; Chung, T. Diamine modification of P84 polyimide membranes for pervaporation dehydration of isopropanol. *AIChE J.* **2006**, *52*, 3462-3472.

168. Shao, L.; Liu, L.; Cheng, S.; Huang, Y.; Ma, J. Comparison of diamino cross-linking in different polyimide solutions and membranes by precipitation observation and gas transport. *J. Membr. Sci.* **2008**, *312*, 174-185.

169. Wang, Y.; Goh, S. H.; Chung, T. Miscibility study of Torlon® polyamide-imide with Matrimid® 5218 polyimide and polybenzimidazole. *Polymer* **2007**, *48*, 2901-2909.

170. Chung, T.; Shao, L.; Tin, P. S. Surface modification of polyimide membranes by diamines for H2 and CO2 separation. *Macromolecular rapid communications* **2006**, *27*, 998-1003.

171. Powell, C. E.; Duthie, X. J.; Kentish, S. E.; Qiao, G. G.; Stevens, G. W. Reversible diamine cross-linking of polyimide membranes. *J. Membr. Sci.* **2007**, *291*, 199-209.

Appendix A - Apparent Activation Energy

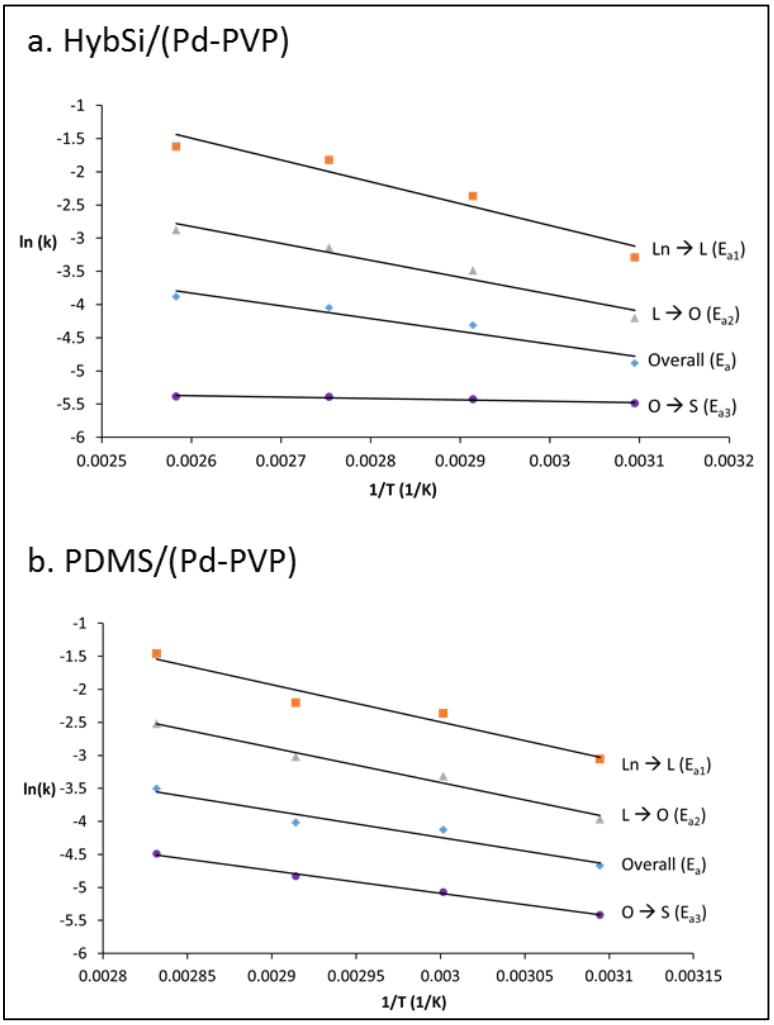

Figure A.1 - Arrhenius plot for PHSO using two different membrane/catalyst: (a.) HybSi/Pd-PVP membrane, (b.) PDMS/Pd-PVP

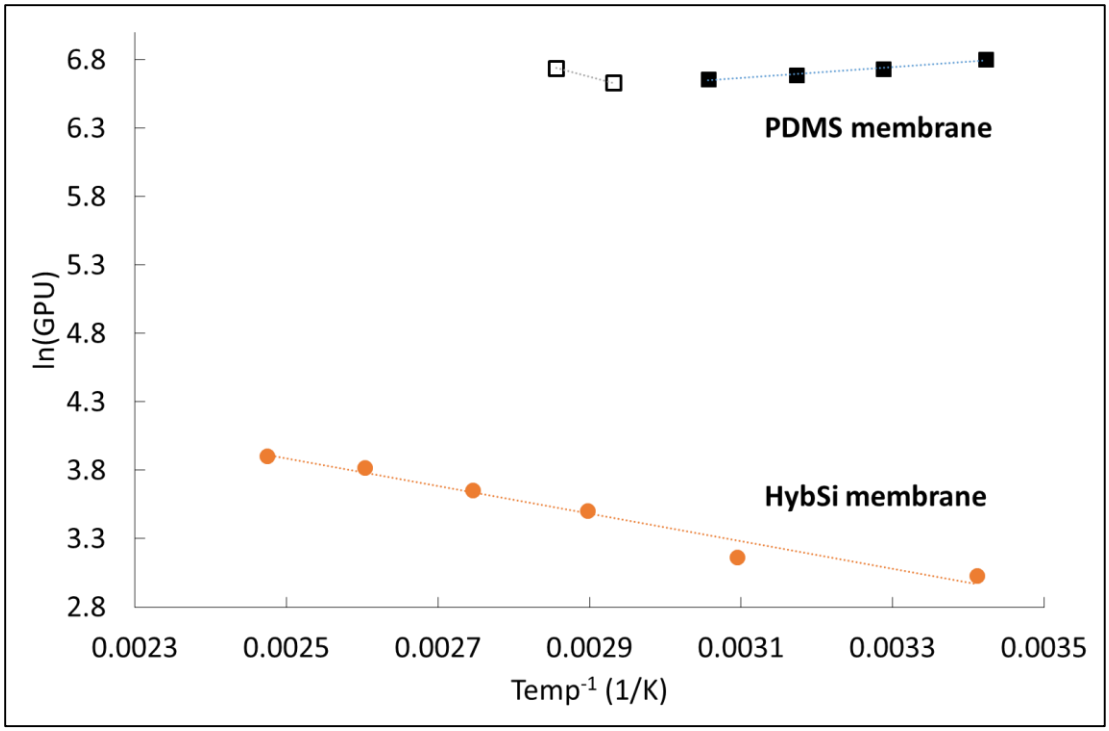

Figure A.2 – Arrhenius plot for hydrogen permeance of virgin membranes: (●) HybSi membrane, (■ and □) PDMS. The two data sets for the PDMS are the same membrane, they are broken up where the Arrhenius plot has an inflection point.

Table A.1 – Apparent Activation Energies for overall and individual reaction in the PHSO.

	PDMS/Pd-PVP		HybSi/Pd-PVP	
	Apparent Activation Energy (kJ/mol)	R^2 of Arrhenius plot	Apparent Activation Energy (kJ/mol)	R^2 of Arrhenius plot
E_a (overall)	34.1	0.9484	16.0	0.9335
E_{a1} (Ln → L)	47.0	0.9503	27.3	0.9294
E_{a2} (L → S)	43.9	0.9835	21.3	0.951
E_{a3} (S → O)	28.7	0.9995	1.7	0.9143

Table A.2 - Apparent Activation Energies for Overall reaction (PSHO)

Apparent Activation Energies for Overall reaction (PSHO)			
System	H_2 Pressure (bar)	Temperature range (°C)	Ea (kJ/mol)
PDMS (Pd-PVP)	4	50-80	36.4
HybSi (Pd-PVP)	4	50-115	16.0
Pd/slurry	51.7	50-110	30.1-35.9

Table A.3 - Apparent Activation Energies for hydrogen Permeance

Apparent Activation Energies for hydrogen Permeance			
System	H_2 Pressure (bar)	Temperature range (°C)	Ea (kJ/mol)
PDMS (virgin)	3.5	19-54	-3.3
PDMS (virgin)	3.5	68-77	11.84
HybSi (virgin)	3.5	19-131	8.4